FREQUENCY RESPONSE OF AN AGRICULTURAL FENCE AND THE IMPLICATIONS FOR
DATA TRANSMISSION

A THESIS SUBMITTED IN FULFILMENT OF REQUIREMENT FOR THE DEGREE

of

Master of Philosophy

at

The University of Waikato

by

Jonathon Guy McMullan

Supervisors

Professor Jonathan Scott and Mr Anthony Smith

School of Engineering

Hamilton, New Zealand

April, 2014

Preface and Acknowledgements

This thesis is for the completion of my master of philosophy. It is a reflection of my interest in communications and in particular of data transmission in difficult environments.

Firstly I would like to thank my supervisors Professor Jonathan Scott and Anthony Smith. Professor Scott was instrumental in getting my project off the ground. He was also very helpful in guiding me around the problems I encountered during my research. Anthony promoted my research to the Callaghan Institute and without him I would not have had the funding to undertake this project.

I would also like to thank the staff in the Energizer Team at the Gallagher Group, in particular Hayden Goble, Robert Surrey and John Croukamp. Your guidance in fine-tuning my measurement procedures and answering my limitless questions enabled my research to make steady progress and your willingness to assist appreciated.

Abstract

The electric fence has been used as a data transmission medium in Gallagher Products for a number of years. This has allowed the energizer to be remotely controlled and, with the current generation, to monitor the performance of the fence remotely. Very little investigation has been conducted into determining the optimum frequency bands to transmit in to give optimum performance.

We propose that the fence spectrum be split into three frequency bands. A Fence Pulse Guard Band which extends from DC to 10 kHz, a Low Frequency Channel which extends from 10 kHz to 250 kHz, and a High Frequency Channel which extends from 250 kHz to 10 MHz.

The fence frequency response is dependent on the length of the fence and is dominated by transmission line effects and radiative losses. For the test fence, the spectrum up to 250 kHz is flat without any frequency selective fading. Above 250 kHz, the spectrum is very unstable and the frequency selective fading can exceed 15 dB. Operating in this region requires an advanced system to utilise the available bandwidth.

The impedance of the human operator in the system is best characterised as a fractional capacitor in series with a resistor. Higher frequencies are attenuated less up to 10 MHz after which the impedance is dominated by the resistance.

The impedance of an insulating joint is best characterised as a capacitor in series with a resistor. Higher frequencies are attenuated less and are the preferred method for reducing the effect of insulating joints.

The Low Frequency Channel is suitable for less robust systems which cannot tolerate frequency selective attenuation. The High Frequency Channel is suitable for robust systems which prioritise performance.

We present a number of possible solutions for improving the efficiency of the modulation and error correction strategies. Solution 3 utilising Phase Shift Keying

(PSK) with eight symbols and Trellis Code Modulation (TCM) is recommended as the first solution to be implemented and evaluated. A forward error correction strategy as outlined in Solution 1 is also recommended for implementation first.

This research suggests that the electric fence system could be significantly improved in performance and reliability using the methods mentioned above but at some cost.

Statement of Originality

The idea to evaluate the response of the electric fence for data transmission was that of the author and was done with support from Professor Jonathan Scott and the Gallagher Group. I collected the data on the fence spectrum. The idea to evaluate the impedance of the human operator and bad joints is that of Professor Jonathan Scott. The modulation strategy and forward error correction designs are mine and are based on research from text books and journal papers.

Table of Contents

Table of Figures

Table of Tables

1. Introduction

Electric Fences are an essential tool that is extensively used in livestock farming, and active monitoring of the fence's condition is important to detecting and fixing faults to ensure livestock are controlled and contained. The current Gallagher system is capable of transmitting data using the fence as the transmission medium between fence monitors and handheld remotes. However the data rate of this system is low and the receiver cannot correct for minor errors in the transmission.

The system in the current generation of energizers was designed to be backwards compatible with the previous generation and very little research has been done into the frequency response of the fence with this application in mind. The current generation continues to be popular with farmers so further improvements should be cognisant of this.

1.1. Thesis Statement

In this thesis we present an improved method for transmitting data along a standard electric fence. It is the aim of this thesis to:

- Evaluate the frequency response of a test fence
- Evaluate the frequency response of the human operator
- Evaluate the frequency response of non-conducting wire joints
- Present and evaluate a number of alternative modulation strategies to improve performance
- Present and evaluate a number of forward error correction strategies to improve performance
- Provide guidance for further research and design

2. The Agricultural Energizer

An electric fence is designed so as to deter an animal from challenging the fence rather than to be able to physically prevent the animal from escaping. Once the animal has been trained to not challenge a fence, the construction of an electric fence need not be as robust as a standard fence and costs can be significantly reduced.

An energizer typically achieves this by storing electrical energy in a capacitor bank and discharging the energy into the primary side of a transformer. One side of the secondary winding is connected to an earth stake and the other to an electrical conductor integrated into the fence. An animal receives an electric shock when it completes the circuit from the fence to the ground. A mains-powered energizer typically targets 8kV as the maximum amplitude of the output pulse and can regulate its stored energy to achieve this.

Section 1

Characterising the Fence System

3. Literature Review

3.1. Communications Utilising Existing Fence Construction

3.1.1. Gallagher Remote (XR1)

The first Gallagher communications system used a handheld device to enable or disable the energizer utilising the fence conductor. The XR1 remote produced a series of five high-voltage pulses which could be interpreted by an energizer such as the MBX2500. The remote produced the pulses using a similar circuit to the one used inside an energizer to produce the main output pulse.

The main advantage of this system was the very high transmission voltage produced by the remote. At 500 Ω load, the remote could produce in excess of 1000 V which was capable of bridging small bad joints and travelling long distances. However the protocol was not capable of transmitting data other than the on/off command.

3.1.2. Gallagher SmartPac

The second generation remote was designed to be used with the flagship MX7500 energizer. The SmartPac used a conventional Frequency Shift Keying (FSK) modulation scheme to transmit data using the fence. The two frequencies used were 42.7 kHz and 38.2 kHz to represent 0 and 1 respectively. This system was capable for transmitting data at a baud rate of approximately 1200. The SmartPac could receive remotely the information presented on the front of the energizer, enable/disable the energizer remotely, and help with fault-finding using voltage and current measurements. One contact point between the remote and the fence was used for all functions.

The main disadvantage of this system was the battery life. In order to encode/decode data, the SmartPac used aTMS320 DSP which consumed 75 mA while in operation. As part of the development process, the two frequencies were chosen to avoid problems with an existing patent, but no research was performed in relation to the fence system.

3.1.3. Tru-Test Fence Compass

Tru-Test Limited released the Fence Compass to compete with the SmartPac. The Fence Compass is capable of enabling/disabling the energizer utilising one way communications but cannot receive information from the energizer. It also uses a separate contact point for communications to prevent the voltage measurement circuitry from loading the transmit stage. Short bursts of FSK data modulation are used, specifically 148.7 kHz and 158.7 kHz for 0 and 1 respectively.

The main disadvantage of this system is the very low baud rate of 70 which is not practical for bi-directional data communications.

3.1.4. Gallagher iSeries

As well as communicating between the remote and energizer, the iSeries adds support for communications with battery powered fence monitors. These monitors are able to measure current and voltage at fixed points around the farm and transmit the data back to the energizer display. The iSeries utilises the same communications protocol as the SmartPac while adding an extra protocol layer to make it possible to add extra functions. This allows it to enable/disable older energizers as well as supporting the new features. A single contact point is used for all functions.

The battery life of this product has been significantly improved with respect to the SmartPac.

3.2. Transmitted Power

Both the Fence Compass and the Gallagher Remote include a measurement function as well as circuitry to communicate with the energizer. The Gallagher Remote combines both of these functions into a single electrical contact point on the remote. The Fence Compass has two separate contact points on the remote, one for fence measurement and one for communications. To make a measurement, the user is expected to contact the fence conductor with the front connection then change to the back connection to enable or disable the energizer. By physically isolating the two circuits, the transmit circuit in the Fence Compass can achieve a significantly higher

transmit power than the Gallagher Remote at the cost of convenience (Figure 1 and Figure 2).

Load Curve
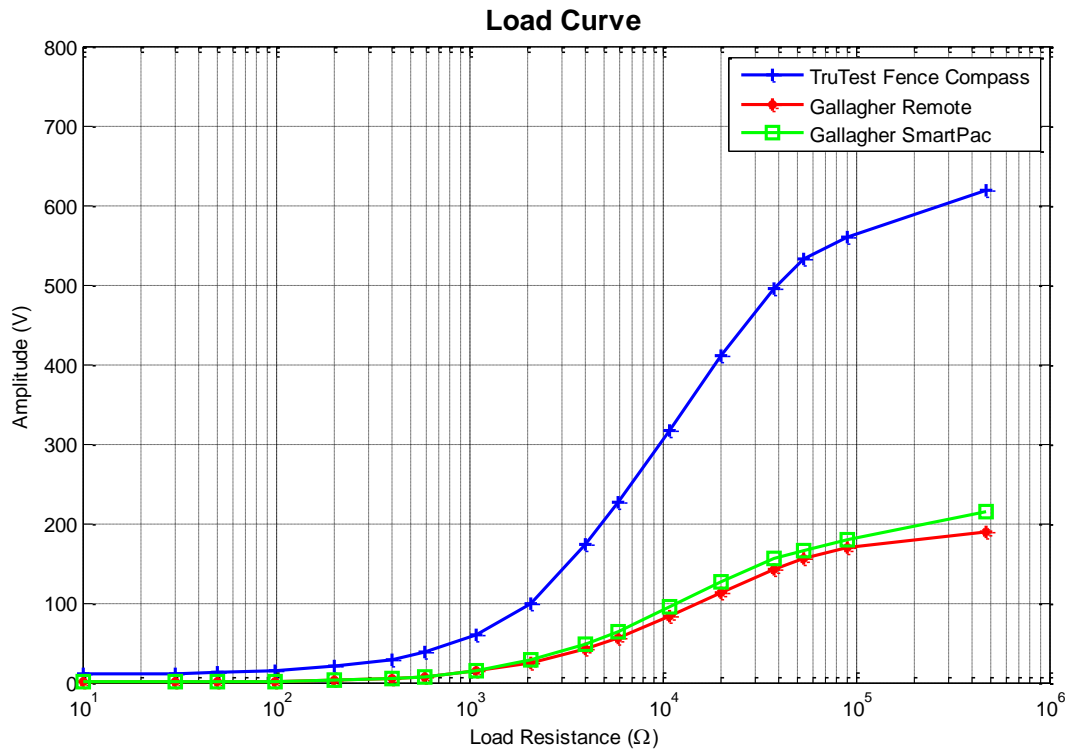
Figure 1 - Graph plotting Amplitude vs. Load Resistance for each remote (excluding XR1). The Gallagher Remote and SmartPac use a very similar circuit which accounts for the similar levels. The TruTest Fence compass is significantly more powerful.

Load Curve
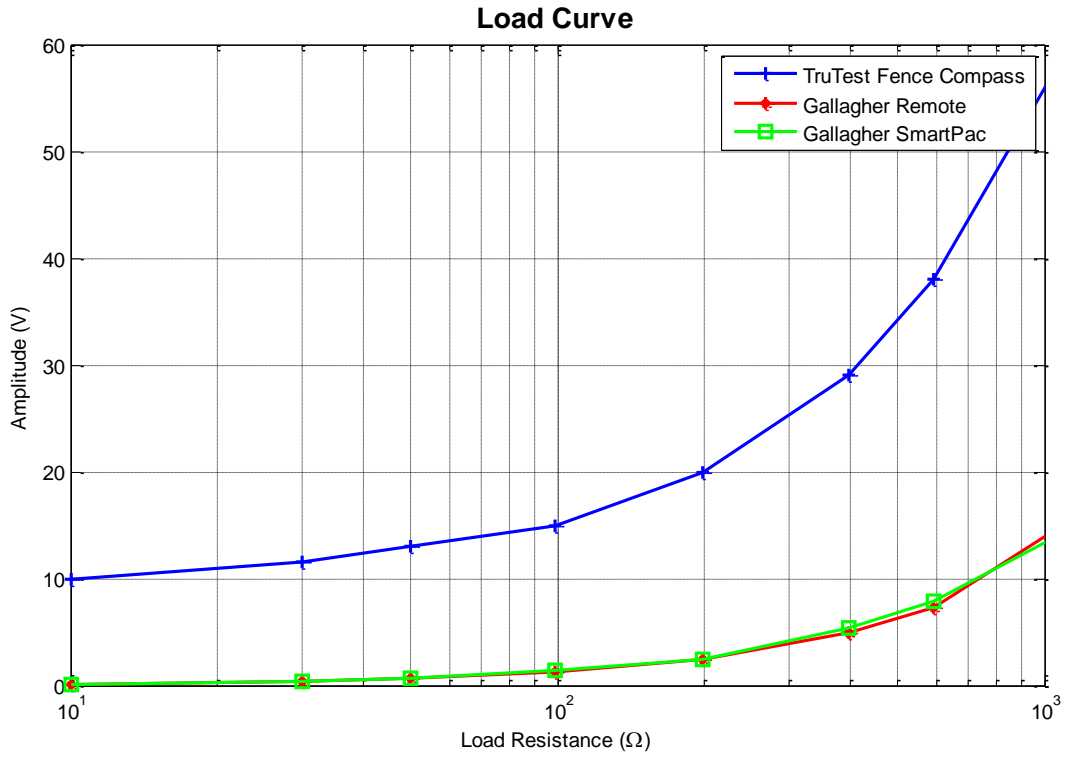
Figure 2 - Graph plotting Amplitude vs Load Resistance for the Range 10Ω to 1000Ω (excluding XR1). The TruTest Fence Compass has a significant advantage at low values of resistance.

The Gallagher XR1 produces a significantly higher voltage than either the Fence Compass or Gallagher Remote (Figure 3).
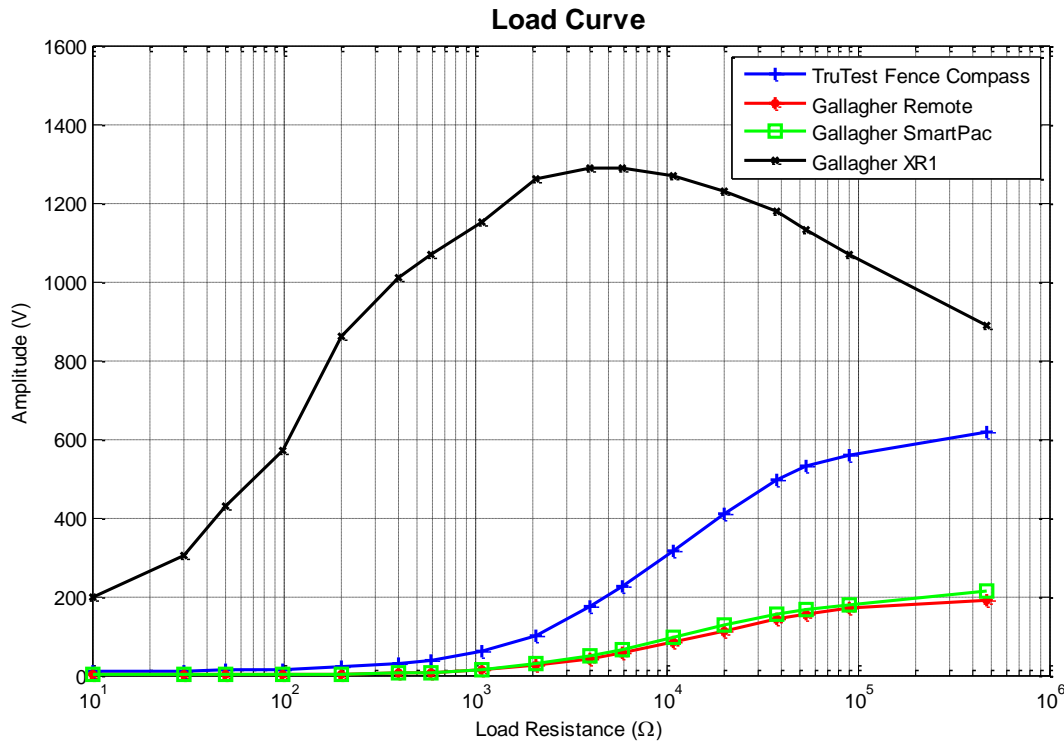
Figure 3 - Graph plotting VPEAK vs. Load Resistance for each remote (including XR1). The XR1 uses a fundamentally different design to produce an output. It has an extremely high output power compared to the other schemes.

3.3. Other Relevant Literature

Of particular note is a thesis completed in 1991 by Hancock [1] while working for the Gallagher Group. A number of detailed models for determining the characteristic load of electric fence are presented for both a single and multi-wire fences. The impedance of a person was also investigated, with particular interest paid to the transfer of energy from the fence pulse. A purely resistive value of 890 Ω was measured as the research was not concerned with the frequency response of the person. The author was primarily interested in how the main fence pulse travelled and did not investigate frequencies beyond 20 kHz.

Another thesis of relevance was completed in 2002 by Saad [2]. A method for the detection of wire deflection in security fences is presented. A sinusoidal signal is transmitted down the fence and its frequency tuned to resonate at the fence's natural frequency. The amplitude of the wave is measured at the terminated end. If the fence is tampered with, the natural resonant frequency will drift and the measured

amplitude will decrease. The author focused on higher frequencies than Hancock, with tests up to 1 MHz.

3.4. Modelling an Electric Fence as a Transmission Line

At low frequencies, an electric fence can be accurately approximated using the resistance of the live wire and the resistance of the return system (earth stakes or return wires). Assuming that the external loading of the fence is minimal, the conductance can be ignored. The capacitance and inductance of the system also has a negligible effect and can be ignored. As the frequency is increased, the effect of capacitance and inductance in the system increases and eventually dominates. A common method for characterising a transmission lines was developed by O. Heaviside [3] and details the modelling of a transmission line using a combination of resistance, inductance, capacitance and conductance (Figure 4). This model can be easily implemented in SPICE although the number of elements required can be prohibitive should the ratio of distance to wavelength become significant.
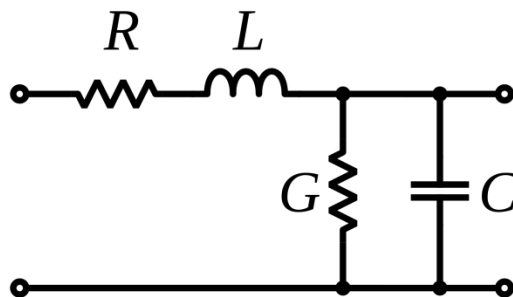
Figure 4 - Single Element of RLCG Transmission Line Model [4]

Capacitance in the system exists between the outgoing conductor and the returning ground. Inductance in the system exists due to the wires themselves or the ground if a ground return wire is not used. The conductance parameter is ignored for this situation because it is effectively zero between the two conductors when no external loading is present. Given a large enough number of elements, this model is effective for modelling a basic lossy transmission line where the losses are due to the resistance of the line. For this research this is insufficient as a general model as it is expected that a significant factor in the losses will be due to the frequency

dependency of the L term. An electric fence commonly uses steel wire with a relative permeability greater than one. This increases the inductance and amplifies the skin effect at frequency[1].

Modelling transmission lines with frequency-dependant components can be achieved using two methods. The first is to use a nodal analysis program such as SPICE with a large number of lumped RLCG elements to approximate the response of the transmission line at frequency such as described by Hyland [5] and others. Alternatively, the transmission line can be modelled using a Finite Element (FE) simulation such as ANSYS HFSS [6]. As the FE simulation solves Maxwell's equations directly based on the physical geometry of the system, it is ultimately more accurate than a SPICE simulation but requires significant computation in order to reach sufficient accuracy.

3.5. Frequency Response between the Remote and Ground utilising the User's Electrical Properties

For the latest generation of energizer remote controls (Gallagher iSeries and TruTest Fence Compass), the human operator forms part of the ground path, from the hand through the body to ground at the feet. A large amount of research has been conducted in the biophysics area for characterising the properties of the body tissue [7].

Gabriel et al. [8] compiled a summary of data from a number of papers which shows a consistent trend towards increasing conductivity and reducing permittivity as the frequency increased. This trend was consistent across most of the body tissues characterised. This would suggest that the attenuation of signals propagating from hand to foot should reduce as frequency increases.

Part two of the study by Gabriel et al. [9] presented further measurements of conductivity and permittivity. The measurement resolution was increased over

---

[1] At high frequency current tends to flow near the surface of the conductor. This is known as the 'skin effect'. 63% of the current flows within one skin depth, $\delta = \sqrt{\frac{2\rho}{\omega \mu_r \mu_0}}$ where δ = skin depth [36].

previous research and provides further confirmation that the conductivity increases and the permittivity decreases with frequency.

Of particular relevance is a study by Foster et al. [10] which focused on a whole body impedance measurement from hand to foot. These results also demonstrated a trend towards reducing impedance as frequency increases.

4. Experimental Facilities

4.1. Measuring Frequency Response of a Fence

4.1.1. Representative Test Fence

Every electric fence installation is different but a common configuration is usually similar to either a tree shape with a large number of branches off a central trunk or a grid pattern with each paddock forming a square in the grid. Such a large number of interconnecting transmission lines makes it very difficult to accurately determine the effect of frequency on the transmission of a signal. To simplify the problem, a fence 200 m in length was constructed from a single run of wire without joints (Figure 5).

Figure 5 - Satellite Map with path of test fence marked. This is located at the back of the Gallagher Site in Hamilton. The total length was closer to 200m than the 210m indicated in the figure. The green marker indicates the transmitter and the red marker indicates the receiver

The fence forms a loop with a break at one end to connect the measuring equipment. This fence will not be representative of all fences, but it enables two important test cases to be examined. The first is a standard test with a single live wire and an earth

return provided by a ground peg. The second is a single live wire with an earth return provided by a separate wire (Figure 6).
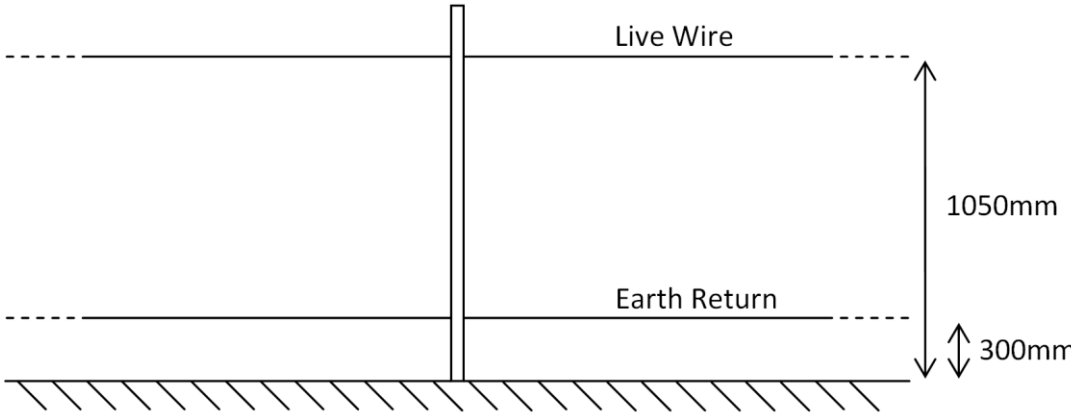
Figure 6 - Diagram of fence construction. The height values are a best guess average over the fence as the ground is not perfectly level.

Standard 2.65mm galvanized high-tensile steel wire was used with a total resistance from end to end of 5.8Ω for the live wire and 5.9 Ω for the earth return wire.

Figure 7 - Photo of Test Fence and connection to equipment

4.1.2. Connecting from the Oscilloscope and Signal Generator to the Fence

Initially the Tektronix 10x probes were connected directly to the fence, with a 600 Ω resistor load at the receiving end (Figure 8).
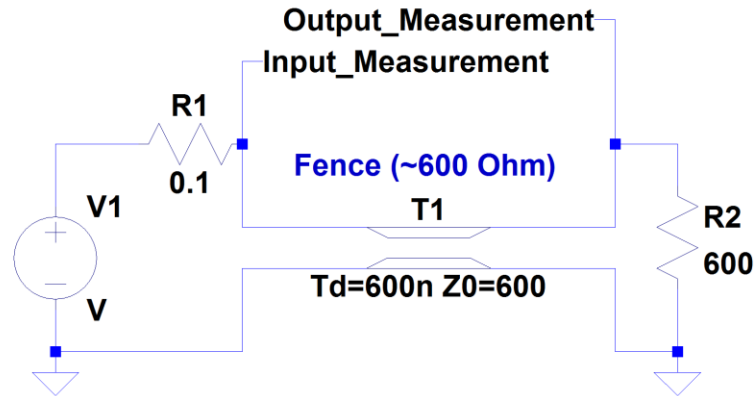
Figure 8 - Standard Lead-out Configuration. The fence impedance is assumed to be approximately 600 Ω.

To improve the matching of the circuit it was modified to use a Coaxial cable and an improved matching circuit. This allows the fence to be more precisely matched and any frequency effects of the connection from the fence to the oscilloscope minimised (Figure 9).
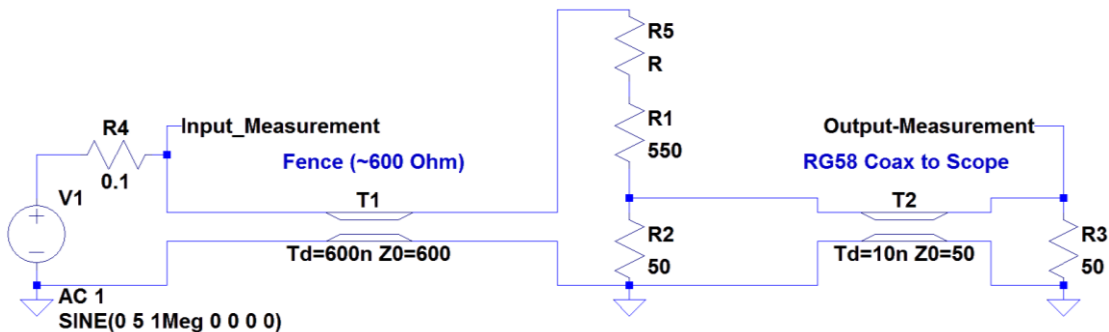
Figure 9 – Improved Measurement Circuit. Coaxial connections are shown with transmission line symbols

Coaxial Cable with a nominal impedance of 50 Ω was used to connect to the fence from the waveform generator and from the fence to the oscilloscope. A board with a series of 0603 package resistors was used to fine tune the impedance matching and is represented by the resistor R5 in the circuit.

Figure 10 - Photo of test equipment

4.1.3. Frequency Generation

For frequencies between 100 Hz and 2 MHz, a Phillips PM821 Arbitrary Waveform
Generator (AWG) was used to generate the test signal. This features a 20 MS/s DAC.
Frequencies between 100 Hz and 20 kHz used a multiplier of 1 which yields 1000
points per cycle. Frequencies between 20 kHz and 200 kHz use a multiplier of 10
which yields 100 points per cycle. Frequencies between 200 kHz and 2 MHz use a
multiplier of 100 which yields 10 points per cycle. The output filter was enabled to
smooth the waveform, particularly when higher multipliers were used.

For frequencies beyond 2 MHz, an Agilent N9310 RF generator was used. A
sinusoidal waveform was produced with modulation disabled. Frequencies between
100 kHz and 50 MHz were produced using this equipment.

4.1.4. Waveform Capture

Initially a Tektronix TPS2014 4-Channel 100 MHz battery powered oscilloscope was used to sample both the input and output waveforms. The captured window was averaged 64 times and converted into 2500 points before being stored using the Tektronix CSV file format on a 512 MB CompactFlash card.

For the final results a TDS2012C 2 Channel 100 MHz oscilloscope was used, powered by a 200W true sine wave inverter. The captured window was averaged 128 times and converted into 2500 points before being stored using the Tektronix CSV file format on an 8 GB USB drive.

4.1.5. Waveform Analysis

Both of the signal generators suffer from distortion in part of their sweep range. The AWG produces a well-defined sine wave when the number of samples is high; however the waveform becomes severely distorted when the number of samples is reduced. The RF generator also suffers from distortion, particularly at low frequencies when attempting to output voltages in excess of 1 V.

To compensate for this, a Fourier Transform is used to measure a single frequency component and to negate the effects of the signal generator. Two methods were used to perform the Fourier Transform and output the resulting frequency response. The first was based on the program written by Scott et al. [11]. A Visual Studio Application loaded and converted the data files from the oscilloscope, loaded the required frequency parameters, and calculated the DFT by calling the program. This data was then loaded into Excel for viewing. The second method used MATLAB and the built in functions to calculate and plot the response.

4.2. Measuring the Impedance of a Human to Ground

4.2.1. Low Frequency

For frequencies between 20 Hz and 2 MHz, an Agilent E4980A Precision LCR Meter was used to measure the impedance of the DUT. It is also capable of selectable output voltages between 1 V and 20 V with high accuracy. The E4980A uses a shielded 4-

terminal pair measurement system to accurately perform the measurement selected
(Figure 11).
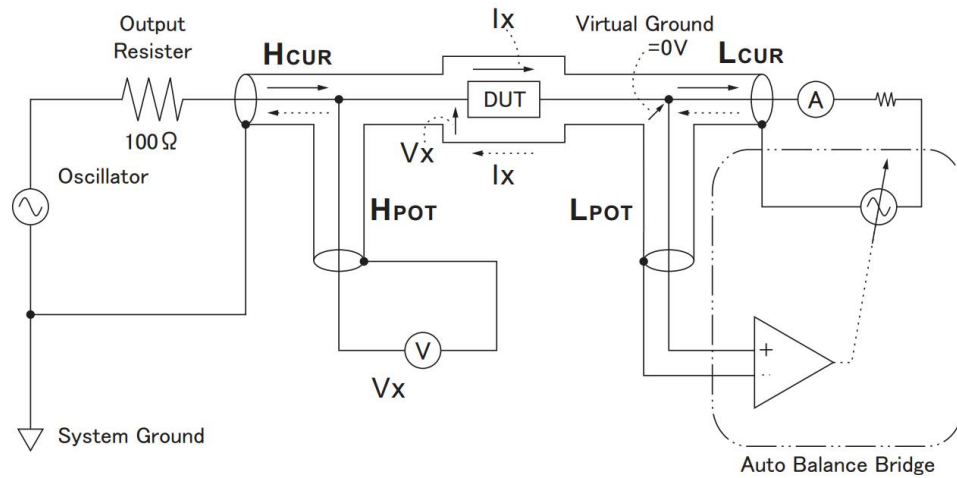
Figure 11 - 4-Terminal Pair measurement system used by Agilent E4980A [12]

This system eliminates additional errors which occur in standard 4-wire measurement
systems by ensuring the same current flows in the outer shield as in the inner
conductor. The self-inductance of the individual leads and mutual inductance between
leads does not have an effect because the same current flows in each conductor. This
further improves the accuracy of the measurement compared to a standard 4-wire
system.

The E4980A was connected to an E5810A LAN/GPIB Gateway which can be
controlled using the Agilent VISA Libraries. The VISA libraries are compatible with
a number of languages, in this instance controlled by Visual Studio 11.0 using the C#
language. Approximately 2100 points are collected between 20 Hz and 2 MHz. For
the majority of the measurements, the test voltage was set at 1 V with a medium
length sample time.

4.2.2. High Frequency
For frequencies in excess of 2 MHz, and an Agilent 4395A
Network/Spectrum/Impedance Analyser was used to measure the impedance of the
DUT. To convert from a two port system to a single port, an Agilent 87512A

Transmission/Reflection Test Set was used (capable of operation from DC to 2 GHz). An Agilent 85032F Type N Calibration Kit was used to calibrate the analyser before measurements were taken.

The source was configured to sweep from 100 kHz to 500 MHz at 0 dBm using a log scale. 801 points were collected with an IF bandwidth of 100 Hz. The total sweep time was 47.32 seconds. The measurement was averaged 16 times for the calibration and 4 times for the measurement.

A female N-type connector was used to adapt the N-type connection to individual wires (Figure 12). No allowance was made for this connector as the rest of the system was so large.
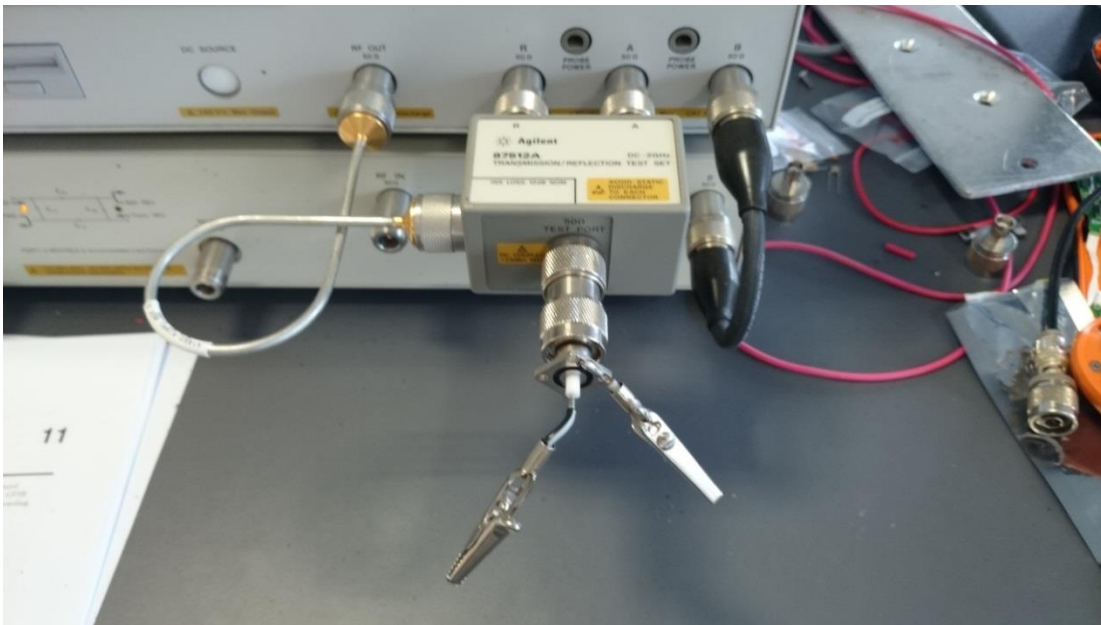
Figure 12 - N-type adaptor to individual wires with Transmission/Reflection Test Set

4.2.3. Connection from Equipment to DUT

To simulate a conductive ground, a plate of aluminium 370 mm x 90 mm x 5 mm was placed on the ground and connected.

The connection from the equipment to the operator's hand depended upon the configuration required.

After some initial testing, it was determined that the application of pressure to the interface between conductive plate and the skin had a large impact on the low frequency measurements. The Remote is designed so that the fingers of the hand are in contact with the back plate. To obtain measurements which were as replicable as possible, the palm of the hand was used instead of the fingers as the pressure can be maintained more evenly over the surface. This is does not match reality perfectly but any differences between these results and reality can be inferred logically.

The pressure distribution across the sole of the feet also had a large impact on the measurements. Increasing the pressure towards the front of the foot improved the conductivity of the measurement so during the measurements, a 'ski stance' was adopted to evenly maintain this pressure for the entire measurement (Figure 13). The knees are brought forward to evenly distribute pressure across the front of the foot as well as the back.
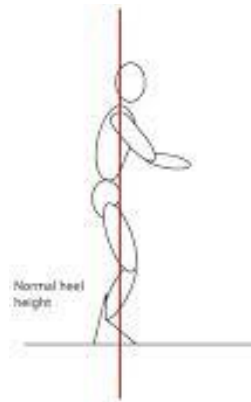
Figure 13 - Ski Stance [13]. Note how the centre of gravity is moved forward over the feet

4.3. Measuring the Impedance of a Bad Joint

4.3.1. Low Frequency

For frequencies between 20 Hz and 2 MHz, an Agilent E4980A Precision LCR Meter was used to measure the impedance of the DUT. Four equal length 50Ω coaxial cables terminated with crocodile clips were used to make the measurement and were connected together at the DUT.

4.3.2. High Frequency

For frequencies in excess of 2 MHz, and an Agilent 4395A Network/Spectrum/Impedance Analyser was used to measure the impedance of the DUT. To convert from a two port system to a single port, an Agilent 87512A Transmission/Reflection Test Set was used (capable of operation from DC to 2GHz). An Agilent 85032F Type N Calibration Kit was used to calibrate the analyser before measurements were taken.

The source was configured to sweep from 1 kHz to 500 MHz at 0 dBm using a log scale. 801 points were collected with an IF bandwidth of 100Hz. The total sweep time was 47.4 seconds. The measurement was averaged 16 times for the calibration and four times for the measurement.

A female N-type connector was used to adapt the N-type connection to individual wires. The test joints were connected as closely to the adaptor as possible.

4.3.3. Test Joints

A number of methods are used to joining fence wire together. Different types of connectors are available on the market to simplify the process but a common way to join wire is to use a reef knot (Figure 14).

Figure 14 - Fence wire joined using reef knot

Tension is usually maintained by the fence strainers; in this case cable ties are used instead. Once the wire had been tensioned into shape, the cable ties could be removed to change the joint configuration before reassembly into the same shape.

4.3.4. Non-linear Properties of Iron Oxide

A signal generator was used to generate a triangle waveform at 10 kHz with an amplitude of 3.3V and 3.8V (Figure 15). A Tektronix TBS1062 Oscilloscope was used to capture 2500 points. A piece of metal 20 mm x 200mm x 4 mm which had a thin layer of rust was used to provide the rust for the junction. A needle was used to establish contact with the rust. Pressure was applied to the needle as necessary to adjust the thickness of the rust layer.
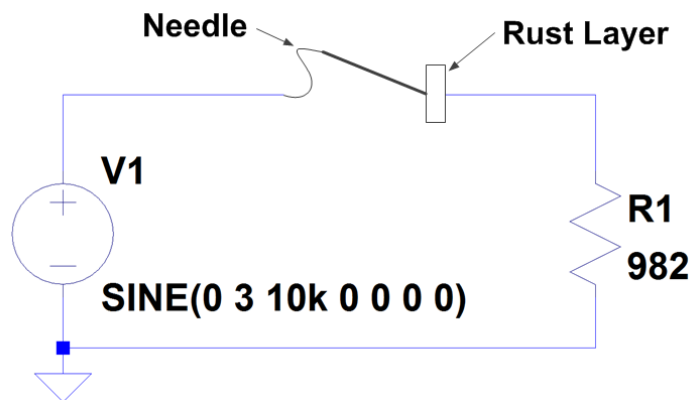
Figure 15 – Schematic of circuit for measuring non-linear effects of iron oxide junctions

4.4. Evaluation of Modulation Schemes and Techniques

The Bit Error Ratio (BER) can be calculated theoretically or simulated to determine the performance of a modulation technique for a given ratio of signal strength to noise. The SNR is dependent on the bandwidth of the signal so noise performance is measured against Energy per bit over Noise Spectral Density (E_b/N_0). Schemes which are highly noise resistant will be able to achieve low error rates at low values of E_B/N_0, or closer to the bottom left corner of the plot.

For Bit Error Rate (BER) simulations, MATLAB includes a specialized tool for producing theoretical and simulated E_b/N_0 plots. This can be configured to simulate PSK, DPSK, OQPSK, PAM, QAM, FSK, MSK and CPFSK with various modulation

orders. It can also be used to test the effects of AWGN, Rayleigh and Rician channel types with both convolutional and block codes. This tool was configured to produce the required plots.

It should be noted that the BER plots produced in MATLAB are based on theory or simulation and as such do not take into effect any reduction in performance caused by the design of the modulator and demodulator.

5. Measuring the Frequency Response of an Electric Fence

The fence is the medium which the data is passed through to communicate between the transmitter and the receiver. The rate at which data can be transmitted is limited by the amount of bandwidth available and the level of interference and noise present. Establishing bands where it is suitable to transmit data efficiently is an important step to designing a communications system.

5.1. Impedance Matching the Test Fence

Transmitting at high frequency requires the fence to be treated as a transmission line and the concepts which are associated with it. Communications systems are commonly constructed using well behaved transmission lines which can be matched to both the transmitter and receiver to reduce interference. Electric fences are constructed in a variety of different ways, and it is unlikely that any construction will be suitable as a well behaved transmission line.

Impedance matching is important because it reduces reflections and interference in a transmission line. In other high speed systems it can be tuned automatically although manual tuning is common as well if the transmission line is well understood and consistent.

It is not feasible to design an automatic impedance matching circuit for an electric fence due to the high voltages which are present. So it is likely that accurate impedance matching will not be available and that any matching will be best guess at the time of design. Based on the dimensions of the test fence, the impedance of the fence is estimated to be approximately 600 Ω [1].

5.2. Initial Frequency Sweep without Accurate Impedance Matching

This sweep was conducted with two Tektronix 10x probes and a 600 Ω 0.25 W resistor connected across the fence at the receiving end. The wire connecting the

signal generator and oscilloscope to the fence was not calibrated in anyway or compensated for its own frequency response. This is close to the worst case scenario for a fence communications system. The Phillips AWG was used to measure 30 points per decade across the frequency range from 100 Hz to 2 MHz (Figure 16).

Frequency Sweep with Live Earth
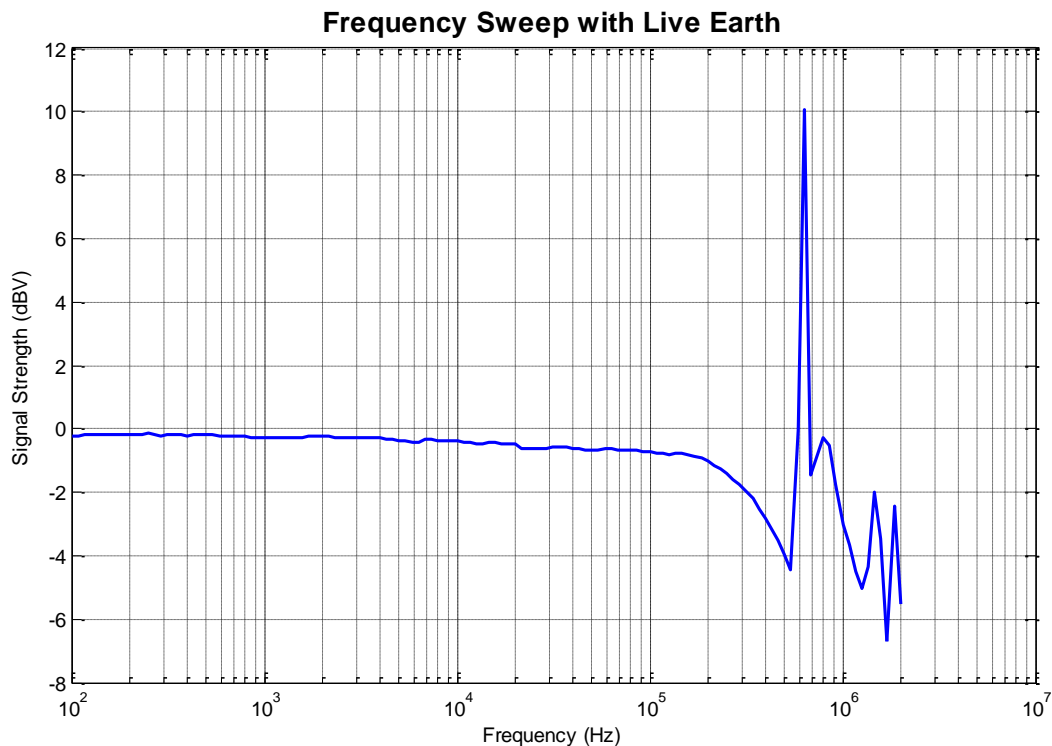
Figure 16 – Frequency Response of Electric Fence matched to a 600 Ω resistor. The response is well behaved before transmission line effects interfere at approximately 200 kHz

The response is predominantly well behaved below 100 kHz however reflections from the mismatched impedance cause interference above 250 kHz.

The frequencies at which standing waves form and cause interference are dependent on the length of the transmission line. Hence the communications system cannot be configured to operate in one of the signal strength peaks as each fence will be different.

5.3. Reducing Reflections using a Matched Lead-out

The oscilloscope and coaxial lead-outs are all matched 50 Ω transmission lines whereas the fence is a 600 Ω transmission line. This creates a mismatch and has a

large effect on the frequency response of the system. An improved test configuration was constructed for this testing (refer Section 4.1.2). To verify the response of the new test configuration, the frequency response was measured without a fence connected. The improved lead-out introduces 27.5 dBV of attenuation into the system but has a very flat frequency response (Figure 17).
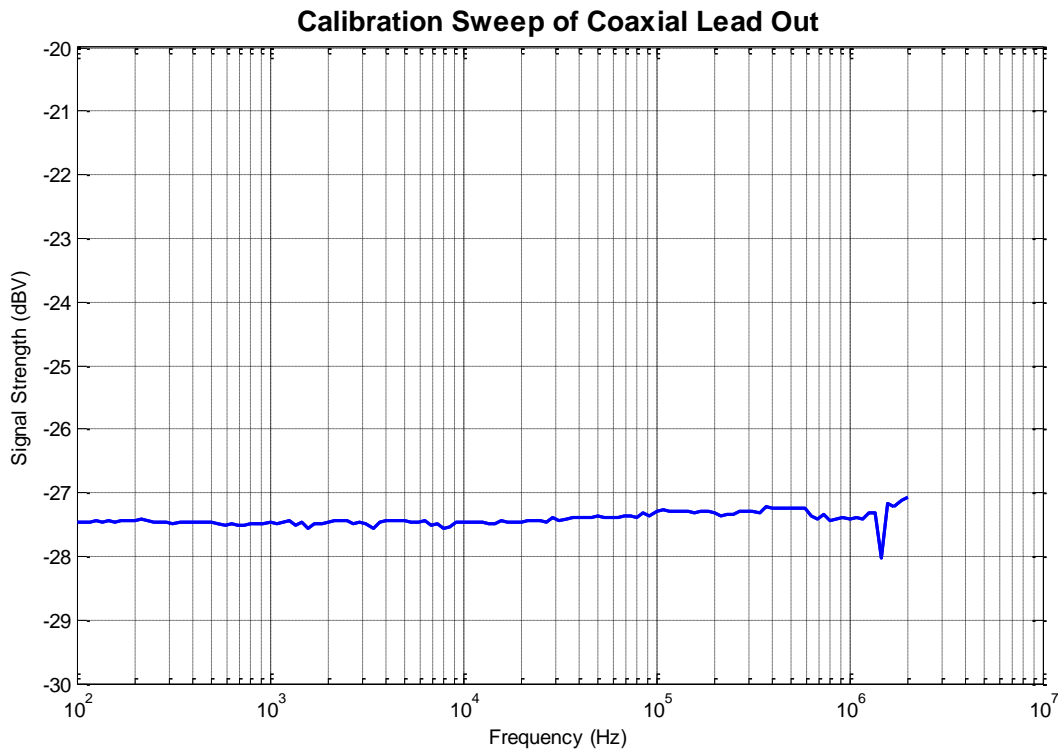
Figure 17 - Frequency Sweep with test fence removed and only the lead-out included. The response is very nearly flat to within a fraction of a decibel

5.4. Accurate Impedance Matching of the Fence

To check whether the impedance matching circuit was having an effect on the results, a peak in the response was chosen, and the matching impedance swept from 575 Ω up to 950 Ω (Figure 18). No discernible pattern is present in the data indicating that the impedance matching is having no major effect. If the impedance matching was dominating the response, an obvious pattern would be present.
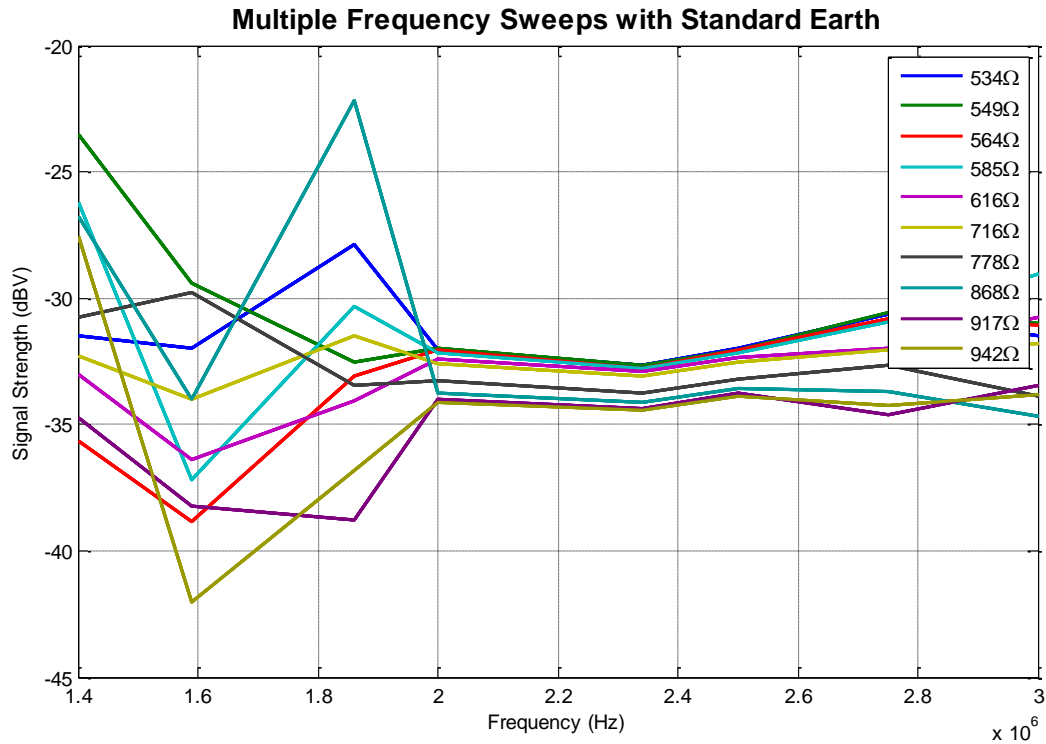
Figure 18 - Impedance Sweep of the test fence. No discernible pattern is present in the figure which indicates that the impedance matching is having little to no effect on the result

5.5. Frequency Sweep with Matched Lead-out

Measuring the frequency response using the matched lead-out and the AWG showed an improvement in the measurement. A number of peaks are eliminated due to the improved matching. A smooth roll off with frequency due to skin effect is expected, however the roll off measured is steeper than accounted for by skin effect and the high frequency response is still highly variable (Figure 19).
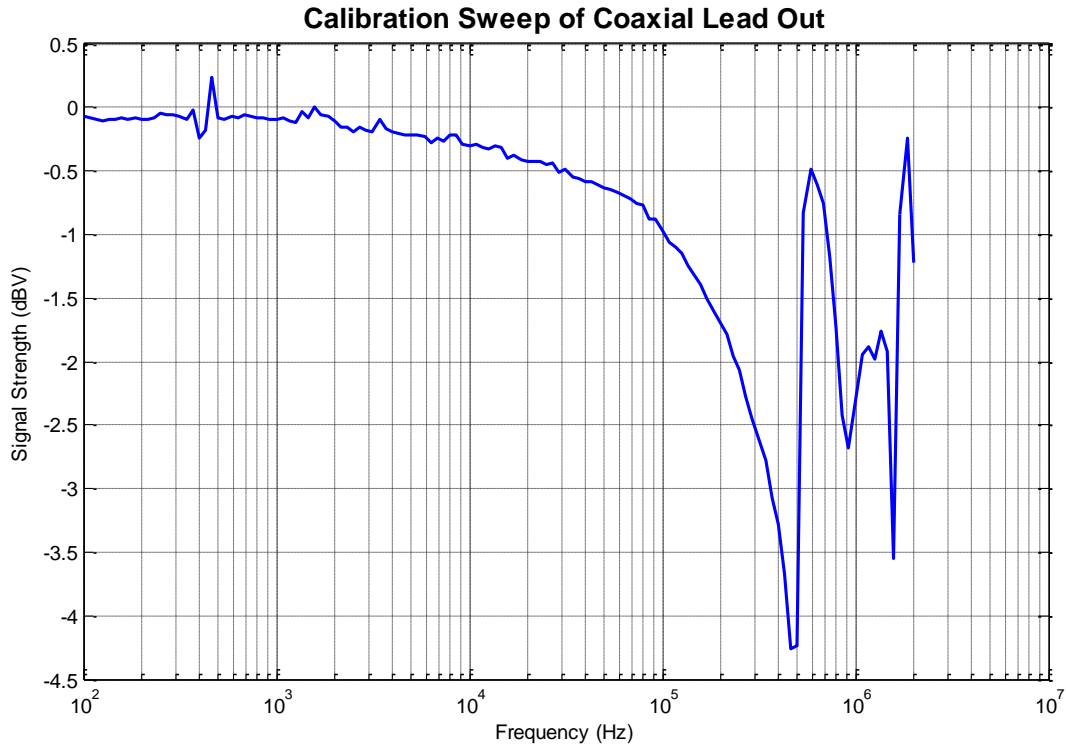
Figure 19 - Frequency sweep with coaxial lead-out and calibration resistor set to zero ohms. The interference caused by the mismatched lead-out is significantly reduced

Replacing the AWG with the N9310A gave similar results which do not appear to match theory if the fence is assumed to be a simple transmission line. The frequency response is still highly variable and it is impossible to discern the expected downwards trend from the data collected. The signals involved cannot be attributed to random noise as a very large number of measurements (128) are averaged to cancel out any Gaussian noise sources. We have no reason to doubt the reliability of these measurements. A number of frequency sweeps are plotted to demonstrate the systems variability (Figure 20 and Figure 21).
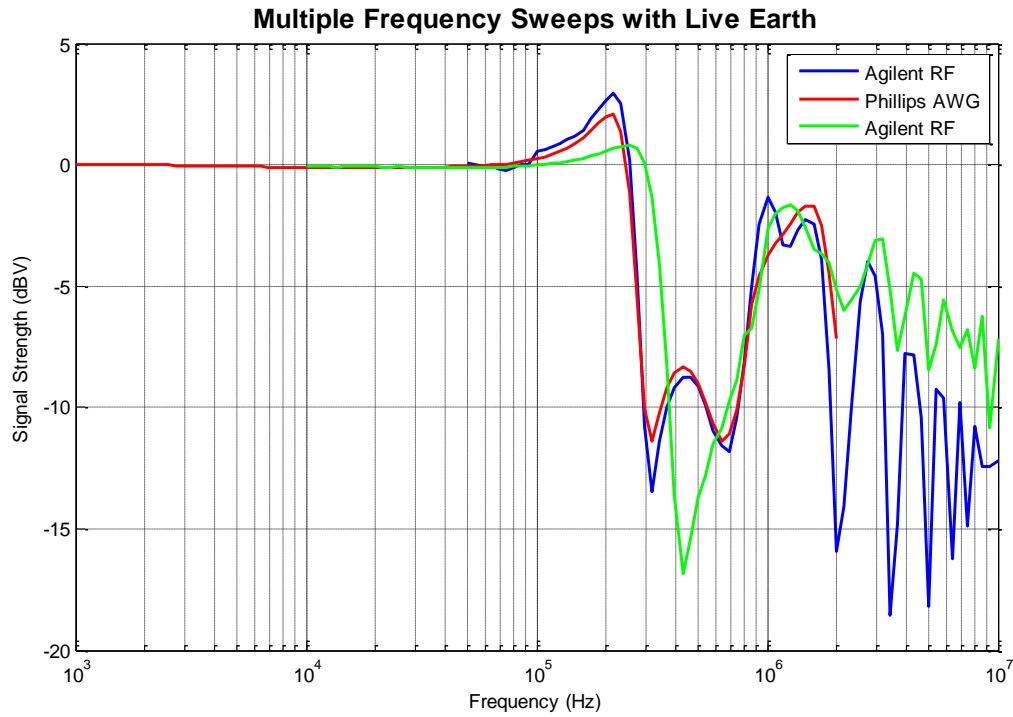
Figure 20 - Frequency Sweep with Live Earth demonstrating variable response. The sweeps do not match perfectly but appear to have a broadly similar pattern. Phillips and Agilent frequency sources used
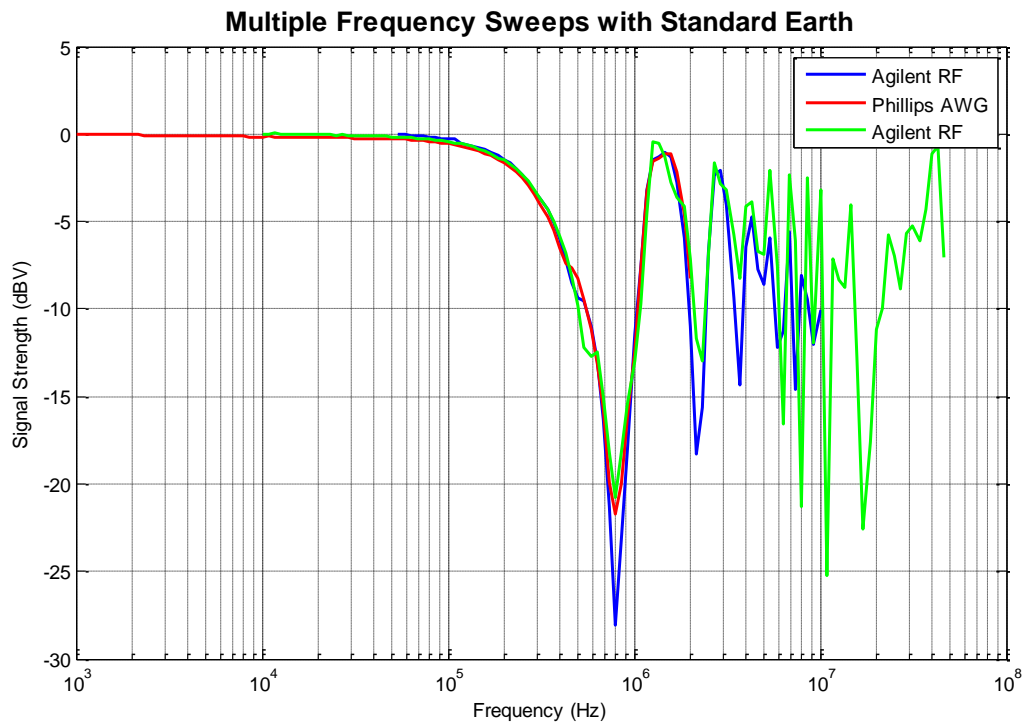
Figure 21 - Frequency Sweep with Standard Earth demonstrating variable response. There is a discernible pattern between each of the sweeps

5.6. Summary of Electric Fence Frequency Response

A sample of the data produced from the tests performed with the improved lead-out was chosen as a representative response for this fence (Figure 22). Data has been normalised to account for the losses in the improved lead-out. The signal generator used is indicated in brackets in the legend, with "AWG" for the Phillips source and "RF" for the Agilent source.
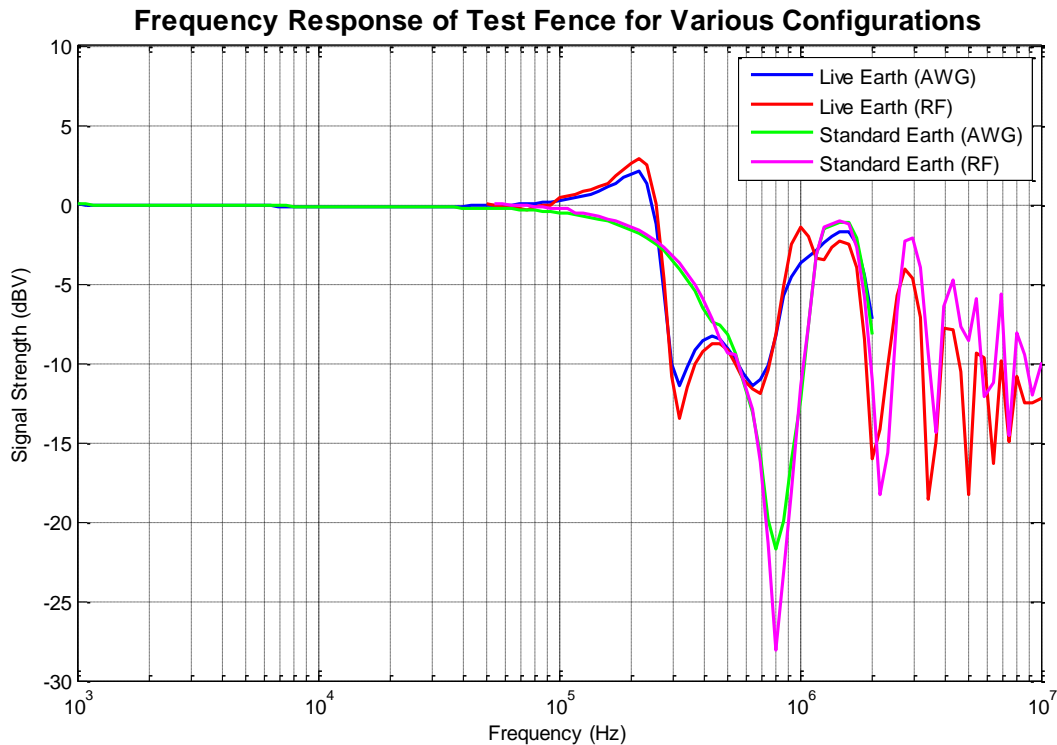
Figure 22 – Representative Frequency Sweep of Test Fence with Improved Lead-out. Presented on a logarithmic scale.

Of particular interest are the differences in the response between the live earth and the standard earth between 100 kHz and 1 MHz, but the measurements are very similar above 1 MHz.

When the data is viewed on a linear axis, a repeating pattern is observed with a regular period (Figure 23). This is very similar to the input impedance of a dipole or folded dipole antenna. Since the fence is effectively a single wire, it is logical to assume it is behaving like a dipole antenna. This pattern cannot be compensated for by matching the transmission line impedance, instead it is a core property of this

transmission line. It should also be noted that the earth stakes have a lower impedance than the live earth. This is because the live earth covers the full 200m distance, whereas the earth stakes do not. This artificially improves the performance of the earth stakes and is an unavoidable artefact of the measurement. The live earth should have a lower impedance at lower frequencies than the earth stakes.

Frequency Response of Test Fence for Various Configurations
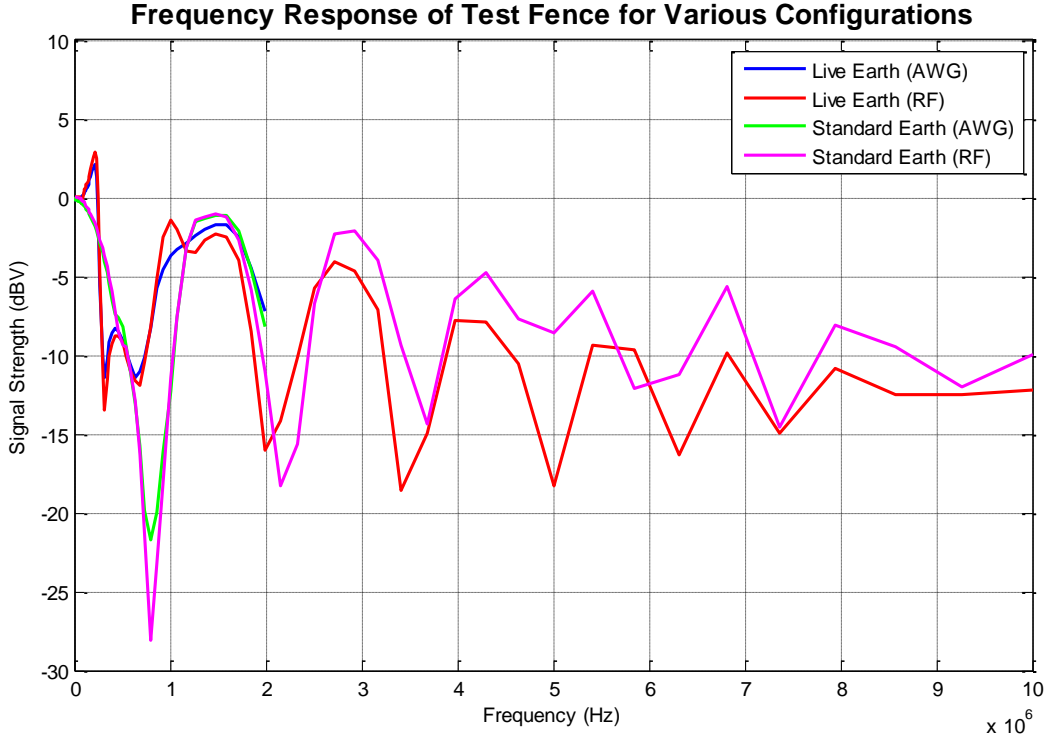
Figure 23 - Representative Frequency Sweep of Test Fence with Improved Lead-out. Presented on a linear scale. The repeating pattern is obvious on a linear scale and is indicative of radiative effects.

In conclusion, the frequency response of the fence is very poor for transmitting data. Above 250 kHz, the response is extremely variable and cannot be characterised with any certainty. To transmit in this region, notches of more than 15 dB must be taken into account. In ideal circumstances, notches in excess of 25 dB are possible but this should be considered an extreme case. The frequencies at which this resonance occurs are dependent on fence geometry. This is a property of the transmission medium and cannot be compensated for with hardware at either end. The impedance of the fence line is approximated to be 600 Ω but attempting to match the fence accurately has

little effect on the overall response. A fence with a live earth has a different response to a fence with just an earth stake.

6. Measuring the Impedance of the Human Operator

The Gallagher Remote is designed to receive and transmit data from the energizer via the electric fence (Figure 24). Earlier versions used a conductive peg to connect to ground but the latest version uses a capacitive back plate to utilise the connection to ground provided by the human operator's body.

Figure 24 – Gallagher iSeries Remote. Conductive plate is insulated by an orange sticker over the battery cover with black dots highlighting the area

The Remote can be modelled at its simplest level as an isolating capacitor (C1) and a measurement resistor (R1). The microcontroller measures the signal imposed across R1 and decodes the data present on the fence transmission line (Figure 25).
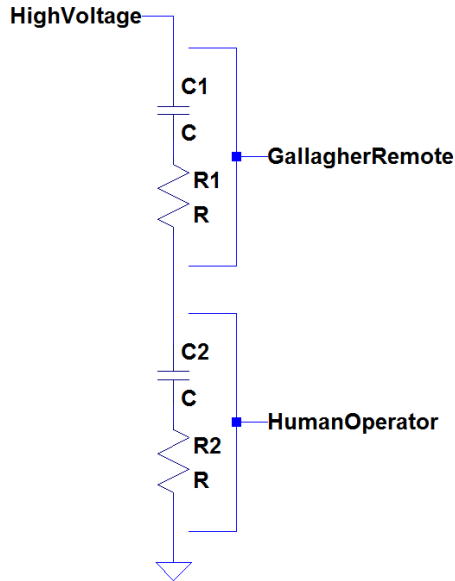
Figure 25 - Simplified Model of System with Gallagher Remote and Human Operator

The operator can be modelled by a lumped capacitance (C2) and a lumped resistance (R2). The impedance of the combination of C2 and R2 at frequency will determine the magnitude of the current which flows through R1 and therefore the signal strength.

A number of variables are combined to produce these two values and it is unlikely that this combination will be well behaved and linear. There are three main areas of interest, the interface between the capacitive back plate on the remote and the hand, the interface between the foot and the ground plane, and the effect of the conductive path through the body.

The interface between the Remote and the hand is heavily influenced by the hand grip of the operator. Without prior instruction, the operator is unlikely to grip the remote in a manner to produce a good connection. It also depends on the surface properties of the skin of the operator using the device. Skin with high moisture content will provide a better connection than skin with low moisture content.

It is unlikely that the operator will be using the device without footwear. Increasing the distance between the skin and the ground is likely to increase the impedance presented by that interface. However the contact will be more consistent than the

interface at the hand due to the fact that a person's stance varies a lot less between individuals compared to an individual's hand grip.

Characterising the conductive path from the operator's hand to their foot is impossible to solve analytically but a general model can be derived from measurements and numerical analysis.

6.1. Impedance of the Receive Path in the Gallagher Remote

The Remote has a single electrical path from the fence connection at the top of the remote to the ground plane. The impedance of this path (Figure 26) can change between hardware revisions but gives a good reference point for considering the performance of the current generation of hardware.
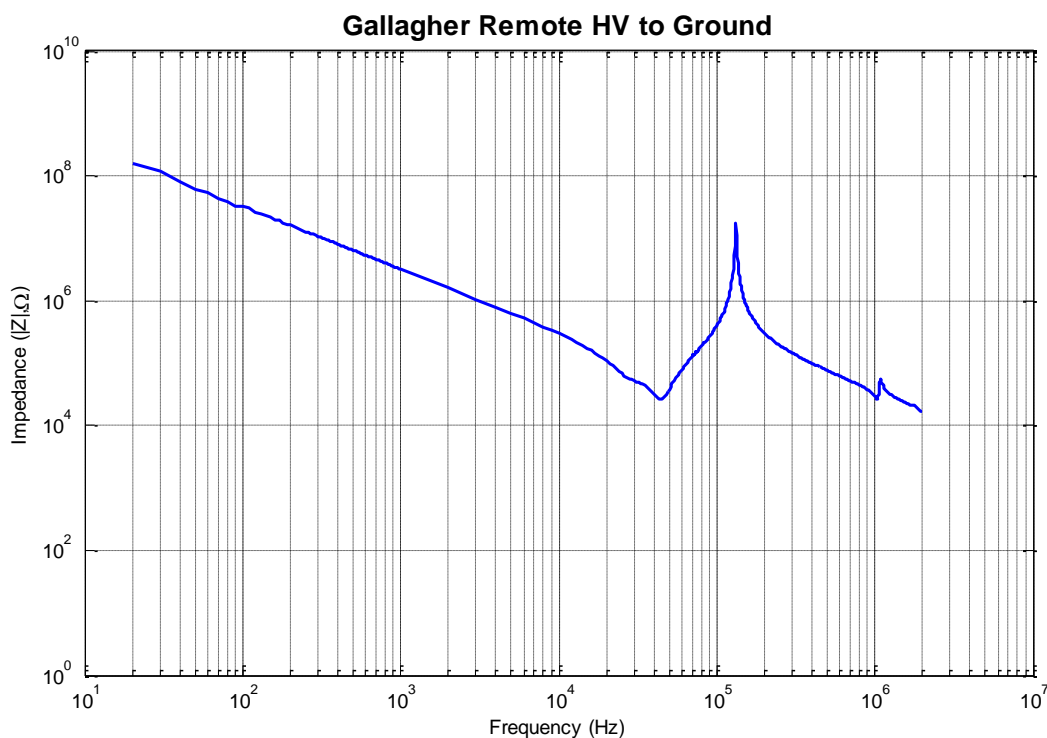
Figure 26 - Magnitude Impedance vs. Frequency for the signal path in the Gallagher Remote. A trough is observed at approximately 40 kHz which is due to the resonant filter network

Up to approximately 100 kHz, the remote works as intended. A high pass filter is present coupled with a resonant filter at 40 kHz. Above this, another resonant peak drives the impedance high, effectively filtering any signals up to 100 kHz. At high

frequencies, the impedance decreases to a level similar to that in the pass-band which increases the sensitivity of the circuit to noise.

6.2. Impedance of the Conduction Path from Hand to Foot

The Gallagher Remote is designed to be held in the hand so the measurement was taken from the palm of the right hand to the sole of the right foot. The black plastic insulating cover was removed from the Remote, exposing the conductive plate (Figure 27). This plate was used to provide a contact with the palm.

Figure 27 - Gallagher iSeries Remote with insulating sticker removed from battery cover

The measurements for this area of the research are primarily focused on the frequencies up to 10 MHz, with frequencies above this included to verify that the measurements are valid and that no important features in the response have been missed. Models are tuned to achieve best fit. Poor fitting models are tuned to fit well at 10 kHz due to its proximity to the current fence communication channel at 40 kHz.

A drop in impedance is measured at approximately 100 MHz in all configurations (Figure 28). This is an artefact of the measurement setup and measurements at such a high frequency are ignored when fitting models.
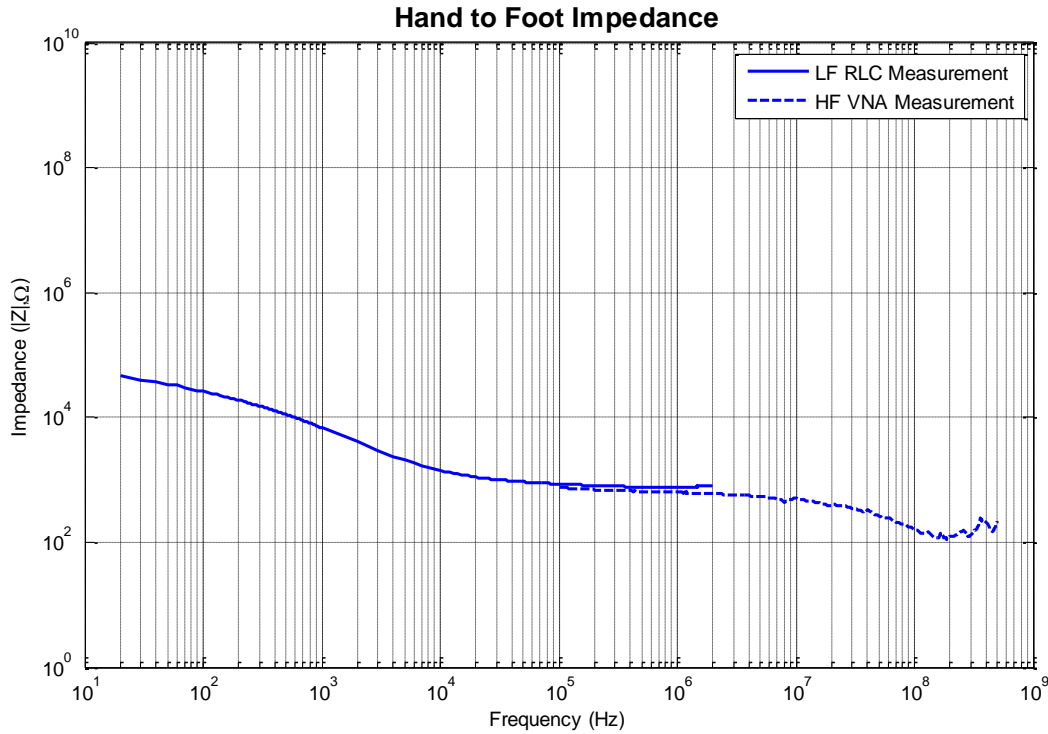
Figure 28 - Graph showing Magnitude Impedance vs. Frequency for the Hand to Foot conductive path

The low frequency measurements closely align with the high frequency measurements, confirming a good calibration on both instruments. A smooth trend is exhibited until 10 MHz, after which the measurement deteriorates.

Attempting to fit a series capacitor-resistor model does not produce satisfactory results (Figure 29 and Table 1). The model could be considered for the high frequencies above 10 kHz but is a very poor match for the low frequencies.
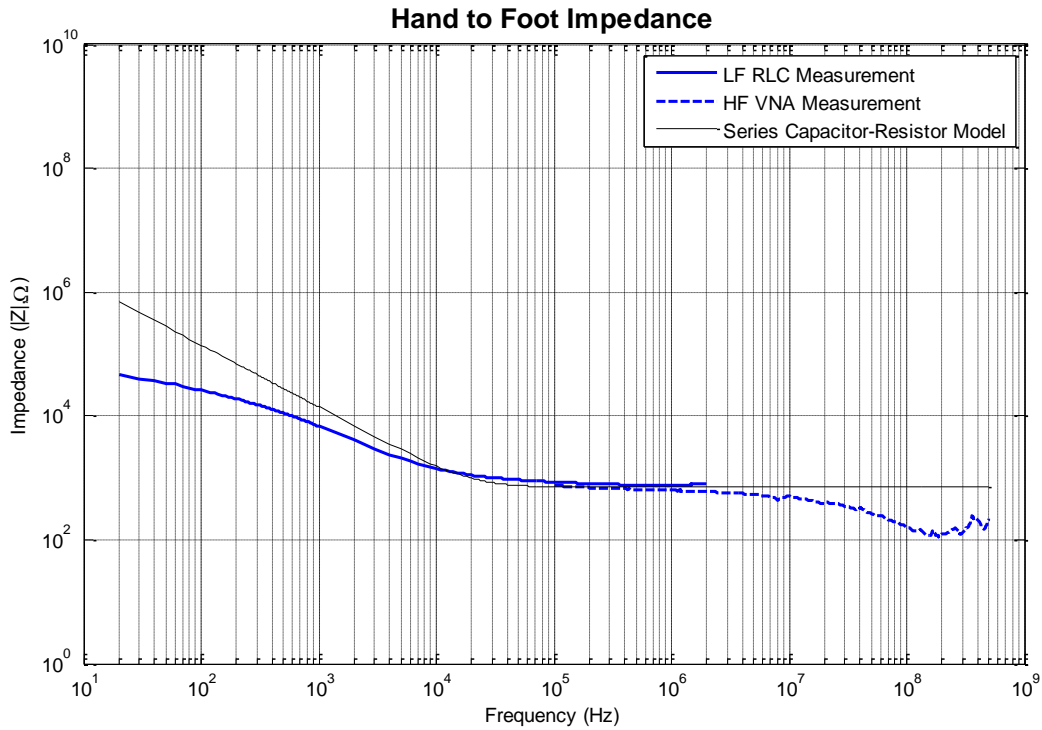
Figure 29 - Graph showing Magnitude Impedance vs. Frequency for the Hand to Foot conductive path. Fitted curve for a series capacitor-resistor model. This model fits poorly at low frequency

Table 1 - Fitted Model Parameters for series capacitor-resistor model of Hand to Foot impedance

Model	Capacitance	Resistance
Hand to Foot	11.4 nF	700 Ω

The human body is a complex biological system and it is not feasible to model analytically. An alternate high level model is the fractional capacitor [14]. When modelling biological tissue, the impedance scales according to Equation 1.

$$Z(s) = \frac{1}{s^\alpha C}$$

Equation 1 – Impedance of a capacitor with modification for fractional capacitance

For a standard capacitor, α is an integer of value one which simplifies the formula to the standard model. For a capacitor which includes biological tissue, α is no longer an integer of value 1 but instead a non-integer value between 0 and 1 non-inclusive.

Based on the idea of the fractional capacitor, Cole et al. proposed the Cole-Cole model which can be used to fit many biological tissues [15].

$$Z(s) = R_\infty + \frac{R_0 - R_\infty}{1 + (\tau s)^\alpha}$$

Equation 2 – Cole-Cole model for the impedance of biological tissue

The Cole-Cole model is a significant improvement over the series capacitor-resistor model. The trend closely matches the data for both low and high frequency measurements (Figure 30 and Table 2).
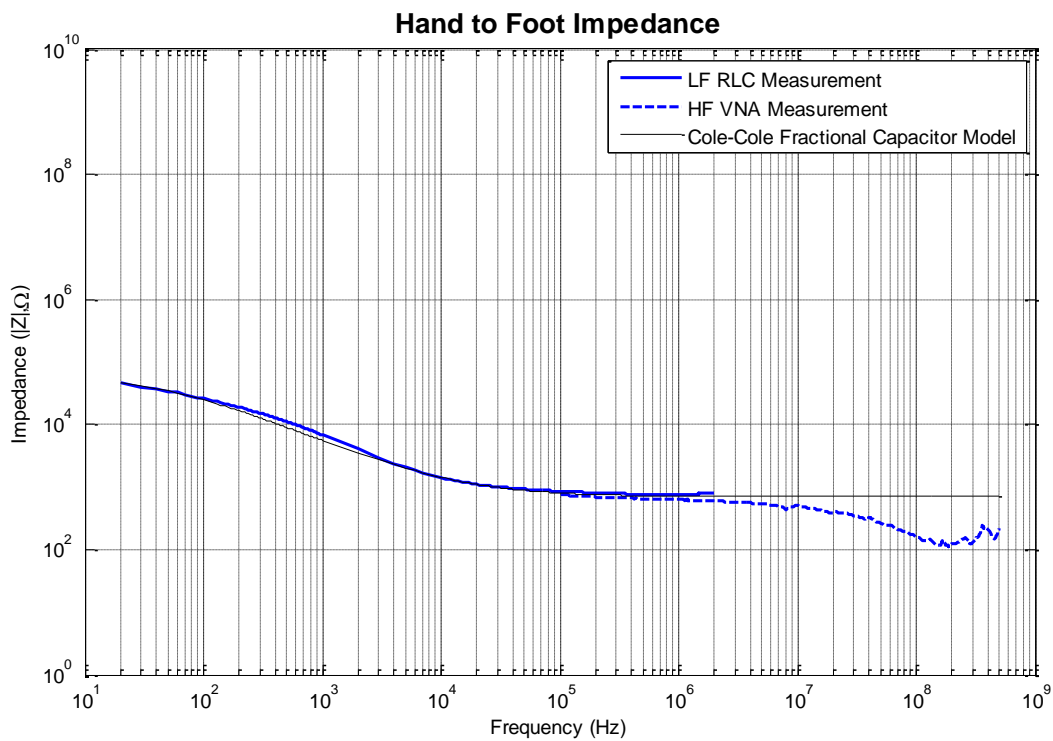
Figure 30 – Graph showing Magnitude Impedance vs. Frequency for the Hand to Foot conductive path. Fitted curve for a Cole-Cole model. This model fits well across the entire frequency range

Table 2 – Fitted parameters for Cole-Cole model of Hand to Foot impedance

Model	τ	α	R_∞	R_0
Hand to Foot	0.02	0.85	700 Ω	68 kΩ

6.3. Effect of the Capacitive Back Plate on the Impedance

The Remote utilises a capacitive back plate to connect the internal circuitry to the operator as part of the ground connection. A capacitor is formed by insulating the conductive plate on the remote battery cover. The measurement was taken between the internal back plate connection and the conductive ground plate at the operator's foot. This includes the capacitive back plate and the human body in the measurement. The plate is approximately large enough to form a capacitor with three fingers but due to a high variability, the palm grip from the Hand to Foot measurement was used again.
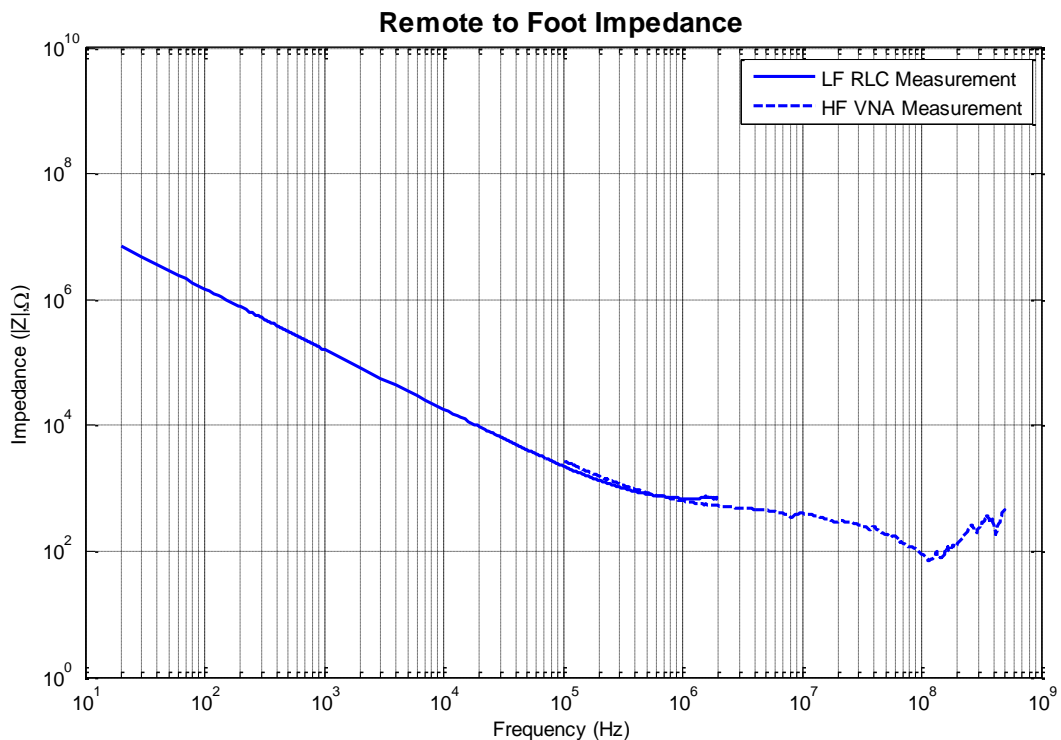
Figure 31- Graph showing Magnitude Impedance vs. Frequency for the Remote to Foot conductive path

Again the low and high frequency measurements closely align, indicating a good calibration between the two instruments (Figure 31).

Attempting to fit a capacitor-resistor model produces reasonable results; however the gradient of the slope is not accurate over the linear region (Figure 32 and Table 3).
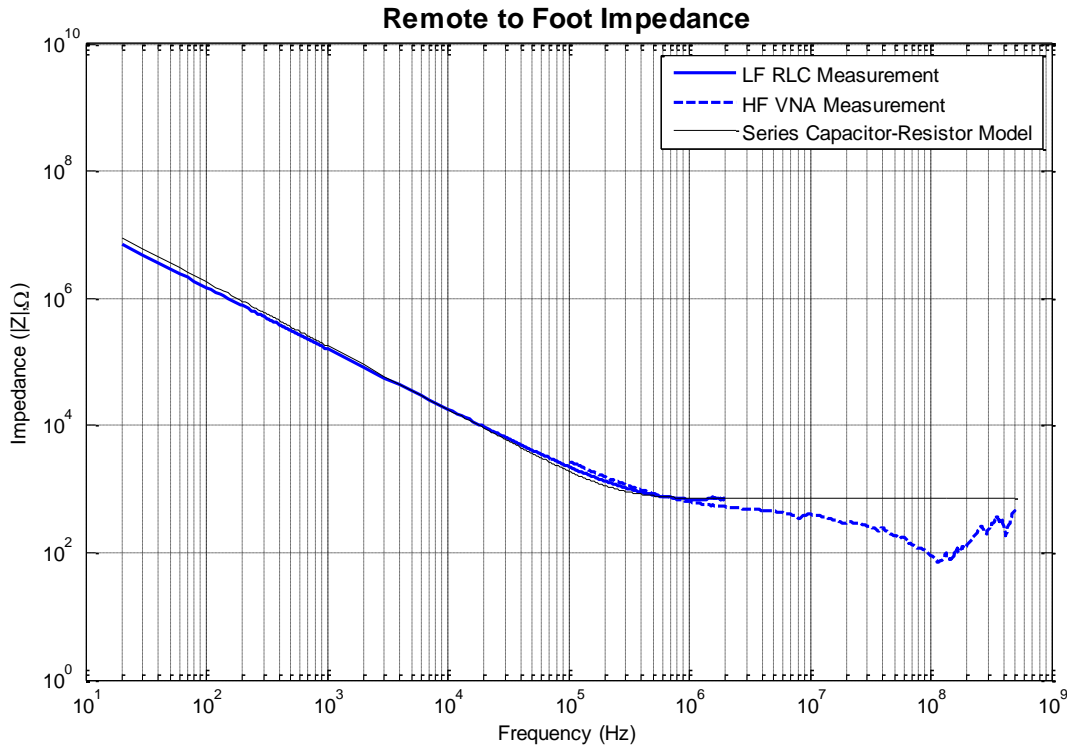
Figure 32 – Graph showing Magnitude Impedance vs. Frequency for the Remote to Foot conductive path. Fitted graph for a series capacitor-resistor model. This model fits the data reasonably well

Table 3 – Fitted parameters for series capacitor-resistor model of Remote to Foot impedance

Model	Capacitance	Resistance
Remote to Foot	884 pF	700 Ω

As with the Hand to Foot measurements, the body of the operator is best modelled by a fractional capacitor (Figure 33 and Table 4). By adding in series the capacitor formed between the back plate and the hand, the body capacitance no longer dominates and the series capacitor-resistor model fits the data better.

The data is fit with the same fractional capacitor-resistor combination as before (refer Equation 1). The value α is now much closer to an integer value of one than it was for previous models.
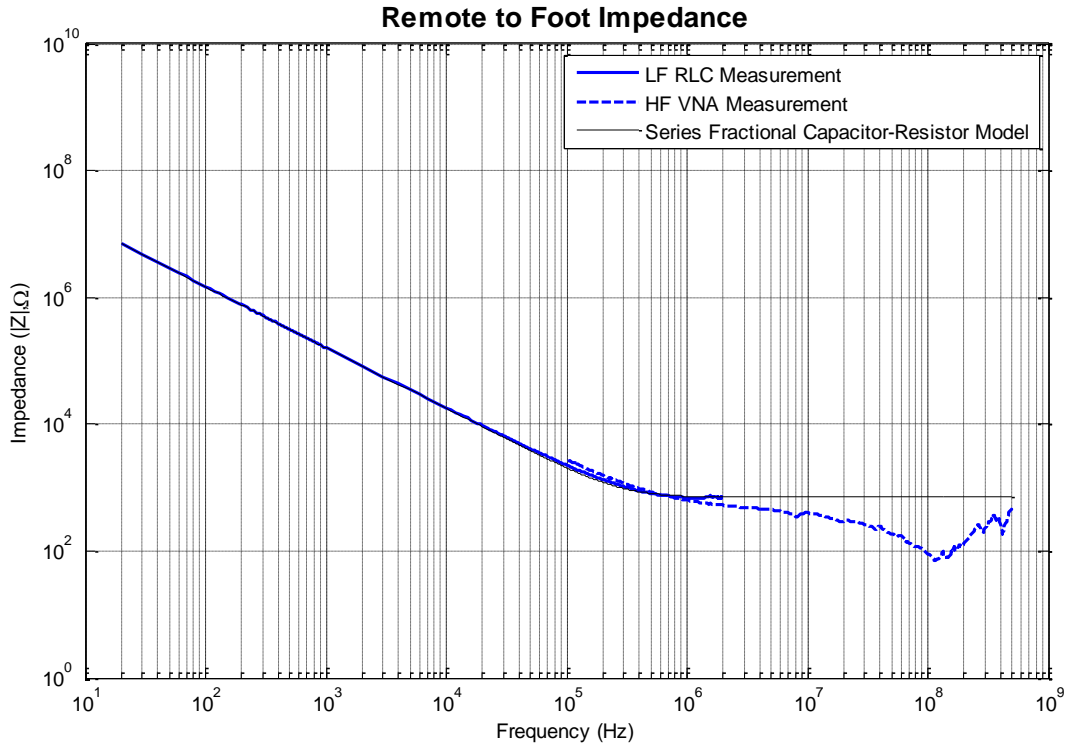
Figure 33 – Graph showing Magnitude Impedance vs. Frequency for the Remote to Foot conductive path. Fitted graph for a series fractional capacitor-resistor model. This model fits the data very well

Table 4 – Fitted parameters for fractional capacitor-resistor model of Remote to Foot Impedance

Model	Capacitance	α	Resistance
Remote to Foot	1.4 nF	0.96	700 Ω

6.4. Effect of Footwear on the Impedance

The footwear worn by the operator can vary significantly and is an important part of the grounding circuit. Footwear can vary between thin-soled shoes and thick-soled gumboots or work boots. The bare capacitive plate was used to interface between the equipment and the operator's hand.

For this test, the operator wore normal shoes with a thin sole when standing on the conductive plate. The measurement was taken between the hand and the capacitive ground plate while wearing thin soled shoes (Figure 34).
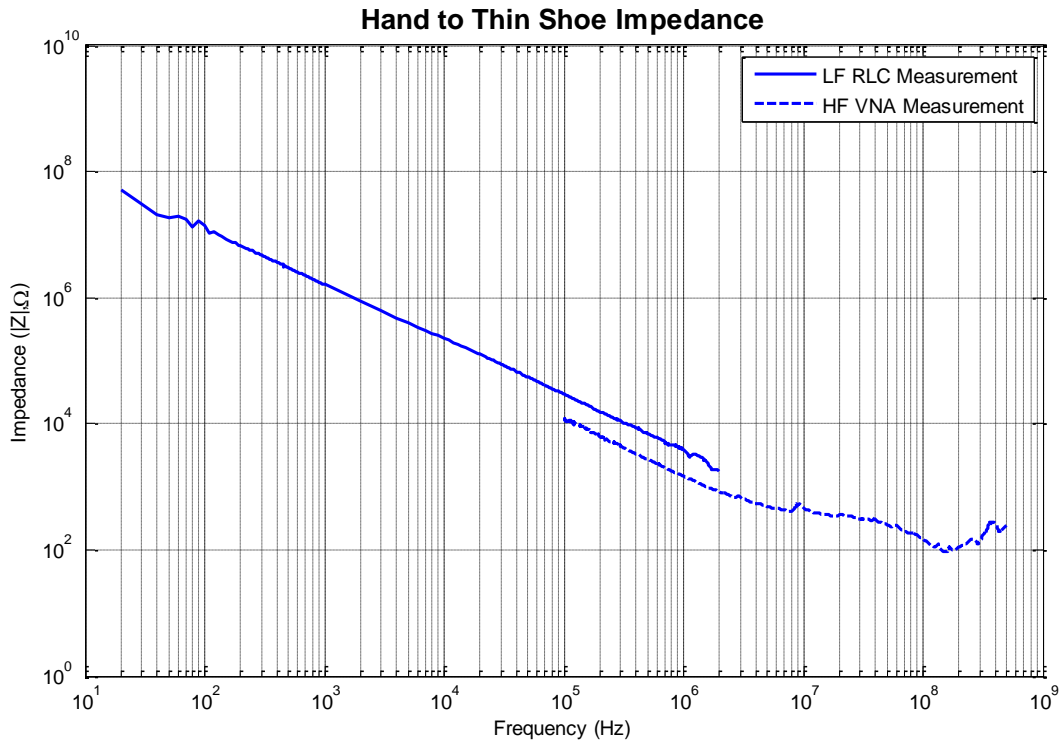
Figure 34 – Graph showing Magnitude Impedance vs. Frequency for the Hand to Thin Shoe conductive path

The high frequency measurement is not aligned as accurately as previous measurements but still confirms the same overall trend. This is repeatable and is being limited by the capacitance of the test equipment. The high frequency measurement is also limited by the sensitivity of the 4395A VNA. This instrument is designed to operate with respect to a standard 50 Ω impedance which makes it difficult to accurately measure high impedance loads such as is the case here.

The standard series capacitor-resistor model is a poor fit for this data and the fractional capacitance of the body dominates the capacitance due to the shoe (Figure 35 and Table 5).
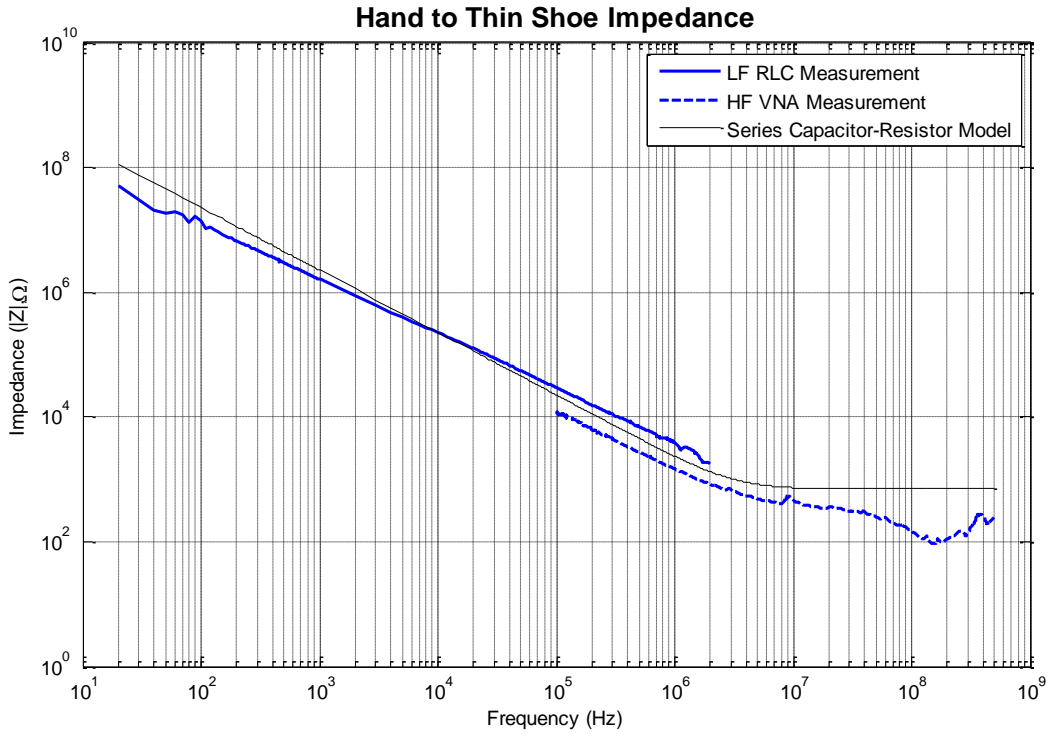
Figure 35 – Graph showing Magnitude Impedance vs. Frequency for the Hand to Thin Shoe conductive path. Fitted graph for a series capacitor-resistor model. This model does not fit the data very well, especially at the two extremes of frequency

Table 5 – Fitted parameters for series capacitor-resistor model of Hand to Thin Shoe impedance

Model	Capacitance	Resistance
Hand to Shoe Thin	70p F	700 Ω

Fitting a curve based on a fractional capacitor is a significant improvement over the standard capacitor (Figure 36 and Table 6), indicating that the fractional capacitance of the body is an important factor in this system.
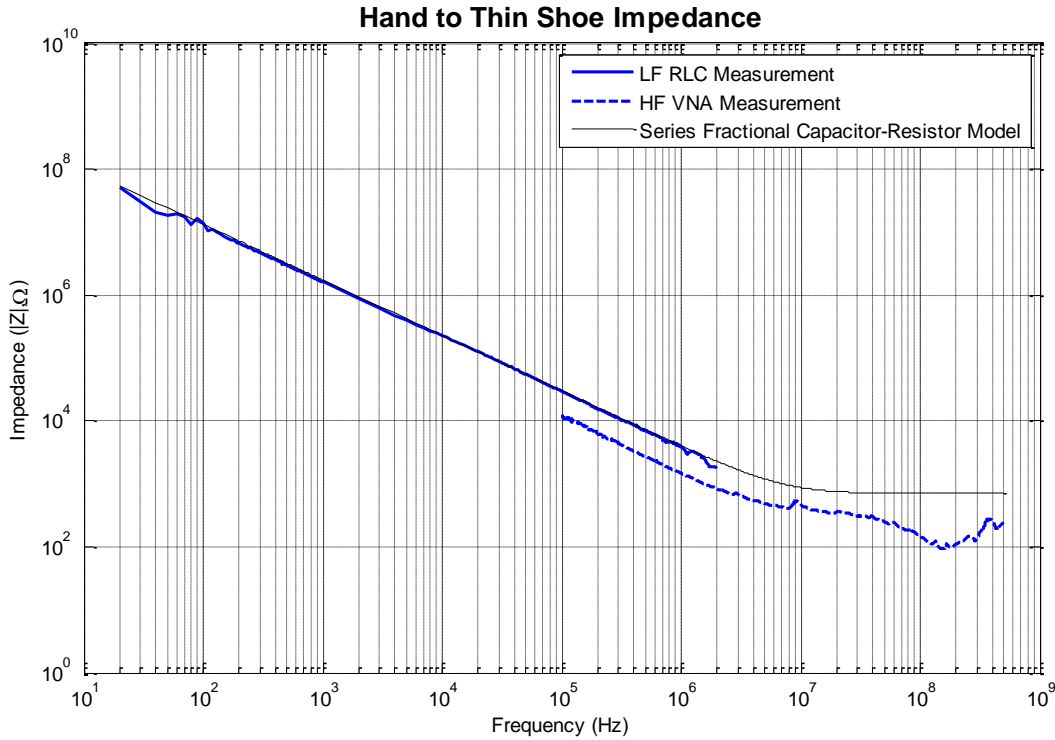
Figure 36 – Graph showing Magnitude Impedance vs. Frequency for the Hand to Thin Shoe conductive path. Fitted graph for a series fractional capacitor-resistor model. This model fits the data very well

Table 6 – Fitted parameters for fractional capacitor-resistor model of Hand to Thin Shoe Impedance

Model	Capacitance	α	Resistance
Hand to Shoe Thin	260 pF	0.88	700 Ω

6.5. Effect of both Footwear and Back Plate on the Impedance

Both the capacitive back plate and footwear are included in this measurement to simulate a real world configuration (Figure 37). The measurement was taken between the internal capacitor connection and the conductive ground plate while the operator was wearing thin soled shoes.
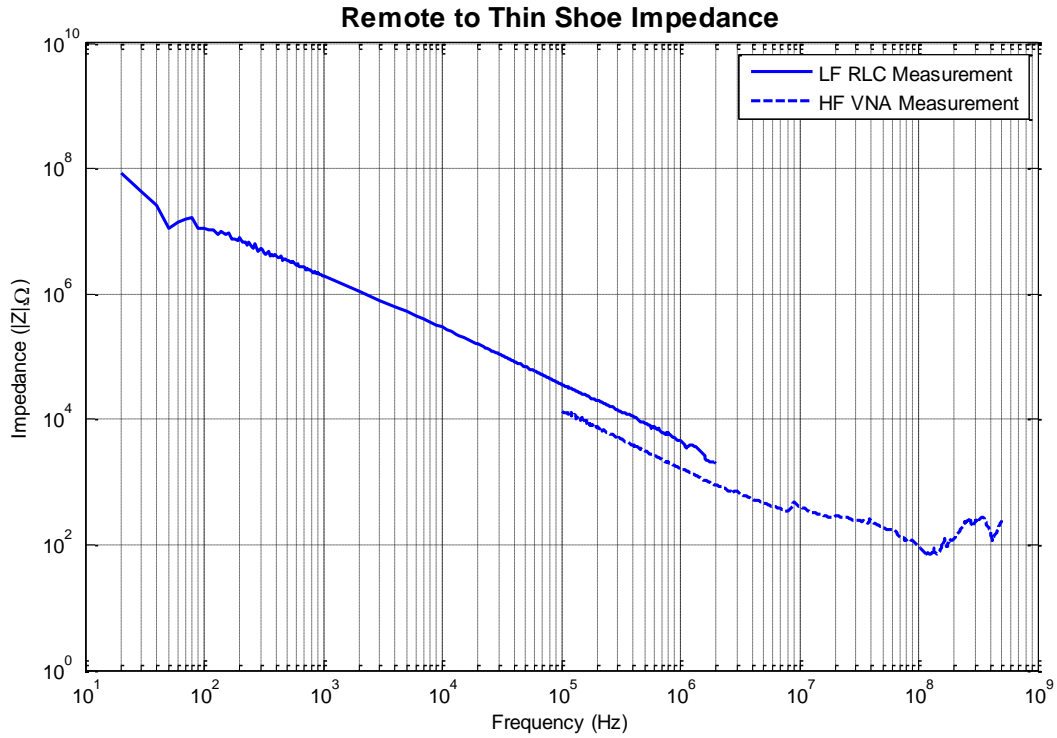
Figure 37 – Graph showing Magnitude Impedance vs. Frequency for the Remote to Thin Shoe conductive path.

The two graphs are misaligned in a similar way to the Hand to Thin Shoe measurement. The series capacitor-resistor model is a poor fit for this data with the fractional capacitive effects dominating (Figure 38 and Table 7).
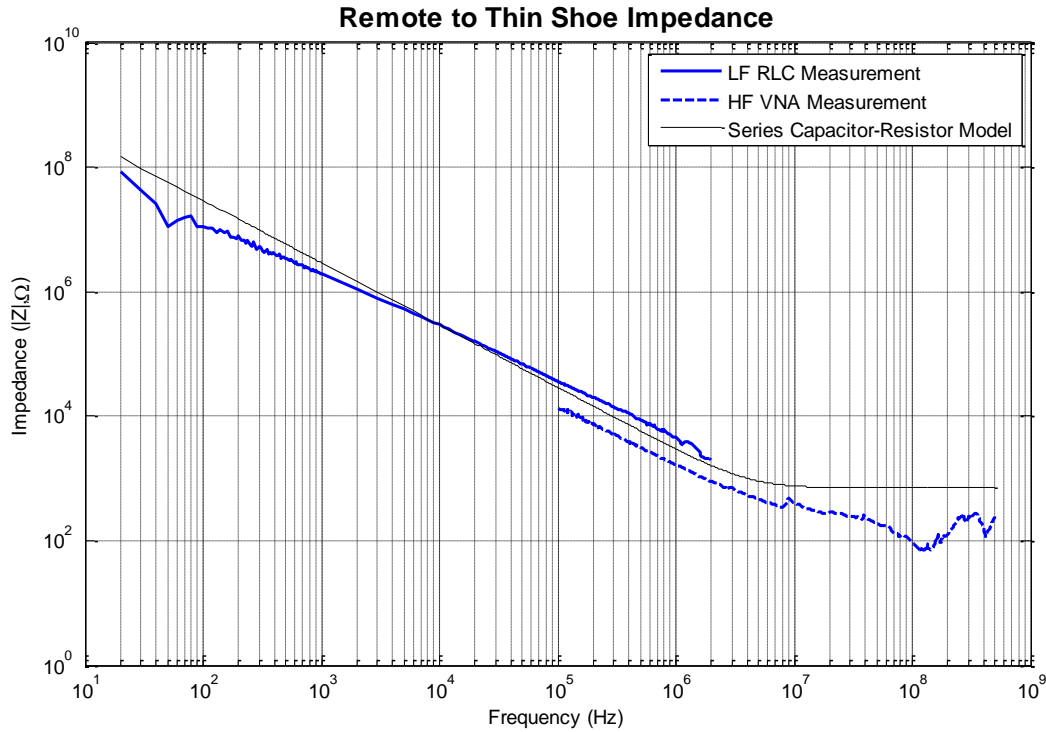
Figure 38 – Graph showing Magnitude Impedance vs. Frequency for the Remote to Thin Shoe conductive path. Fitted graph for a series capacitor-resistor model. This model does not fit the data very well, particularly at the extremes of frequency

Table 7 – Fitted parameters for series capacitor-resistor model of Remote to Thin Shoe impedance

Model	Capacitance	Resistance
Remote to Shoe Thin	54.3 pF	700 Ω

Fitting a series fractional capacitor-resistor model fits the data accurately, indicating a strong fractional component (Figure 39 and Table 8).
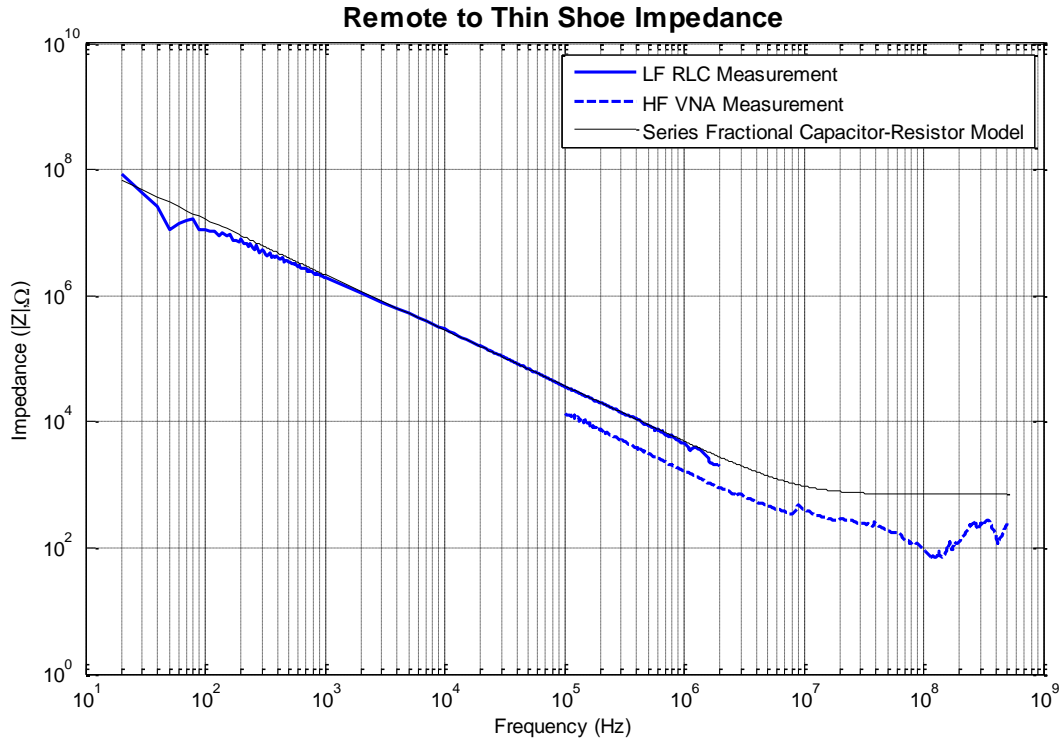
Figure 39 – Graph showing Magnitude Impedance vs. Frequency for the Remote to Shoe Thin conductive path. Fitted graph for a series fractional capacitor-resistor model. This model fits the data well

Table 8 – Fitted parameters for fractional capacitor-resistor model of Remote to Shoe Thin Impedance

	Capacitance	α	Resistance
Remote to Shoe Thin	210 pF	0.88	700 Ω

For comparison, the thin shoes were replaced with gumboots and the measurement repeated (Figure 40 and Table 9).
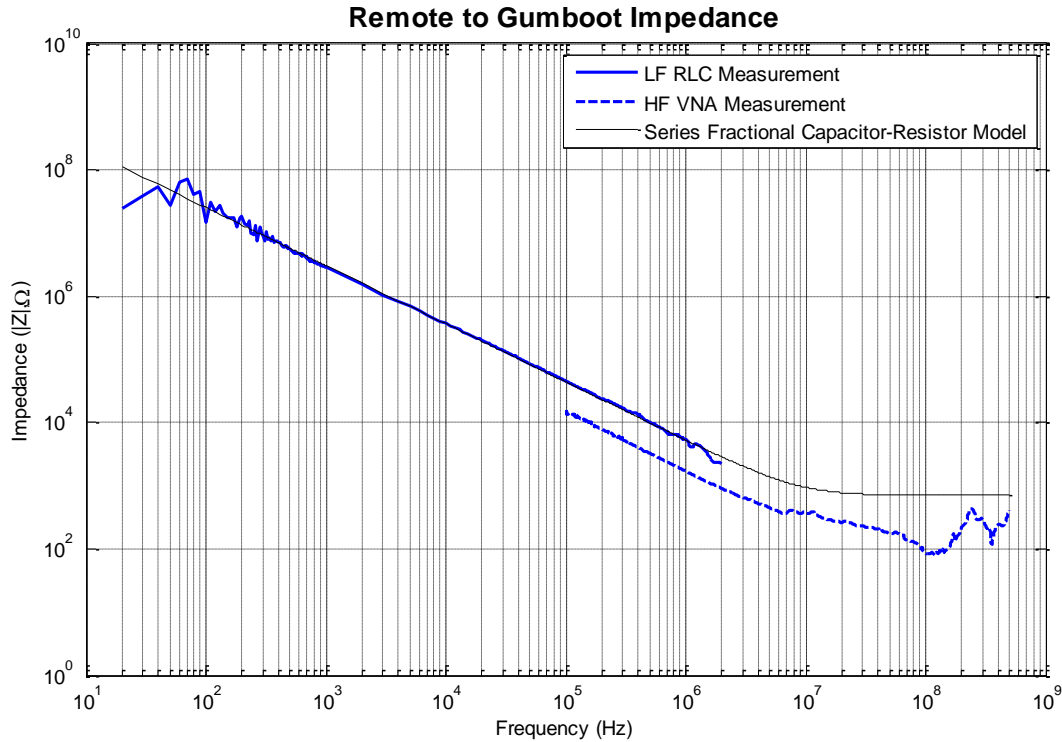
Figure 40 – Graph showing Magnitude Impedance vs. Frequency for the Remote to Gumboot conductive path.

Table 9 – Fitted parameters for fractional capacitor-resistor model of Remote to Gumboot Impedance

Model	Capacitance	α	Resistance
Gumboot to Shoe Thin	105 pF	0.92	700 Ω

6.6. Summary of Human Operator Impedance

The measurements conducted previously are summarised in Figure 41. The data series represented by continuous lines is measured at low frequency using the E4980A LCR meter. The non-continuous lines are the high frequency measurements using the 4395A Network Analyser.
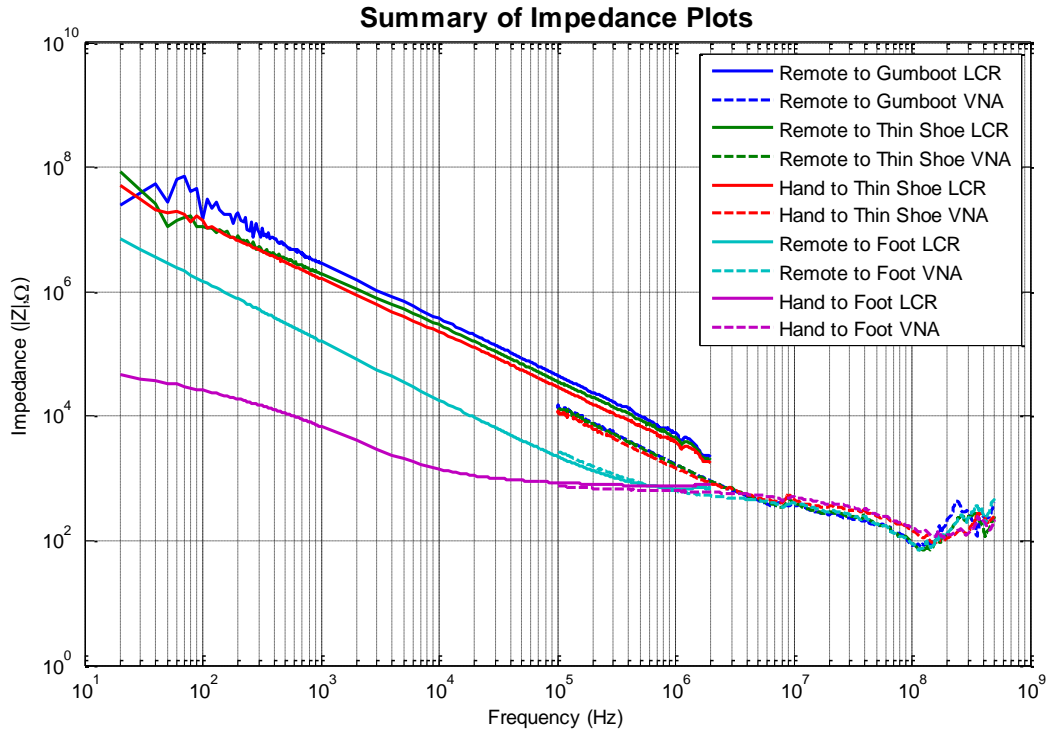
Figure 41 – Summary of the measured Impedance for all configurations

The impedance of the configurations involving footwear is an order of magnitude greater than those without. This indicates that the footwear is the dominant component in the system.
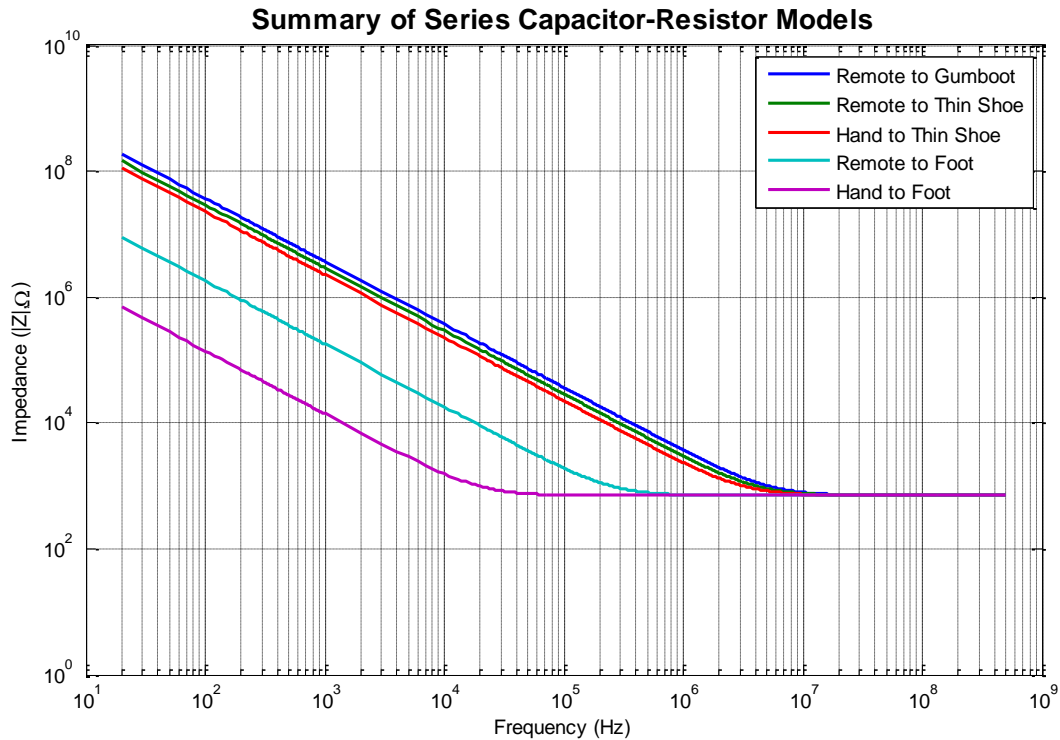
Figure 42 – Summary of Series Capacitor-Resistor models for the impedance of the system. All of the models converge to a similar impedance at high frequency which is due to the series resistance component of the model. The differences between the models is apparent at lower frequencies

The primary intent of this research is to characterise the system and develop models which can be incorporated into future design work. From this point of view, initial design work would be well served by using the standard capacitor model (Figure 42 and Table 10). After the initial design has been completed, it would be more rigorous to use the fractional capacitor model to check the details of the design (Figure 43, Table 11 and Table 12).

Summary of Series Fractional Capacitor-Resistor Models
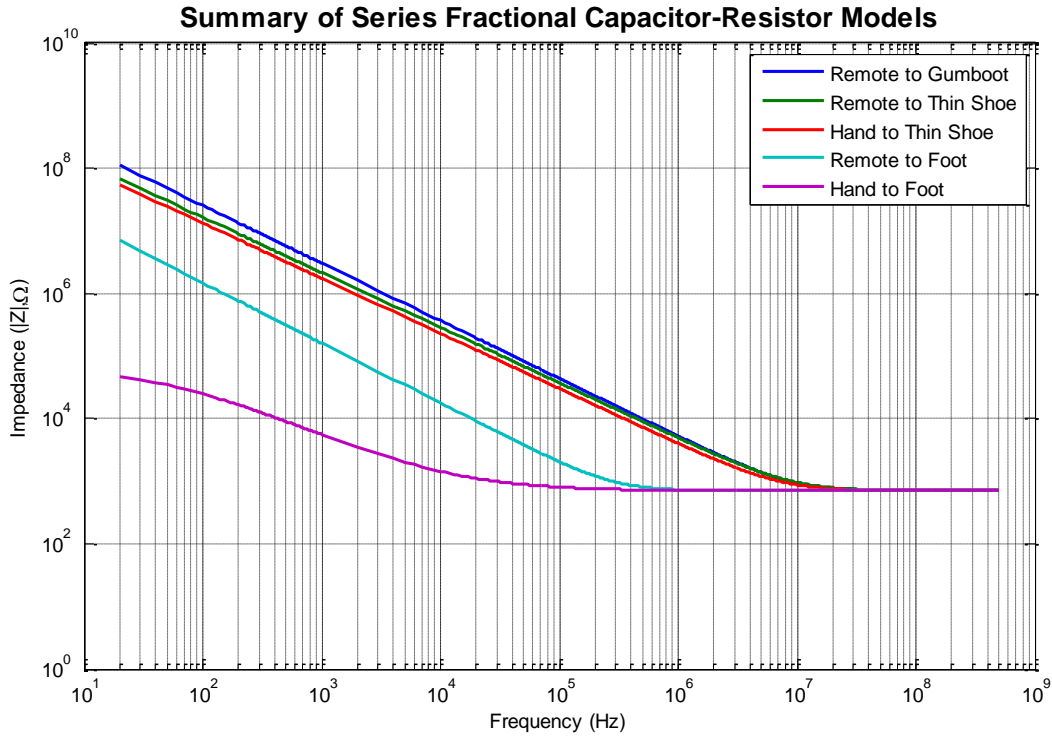
Figure 43 – Summary of Series Fractional Capacitor-Resistor models for the impedance of the system. All of the models converge to a similar impedance at high frequency which is due to the series resistance component of the model. The differences between the models is apparent at lower frequencies

For both fractional and standard models, the impedance has reached an asymptote at approximately 10 MHz. Increasing the carrier frequency further beyond this point will have no advantage with respect to the signal strength at the receiver.

Table 10 - Summary of model parameters for series capacitor-resistor model

Model	Capacitance (pF)	Resistance (Ω)
Hand to Foot	11400	700
Remote to Foot	1400	700
Hand to Thin Shoe	70	700
Remote to Thin Shoe	54	700
Remote to Gumboot	43	700

Table 11 - Summary of model parameters for Cole-Cole Fractional Capacitor model

Model	R_∞ (Ω)	R_0 (Ω)	α	τ
Hand to Foot	700	68000	0.85	0.02

Table 12 – Summary of model parameters for series fractional capacitor-resistor model

Model	Capacitance (pF)	Resistance (Ω)	α
Remote to Foot	1400	700	0.96
Hand to Thin Shoe	260	700	0.88
Remote to Thin Shoe	210	700	0.88
Remote to Gumboot	105	700	0.92

7. Measuring the Impedance of a Simulated Bad Joint

Agricultural fences are exposed to extreme cycles of weather over the course of their lifetime. Joints between fence wires are particularly vulnerable due to their ability to retain water in the joint. Corrosion is likely to occur and can form an insulating layer between the conductors. The main energizer pulse will likely arc over the insulating layer due to its high voltage but the fence communications signal is unlikely to achieve high enough voltage.

A bad joint can be modelled at its simplest level as a capacitor with series resistance (Figure 44).
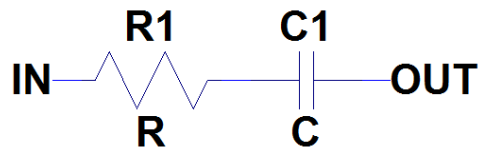
Figure 44 - Simplified model of a bad joint

7.1. Artificially Created Bad Joint

By disassembling the joint and insulating the wires with several layers of 250 µm high voltage insulation tape, a replicable bad joint could be created. By using insulation tape instead of an oxide layer, the joint is significantly less fragile and consistent results can be measured (Figure 45).
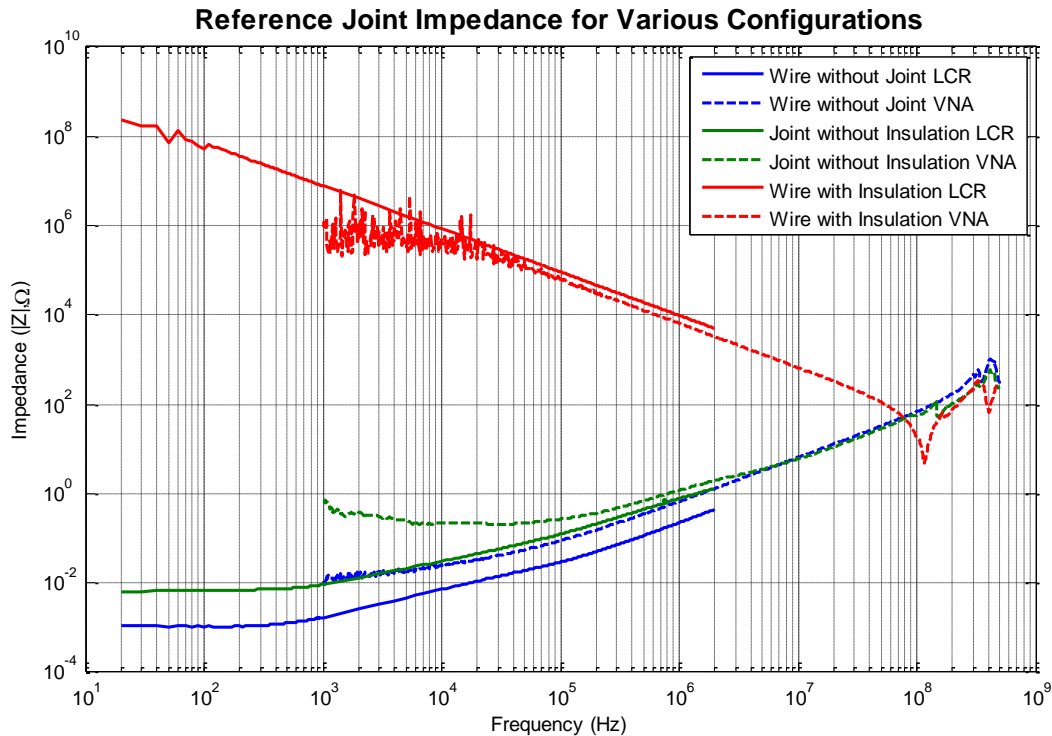
Figure 45 - Measured Impedance of various fence joint configurations. The insulating joint impedance is clearly dominated by capacitance up to a very high frequency. There is also a clear distinction between conducting joints and insulating joints

The data falls into two distinctive groups, either a clear connection (green and blue) or a clear disconnection (red). There are two conducting configurations, a conducting wire joint and a length of wire with no joint at all. The wire with no joint has an impedance value which is too low for the 4395A to measure but it still confirms the trend measured by the more sensitive E4980A LCR.

The 4395A is unable to make an accurate measurement of the impedance of the joint below 100 kHz but closely tracks the low frequency measurement made by the E4980A up to 2 MHz, confirming the overall trend.

There is also no data in the intermediate region between the conductive measurements and the insulating measurements. This indicates a rapid change occurs between a joint conducting and insulating.

The non-conducting measurement clearly shows a capacitively dominated circuit, with a linear trend on the log-log plot (Figure 46 and Table 13).
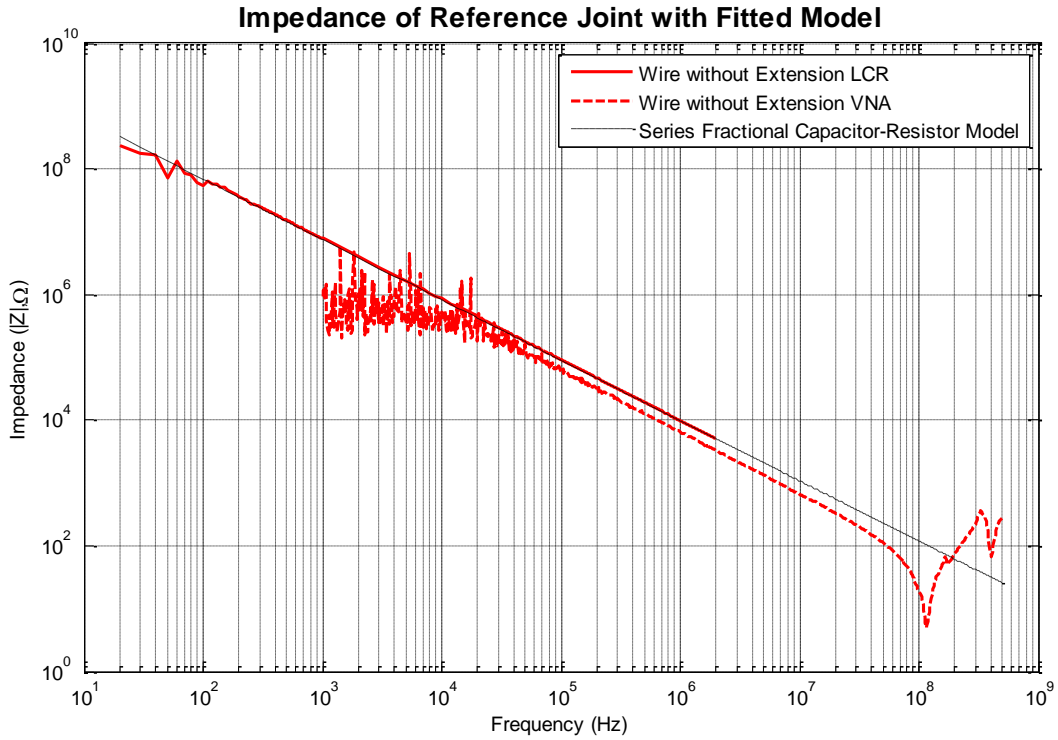
Figure 46 – Impedance of Reference Joint with a fitted Series Fractional Capacitor-Resistor Model. This model fits very well

Table 13 - Fitted parameters for fractional capacitor-resistor model of Bad Joint Impedance

Model	Capacitance (pF)	Resistance (Ω)	α
Remote to Foot	30	5.78	0.96

Above 100 MHz, the joint configurations start to form resonant circuits with the parasitic capacitors and inductors in the measurement circuits (Figure 47). This behaviour was confirmed by increasing the length of lead in wire by 1 m and observing the reduced resonant frequency.
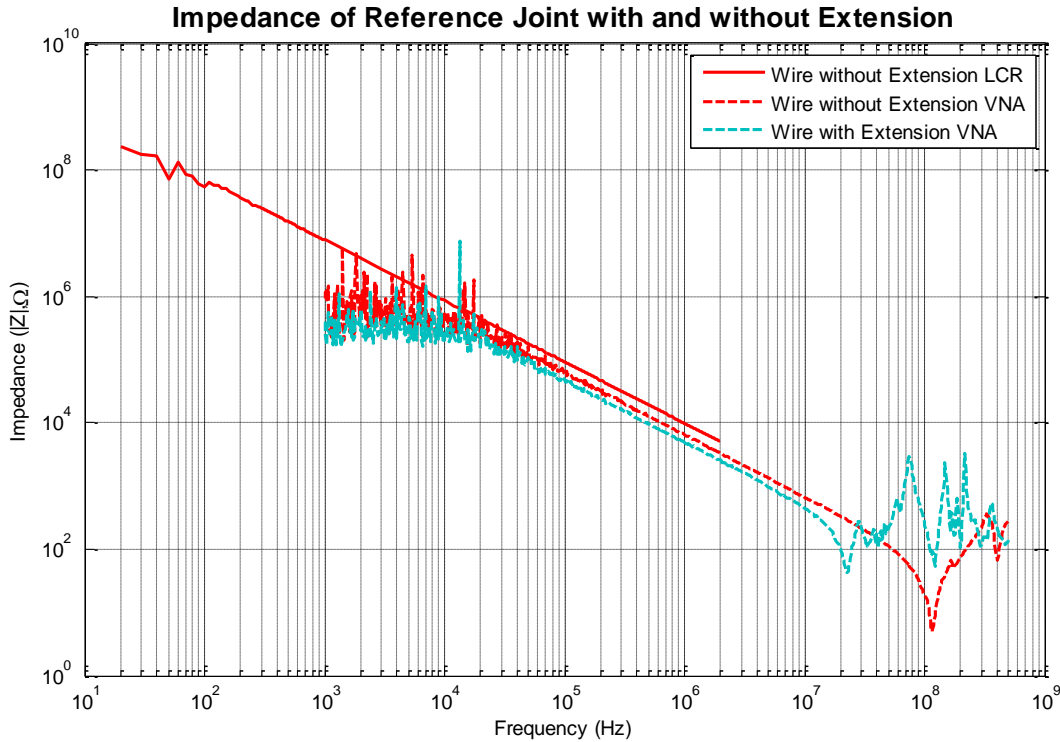
Figure 47 – Comparison between joint without lead extensions and with lead extensions. The measurement with extended leads has a resonant peak at a lower frequency than the measurement without. This indicates that the resonant peaks around 100 MHz are an artefact of the measurement

7.2. Non-linear Properties of Iron Oxide

It is a simple exercise to simulate the insulating properties of iron oxide using another form of insulator. A number of other properties of the material can also have a significant effect with respect to communications systems. It is important to verify that these other properties of the iron oxide layer which forms in a degrading joint will not have a significant impact on the frequency response of the joint. In particular asymmetrical semi-conducting effects such as occurs in a diode are of concern.

Figure 48 – Corroded Joint Simulator. A steel needle is used to form one electrical connection to the junction while the electrical connection through the crocodile clip forms the other

An ideal situation was created in the lab which allowed the conducting properties of the iron oxide layer to be tested (Figure 48). The oxide layer does exhibit significant nonlinear effects when the layer is of a specific thickness (Figure 49 and Figure 50). Significant effort was required to achieve the correct thickness of oxide layer to produce this effect, so it is not expected to be a common occurrence in the field. It is not an asymmetrical junction and as such does not produce a rectifying effect on the signal without a DC bias (Figure 51).
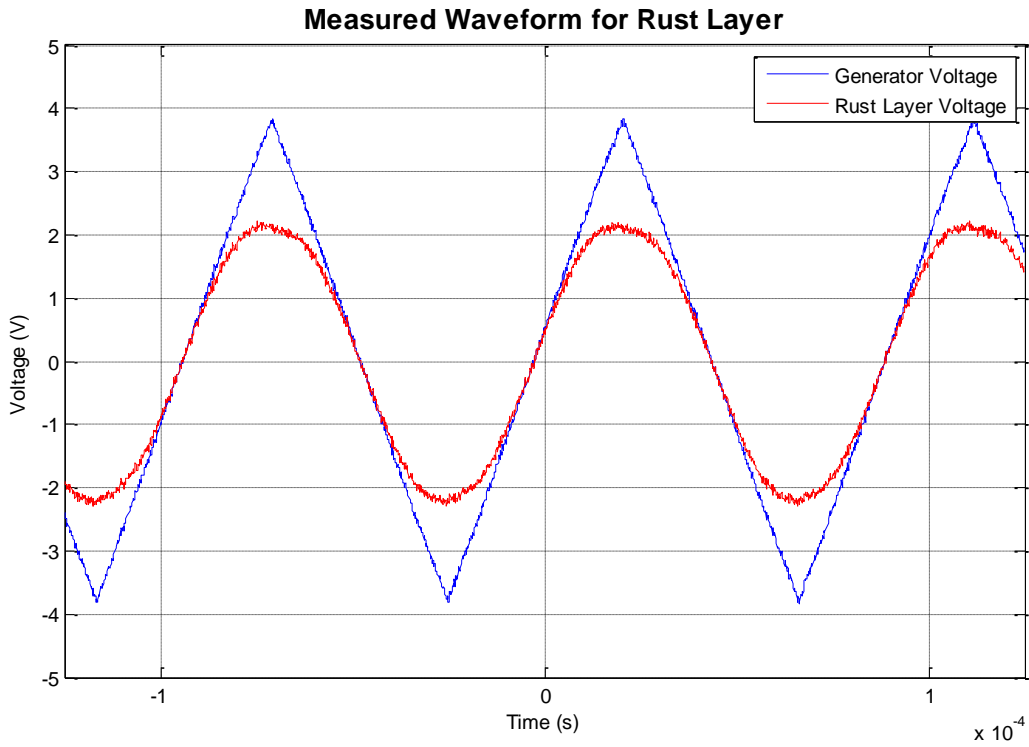
Figure 49 – Capture of voltage waveforms measured at the signal generator and across the rust layer. The non-linear conductivity of the rust results in the waveform being clipped
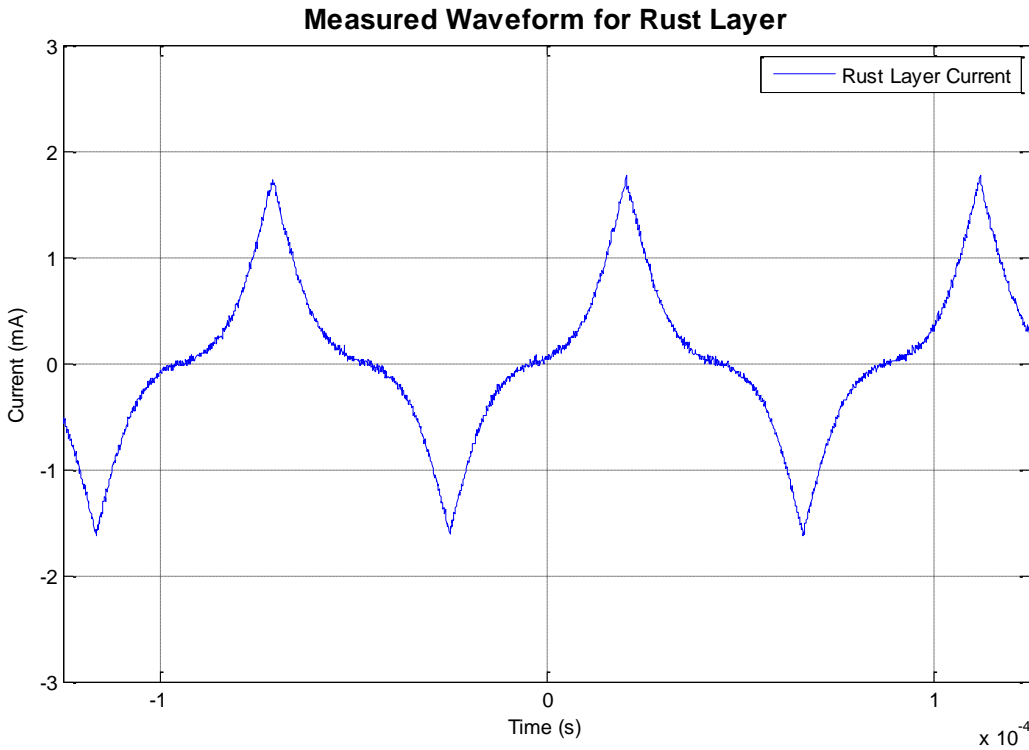
Figure 50 – Capture of current flowing through the rust layer. The current peaks when the waveform is being clipped by the rust layer component

I-V Characteristic for Rust Layer
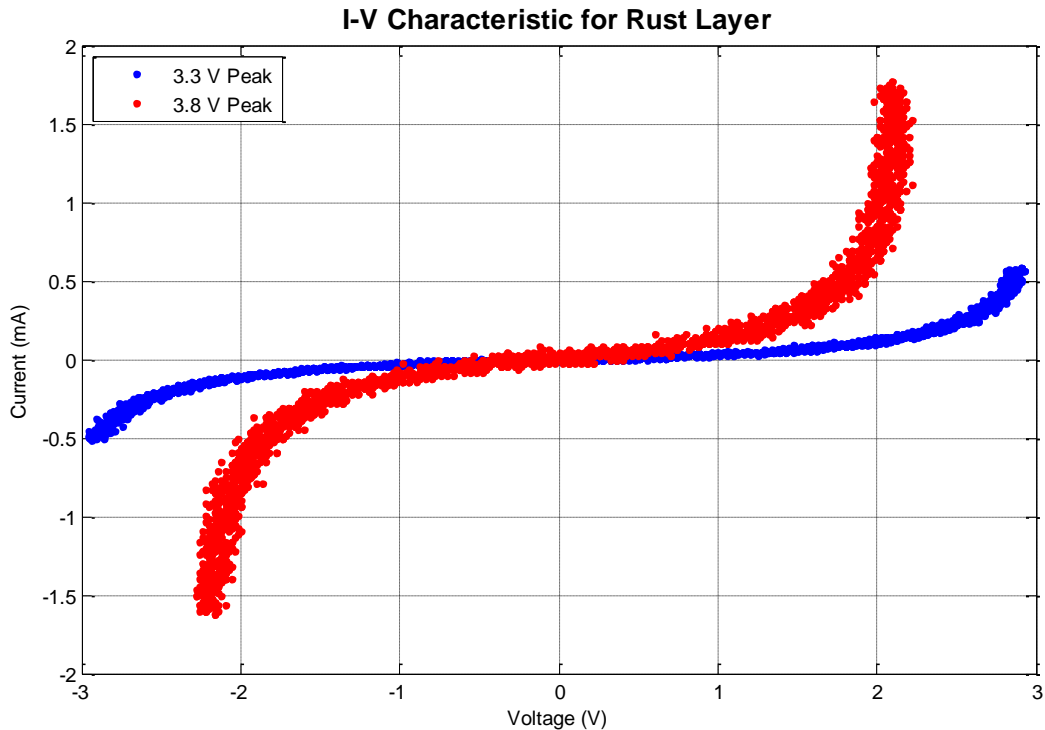
Figure 51 – Measured I-V Characteristic of Rust layer for varying signal amplitudes. As the voltage at the signal generator is increased, the I-V characteristic begins to collapse towards a short circuit.

As the signal amplitude applied to the circuit is increased, the conducted current increases and the voltage drop decreases. Increasing the voltage further causes the layer to fail, producing a short circuit.

Non-linear devices introduce spurious harmonics into the transmission as a result of intermodulation distortion. However, the conditions required to produce this effect are non-trivial and require that the joint have a very precise layer of rust. The fence is also subject to repeated high voltage pulses which will destroy the delicate rust layer. It also requires that the signal amplitude be within a very narrow window. The Gallagher iSeries Remote is capable of signal amplitudes in excess of 100V at light loads which will cause the junction to fail.

There is a remote possibility that with current designs, a remote may be able to turn an energizer off but not be able to turn it back on. If the signal amplitude was in the correct range, and the bad joint had sufficient time to recover a layer of iron oxide, then the signal would not be received be the energizer.

Based on this, the chance of a corroded fence joint displaying non-linear characteristics and producing distortion is very small and can be safely ignored when considering the overall communications system.

Section 2

Evaluating Methods for Data Transmission

8. Literature Review

8.1. Overview of Gallagher Protocol

The Xport Protocol is designed for bi-directional communications between the iSeries energizer and the fence monitors and remotes. The protocol is also designed to be backwards compatible to a limited extent, specifically on/off functions. A single bit of data is modulated using FSK with 42.7 kHz and 38.2 kHz representing 0 and 1 respectively (Figure 52). The overall baud rate is 1190 which corresponds to a bit time of 840 μs.
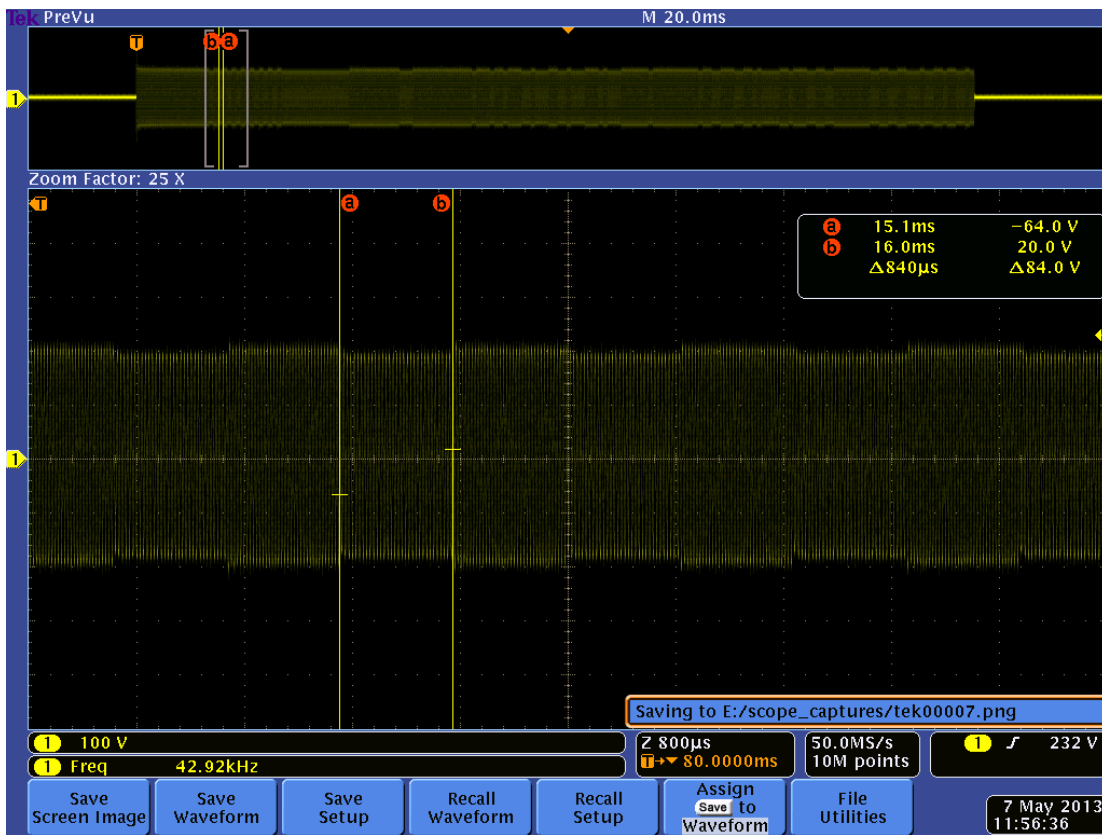
Figure 52 – Capture of a data transmission on a Gallagher Fence, with single bit highlighted between cursors. Although the two frequencies, 38.2 kHz and 42.7 kHz, cannot be resolved given the scale of the plot, the two frequencies have slightly different amplitude and can thus be distinguished in the figure. Captured using Tektronix DPO4034

Each bit occupies an 840 μs interval, with the entire packet having a length of up to a maximum of 1.74 s. The number of bits in a transmission can vary but the total transmission length for sending an ON command is 155 ms (Figure 53).

Figure 53 – Capture of a data transmission on a Gallagher fence. Figure shows an entire capture of an ON transmission, length approximately 155 ms. The various parts of the transmission can be distinguished such as the preamble and the main message

The number of bits per transmission depends on the data being sent up to a protocol limit of 2072 (Figure 54).

Preamble	Start Bit	Destination ID	Source ID	Sequence	Message Type	Length	Data	CRC
31 bits	1 bit	24 bits	24 bits	2 bits	6 bits	8 bits	Up to 1960 bits	16 bits

Figure 54 - Diagram detailing format of data used in Gallagher Xport Protocol

8.2. Overview of Tru-Test Protocol

The Fence Compass is the only device which can transmit data in a Tru-Test system as of 7th of May, 2013. This negates any timing requirements as there are no other devices for the messages to collide with. A single bit is comprised of a short burst of FSK modulated data followed by a delay (Figure 55).
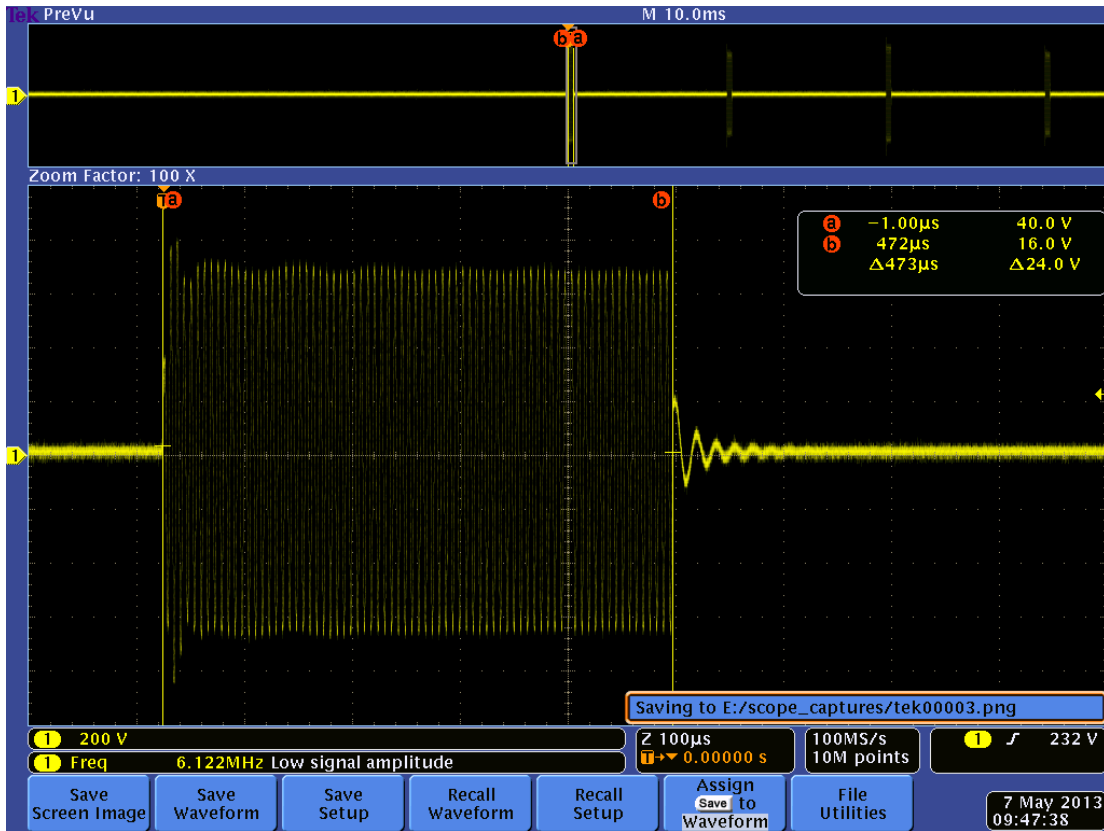
Figure 55 – Capture of a single high frequency burst on a TruTest Fence. The length of the pulse is approximately 473 μs as indicated by the cursors
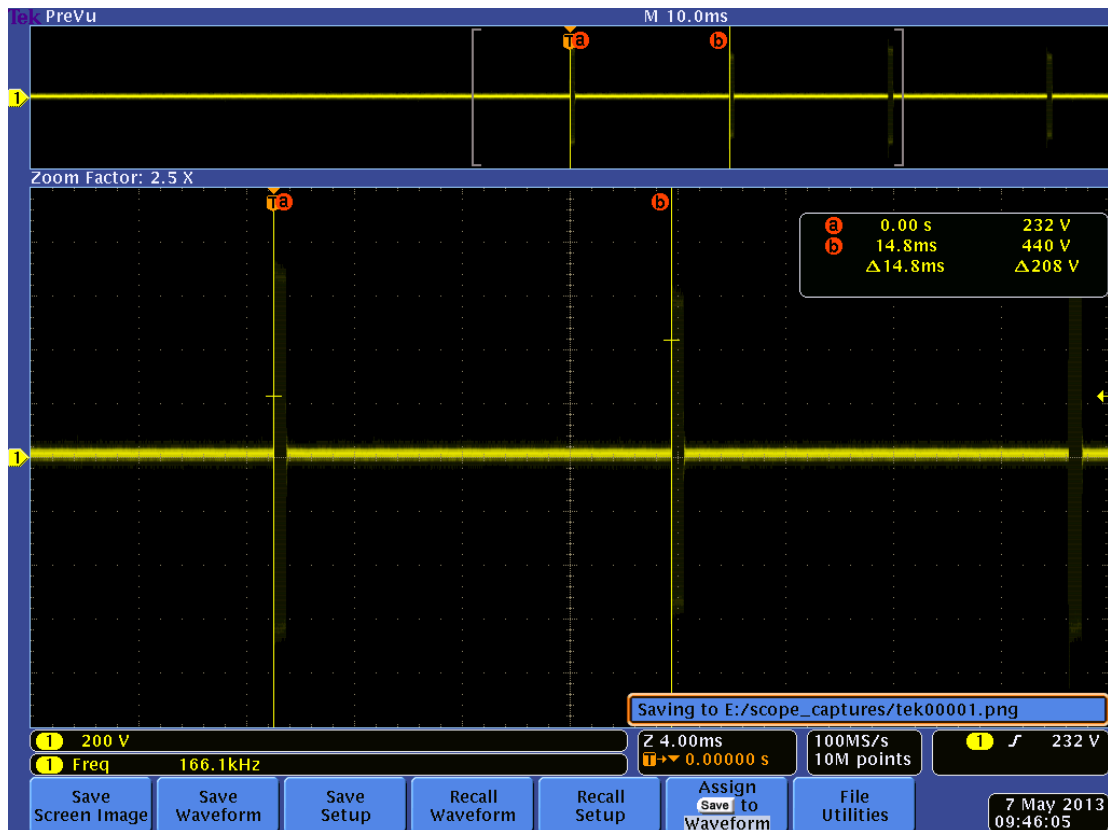
Figure 56 – Capture of a series of high frequency bursts on a TruTest fence. The interval between bursts is approximately 14.3 ms. This equates to a baud rate of 68 when the length of the burst is added

The frequency of the burst encodes the value of the bit, 148.7 kHz for 0 and 158.7 kHz for 1. The burst is transmitted for approximately 470 μs followed by a delay of approximately 14.3 ms (Figure 56). From the beginning of the first bit to the end of the last bit is approximately 400 ms (Figure 57). There are only two commands (ON and OFF) so the length of the transmission never varies.
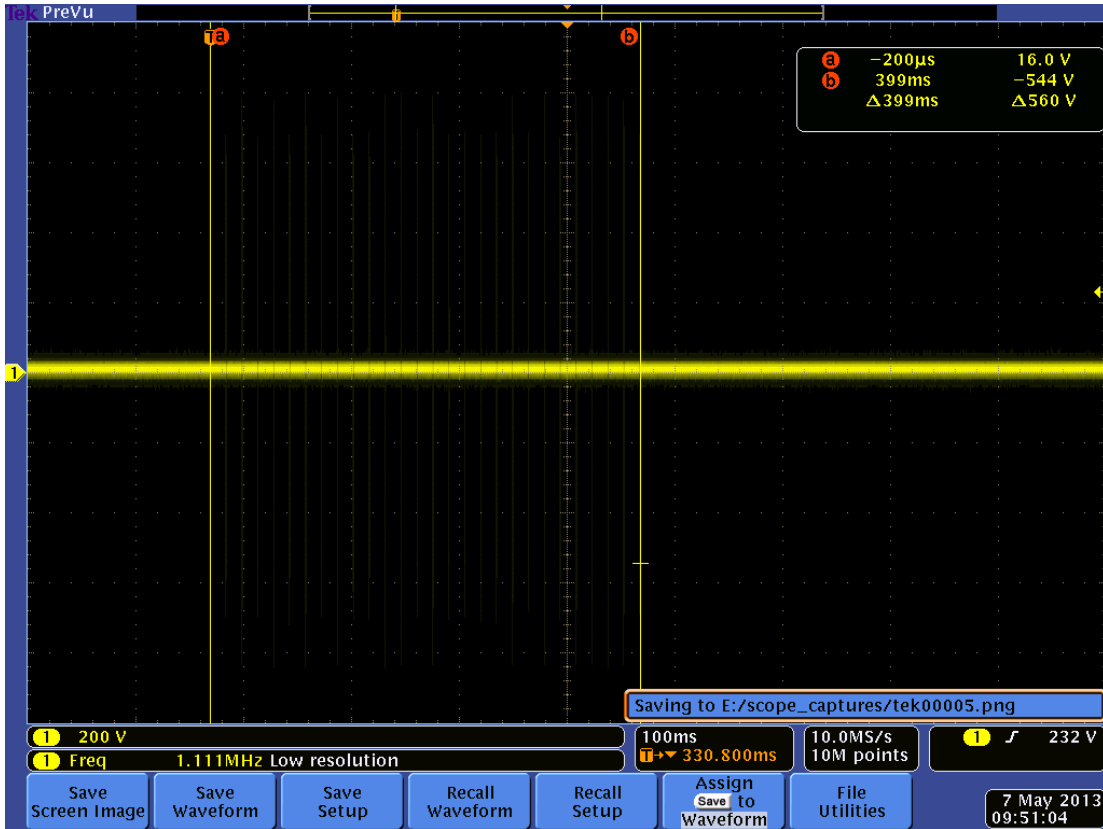
Figure 57 - Capture of full transmission on a TruTest fence. It is very difficult to resolve the individual bursts at this scale due to the very short length of a burst

A total of 28 bits are sent per transmission, comprising of 10 preamble bits, 2 start bits, and 16 message bits (Figure 58).

Preamble										Start Bits		Address				Checksum				Inverted Address				Inverted Checksum			
1	0	1	0	1	0	1	0	1	0	0	1	X	X	X	X	0	0	0	X	X	X	X	X	1	1	1	X

Figure 58 - Diagram detailing format of transmitted bits for an OFF message using the TruTest Protocol. Note that the inverted checksum follows the non-inverted checksum

The address is a number programmed into both the energizer and the remote and can be any value from 1 to 15. The checksum is calculated based on the number of 1s in the address, for even numbers the checksum is 1, for odd numbers the checksum is 0. For an off message, the order of the non-inverted and inverted checksum bytes are swapped (Figure 59 and Figure 60).

Preamble								Start Bits		Address				Inverted Checksum				Inverted Address				Checksum			
1	0	1	0	1	0	1	0	0	1	X	X	X	X	1	1	1	X	X	X	X	X	0	0	0	X

Figure 59 - Diagram detailing format of transmitted bits for an ON message using the TruTest Protocol. Note that the non-inverted checksum follows the inverted checksum

Address 3			
Off Command		On Command	
Bit	Binary Value	Bit	Binary Value
1	1	1	1
2	0	2	0
3	1	3	1
4	0	4	0
5	1	5	1
6	0	6	0
7	1	7	1
8	0	8	0
9	1	9	1
10	0	10	0
11	0	11	0
12	1	12	1
13	1	13	1
14	1	14	1
15	0	15	0
16	0	16	0
17	0	17	1
18	0	18	1
19	0	19	1
20	1	20	0
21	0	21	0
22	0	22	0
23	1	23	1
24	1	24	1
25	1	25	0
26	1	26	0
27	1	27	0
28	0	28	1

Figure 60 - Diagram detailing example ON/OFF Transmission signalling an energizer at address 3. Note that only bits 17 to 20 and 25 to 28 change between commands. Note also that the least significant bit of the address is transmitted first.

8.3. Relevant Patents

In 1993 the Gallagher Group patented a technique for controlling an energizer remotely [16]. The main claim was the electronic control of an electric fence energizer along the fence via a coded signal. The coded signal is specifically mentioned to vary in the time domain.

This technology was developed further, resulting in the XR1 Remote. A new patent was granted, covering the use of a second energy storage device to produce the coded high voltage pulses [17]. Data was encoded using Pulse Position Modulation (PPM) and used to enable/disable the energizer from the remote.

In 2000 the Tru-Test Group patented a technique for transmitting analog voltage measurements down a fence line [18], using single high voltage pulses. The integrator voltage rises at a constant rate and is reduced by a fixed amount at each received pulse (Figure 61). Data is then decoded by sampling at the correct time.
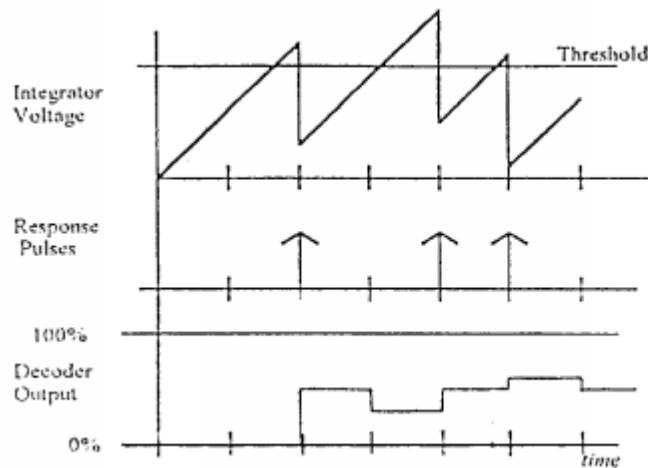
Figure 61 - Figure demonstrating data decoding [18]

As part of the development of the Fence Compass, Tru-Test developed a FSK based system to transmit messages down the fence to the energizer [19]. This system was designed with enabling/disabling the energizer in mind and as such has a low bit rate. The patent specifically mentions producing a signal with short high frequency bursts to encode the data. The frequency range mentioned lies primarily between 50 kHz and 190 kHz. The length of the burst is specified to be between 100 µs and 1000 µs

which matches the current generation Fence Compass. The target voltages mentioned vary from a fraction of a volt to several thousand which also matches the current generation.

A third patent was issued to Tru-Test in 2005, relating to fence communications utilising Phase Shift Keying (PSK) [20]. This patent details the design of a system to communicate between a base station and either remotes or other devices connected to the fence. The microcontroller modulates the data by changing the phase of the carrier by 90°. The receiver passes the signal through two mixer stages, one with a cosine, the other with a sine. The two outputs are then compared to determine the phase of the signal.

8.4. Relevant Standards

8.4.1. CISPR 14-1 Ed. 5.0 (Bilingual 2005) Electromagnetic compatibility – Requirements for household appliances, electric tools and similar apparatus – Part 1: Emission

This standard covers the frequency range from 9 kHz to 400 GHz. A number of exclusions are specified but electric fence energizers are still included. There are a number of points in this standard which are particularly relevant to fence communications.

Section Four specifies the following: *Radio disturbance measurements below 148.5 kHz and above 300 MHz need not be carried out, unless otherwise specified in this standard for specific appliances*. This allows the current generation of Gallagher communications products to operate at 40 kHz without violating this standard. Because this standard does not apply to battery operated devices, the TruTest system can be implemented as a one-way system but not as a two way communications protocol as it operates at 150 kHz.

Section 4 also specifies a maximum output voltage at the output terminals of the device. A quasi-peak measurement of 74 dB(µV) is specified from 500 kHz to 30 MHz. An average measurement of 64 dB(µV).

Section 5 covers testing methods and specifies that the frequency measurements be conducted with a voltage probe of at least 1500Ω.

9. Evaluation of Modulation Strategies and Techniques

The construction of the electric fence system makes it impossible for baseband signals to be transmitted directly. To compensate for this, the data is modulated onto a carrier wave and transmitted down the fence. This allows parts of the spectrum which are less hostile to data signals to be exploited by the communications system and the performance improved.

9.1. Common Sources of Interference in the Fence system

A suitable modulation scheme should be resistant to a number of forms of interference, some of which are unique to the fence system in particular.

- Gaussian background noise is present in all communication systems. Common sources include thermal effects due to resistance and shot noise due to the discrete nature of electricity.
- The energizer produces a high voltage electric pulse with a peak voltage of approximately 8 kV. This occurs regularly on the fence and will likely cause the receiver to saturate.
- Each fence has slightly different dimensions. This changes the frequencies at which standing waves will form and therefore attenuation due to the fence construction will not be constant across the spectrum (Chapter 5.6).
- The fence is extremely long and is capable of functioning as an antenna, coupling in outside continuous wave signals such as those from marine radios and other radio stations. These signals can also produce beat patterns which appear in unexpected parts of the spectrum (Chapter 5.6).
- For long enough fences, transmission line effects can become more important. Multipath interference occurs in the system due to reflections caused by unterminated branches, bad joints and vegetation loading.

- It is not uncommon for two fences to run parallel for long distances. This increases the likelihood that two separate fence communications systems could couple in and interfere with each other.

- A number of the components in the fence system have an impedance which changes with frequency (especially capacitive effects). This causes components of the transmission to reach the receiver with different amplitudes (Chapter 6.6 and 7.1).

- Non-linear materials in the fence construction can cause intermodulation distortion (Chapter 7.2). This is expected to be a relatively minor source compared to other sources.

9.2. Other Considerations for Modulator/Demodulator Design

As well as considering the theoretical performance of a particular modulation scheme, a number of other practical considerations must be evaluated in the choice of scheme.

- The transmitter and receiver must be isolated and protected from the high voltage pulse produced by the energizer. A number of safety standards dictate how this must be implemented.

- In certain bands, there are local laws and regulations which limit the maximum transmit power of the system (Chapter 8.4.1).

- For battery powered devices, minimizing power use is a high priority. This adds further complexity to a number of areas of the design:
  - Synchronization between modulator and demodulator
  - Sampling frequency and accuracy of the received waveform.

- Filtering is required at the receiver and possibly at the transmitter. The complexity of the filter is dictated by factors such as the width of the filter and how much effect it has on the phase of the signal.

- It is possible that the system may be extended to support multiple channels either at the time of design or further on in the products life cycle.

9.3. Modulation Schemes

9.3.1. Frequency Shift Keying

Frequency Shift Keying (FSK) is used by the current generation Gallagher Remote and the TruTest Fence Compass. Data is modulated on the carrier wave by increasing or decreasing the frequency of the carrier wave [21].

$$BW_{0.95} = \Delta f + \frac{3}{T_b}$$

Equation 3 – General solution for bandwidth occupied by BFSK (95% of transmitted power) [22]

$$BW_{0.95} = \frac{4}{T_b}$$

Equation 4 – Bandwidth occupied by BFSK with a minimum frequency separation ($\Delta f = 1/Tb$ for orthogonal non-coherent carriers)

Table 14 - Performance Summary of M-ary FSK at BER = 10^{-5}

M	$\dfrac{M\text{-ary bandwidth}}{\text{binary bandwidth}}$	E_b/N_0	$\dfrac{M\text{-ary energy}}{\text{binary energy}}$
2	1/1	12.6 dB	0 dB
4	2	9.88 dB	-2.70 dB
8	3	8.40 dB	-4.18 dB
16	4	7.42 dB	-5.16 dB

When transmitting a single bit per symbol, FSK exhibits poor noise performance compared to the other modulation strategies presented here (Table 14 and Figure 62). It also has a poor spectral efficiency (Equation 3and Equation 4). However as the number of bits encoded per symbol increases, the noise performance improves. This is because FSK is only limited by the bandwidth available, unlike PSK and QAM which are limited by the total phase of 360°. According to the Shannon-Hartley Theorem [21], an increase in bandwidth has a much bigger effect on the available channel capacity than the limitation due to noise. FSK can exploit this to increase its available bandwidth [22]. Only FSK exhibits this feature but it is at the cost of a more

complex modulator and demodulator (wider filters, increased number of generator frequencies) as well as a much larger bandwidth.
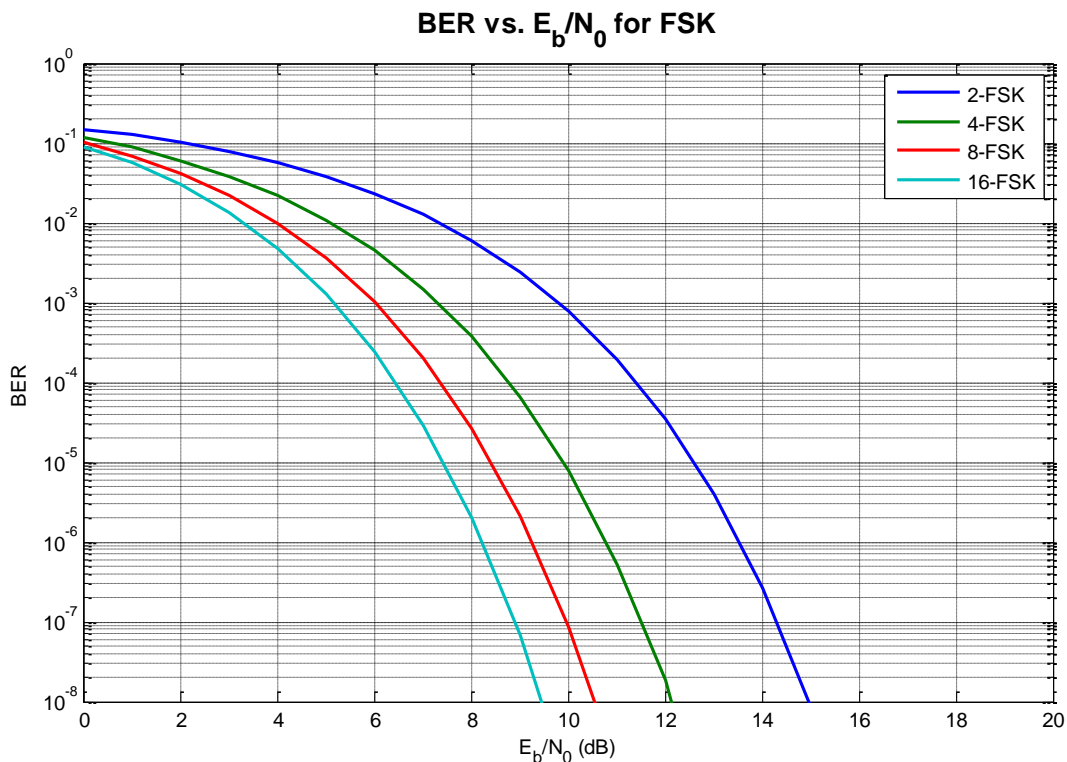
BER vs. E_b/N_0 for FSK

Figure 62 - Plot of BER vs. E_b/N_0 for FSK modulation with one to four bits per symbol. The signal strength required to achieve a set BER decreases as the number of symbols increases

9.3.2. Pulse Position Modulation

Pulse Position Modulation (PPM) has identical noise and bandwidth performance to that of FSK [23] [24]. Information is encoded onto the time delays between pulses.

PPM is less common than the other modulation schemes presented here but is an important scheme in the area of ultra-wideband (UWB) communications [24]. It is extremely resistant to changes in amplitude due to fading caused by multipath interference. The UWB nature of this strategy makes it less susceptible to frequency selective fading as well.

Because the information is encoded into the time-delay between pulses, it is extremely sensitive to the time delays caused by multipath interference. This reduces the strategy's suitability for M-ary signalling. PPM occupies a very wide bandwidth

if its duty cycle is kept low (< 0.5 %) [25]. This gives the strategy a very high peak to average power ratio. The minimum bandwidth of an UWB system is at least 20 % of its arithmetic carrier frequency [25]. Simple UWB is susceptible to narrow bandwidth interference unless it is modified with further redundancy [26].

9.3.3. Phase Shift Keying

Phase Shift Keying (PSK) modulates data onto a carrier wave by varying the phase of the carrier. For 2-PSK, 0° and 180° are used which is functionally identical to toggling the polarity of the carrier wave. For encoding more bits, intermediate phases are used as well, for example 90° and 270° are used for 4-PSK.

$$BW_{0.95} = \frac{3}{T_b}$$

Equation 5 - General solution for bandwidth occupied by BPSK (95% of transmitted power) [22]

Table 15 - Performance Summary of M-ary PSK at BER = 10^{-5}

M	$\dfrac{M\text{-ary bandwidth}}{\text{binary bandwidth}}$	E_b/N_0	$\dfrac{M\text{-ary energy}}{\text{binary energy}}$
2	1/1	9.61 dB	0 dB
4	1/2	9.61 dB	0 dB
8	1/3	13.0 dB	3.36 dB
16	1/4	17.5 dB	7.86 dB

PSK has good noise performance when transmitting a single bit and improves significantly on FSK (Table 15 and Figure 63). Increasing the number of bits per symbol to two has no effect on the noise performance because both an in-phase and quadrature component is used to transmit data. Increasing the number of bits beyond two negatively impacts the scheme's noise performance.
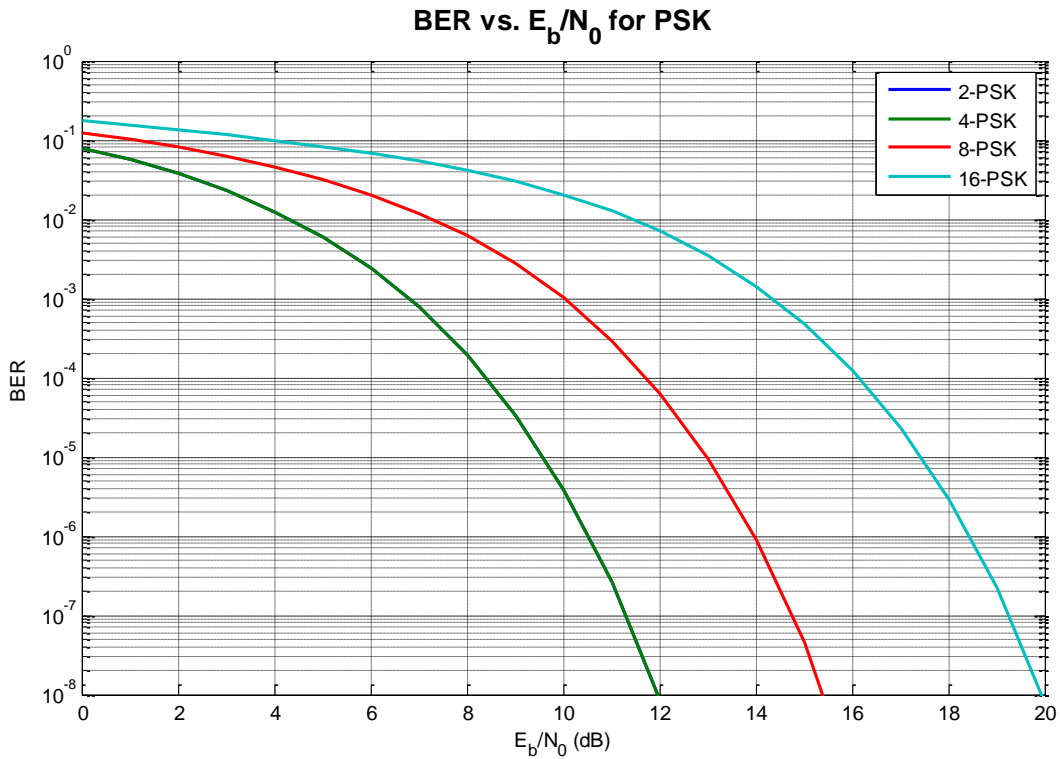
BER vs. E_b/N_0 for PSK

Figure 63 - Plot of BER vs. E_b/N_0 for PSK modulation with one to four bits per symbol. Note that 2-PSK and 4-PSK have identical performance and overlap

9.3.4. Differential Phase Shift Keying

Differential Phase Shift Keying (DPSK) modulates data onto the carrier in the same way as PSK except that with each new symbol, the phase must change even if the binary value of the symbol does not. This removes the need for synchronization with the receiver, as it determines the value of the symbol by the change in phase from the previous symbol.

The performance of DPSK regresses slightly from that of PSK (Table 16 and Figure 64), due to the incoherent receiver. The difference in performance further increases as the number of bits per symbol increases.

Table 16 - Performance Summary of M-ary DPSK at BER = 10^{-5}

M	$\dfrac{M\text{-ary bandwidth}}{\text{binary bandwidth}}$	E_b/N_0	$\dfrac{M\text{-ary energy}}{\text{binary energy}}$
2	1/1	10.4 dB	0 dB
4	1/2	11.9 dB	1.53 dB
8	1/3	15.8 dB	5.41 dB
16	1/4	20.4 dB	10.0 dB
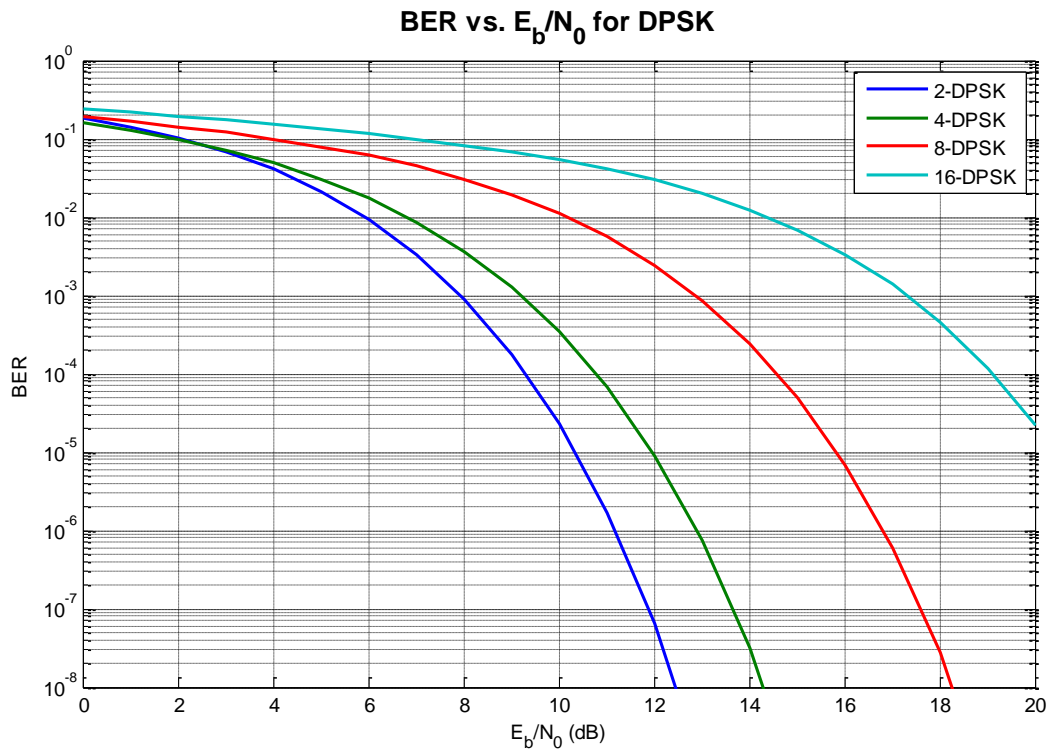
Figure 64 - Plot of BER vs. E_b/N_0 for DPSK modulation with one to four bits per symbol. Unlike PSK, 2-DPSK and 4-DPSK do not overlap

9.3.5. Quadrature Amplitude Modulation

Quadrature Amplitude Modulation (QAM) combines Amplitude Shift Keying (ASK) and PSK to modulate data using both the amplitude and phase of the carrier. QAM cannot encode less than two bits per symbol and to maintain a uniform constellation must increase from two bits per symbol to four bits and so on. Non-uniform constellations are also possible but are beyond the scope of this research (although 8-QAM and 32-QAM are included for interest).

Table 17 - Performance Summary of M-ary QAM at BER = 10^{-5}

M	$\dfrac{M\text{-ary bandwidth}}{\text{4-QAM bandwidth}}$	E_b/N_0	$\dfrac{M\text{-ary energy}}{\text{4-QAM energy}}$
4	1/1	9.57 dB	0 dB
8	1/1.5	12.5 dB	2.93 dB
16	1/2	13.4 dB	3.85 dB
32	1/2.5	16.5 dB	6.97 dB

4-QAM is functionally identical to 4-PSK so, even though they are generated using different techniques, they have identical noise performance. When the number of bits per symbol is increased to four, QAM gains a significant advantage over every other modulation scheme mentioned here. However it still requires good signal strength for reliable operation (Table 17 and Figure 65).
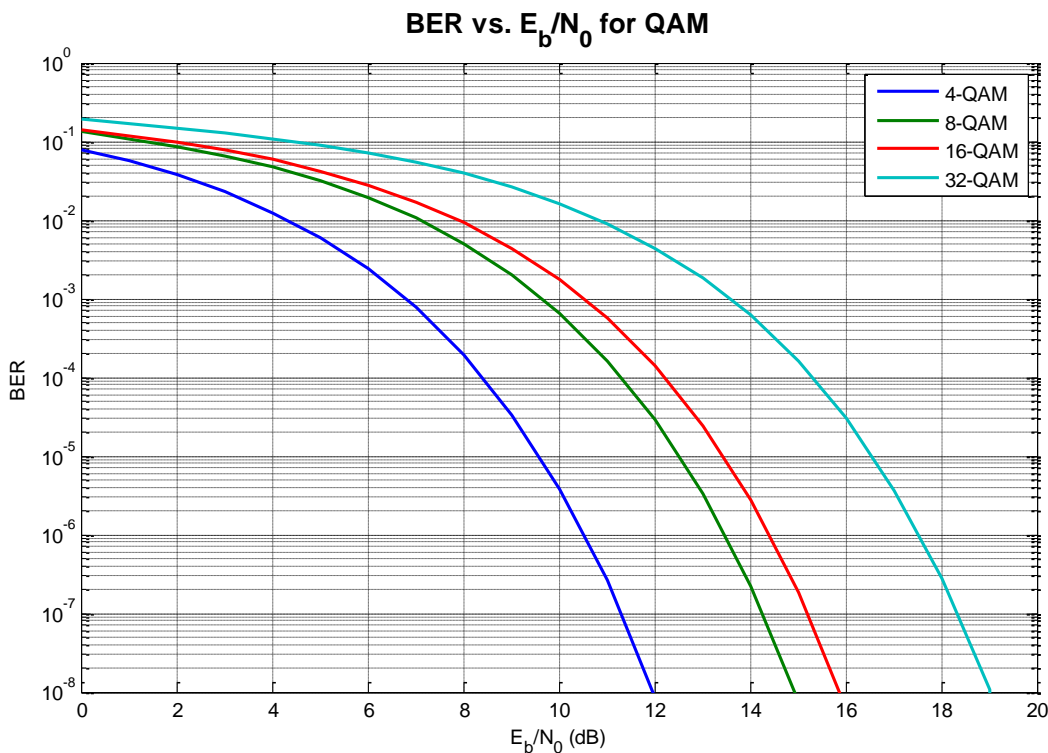
Figure 65 - Plot of BER vs. E_b/N_0 for QAM modulation with two to five bits per symbol. The shape of the constellation has a large effect on the BER plot. The increase in signal strength from 4-QAM to 8-QAM is much greater than the increase from 8-QAM to 16-QAM due to the non-symmetrical constellation shape.

9.3.6. Spectral Efficiency

The spectral efficiency of a modulation scheme is a metric for comparing how much data can be fitted into a limited bandwidth channel given a particular modulation technique. Data transmission is limited by the Shannon-Hartley Theorem [21], a measure of the fundamental limit of an AWGN channel. This limit defined by Equation 6.

$$\frac{E_b}{N_0} = \frac{2^{\frac{C}{W}} - 1}{\frac{C}{W}}$$

Equation 6 - Shannon Limit

PSK and QAM (Single Sideband Amplitude Shift Keying or SSB ASK is not included in the scope of this research) are spectrally efficient and this increases as the number of bits per symbol increases. They are less power efficient though due to the higher required signal strength. They are used most often in systems which are limited by bandwidth and not by power.

FSK is significantly less spectrally efficient than the other modulation schemes. However the number of bits per symbol can be increased without requiring an increase in power which makes it a plausible option for power-limited systems which have a wide bandwidth available.

Standard modulation schemes cannot get particularly close to the Shannon Limit (Figure 66); however convolutional codes such as turbo codes can narrow the gap significantly and are extensively used in communications to achieve this.
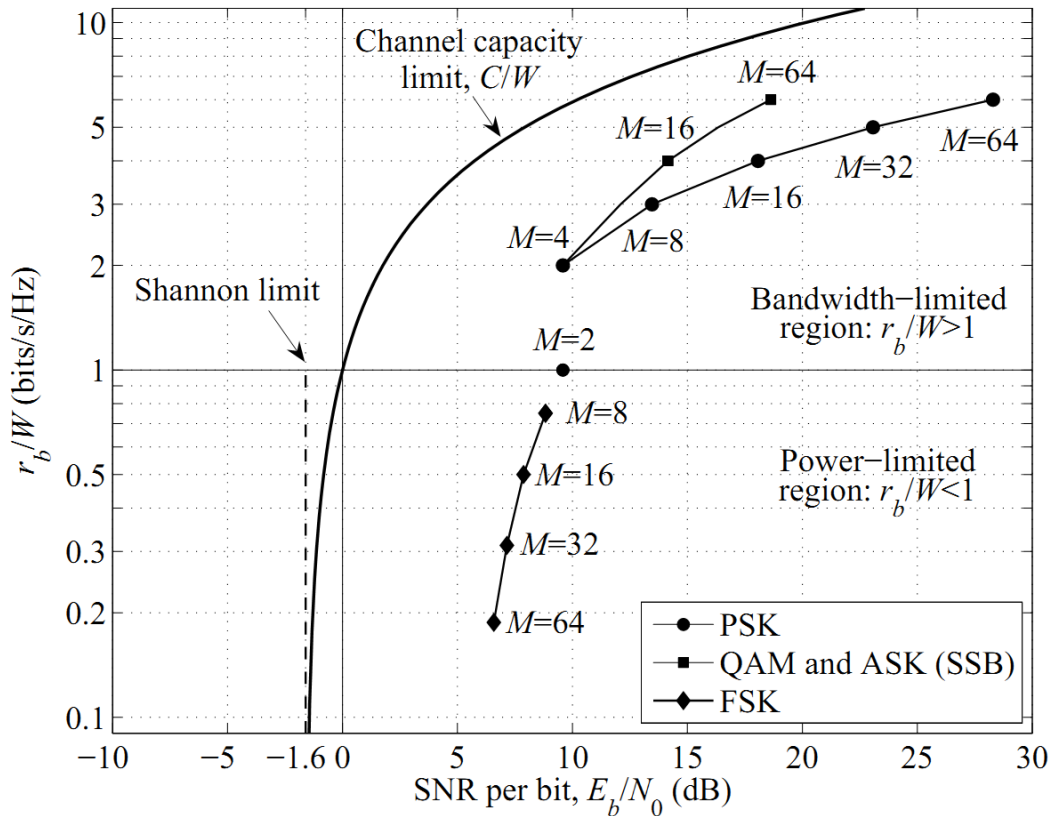
Figure 66 – Spectral Efficiency of several modulation schemes with respect to the Shannon Capacity Limit [22]. No modulation scheme can get close to the Shannon Limit without further modification

9.4. Spreading and Multiple Access Techniques

9.4.1. Frequency Division Multiple Access

Frequency Division Multiple Access (FDMA) splits the available spectrum into frequency channels (Figure 67). The resulting channels can be used in several different ways to achieve different performance advantages. Channels can be allocated to different users to allow multiple devices to communicate simultaneously. The same device can also use multiple channels to increase the bandwidth available if necessary.

Of particular importance to this research is the ability to use FDMA to compensate for a non-uniform spectrum. As noted previously (Chapter 5.6) the response of the fence has peaks and troughs which are unique to each fence. FDMA can check a number of preconfigured channels to determine which channel will provide the greatest reduction in attenuation.

FDMA has a number of disadvantages. It reduces the spectral efficiency of the system by requiring the use of guard bands to account for non-ideal filtering. Separate modulators and demodulators are required for each channel. This increases the hardware requirements for each device and likely increases power consumption. Each channel is likely to have a narrow available bandwidth which makes PSK more suitable than FSK for modulating the data.
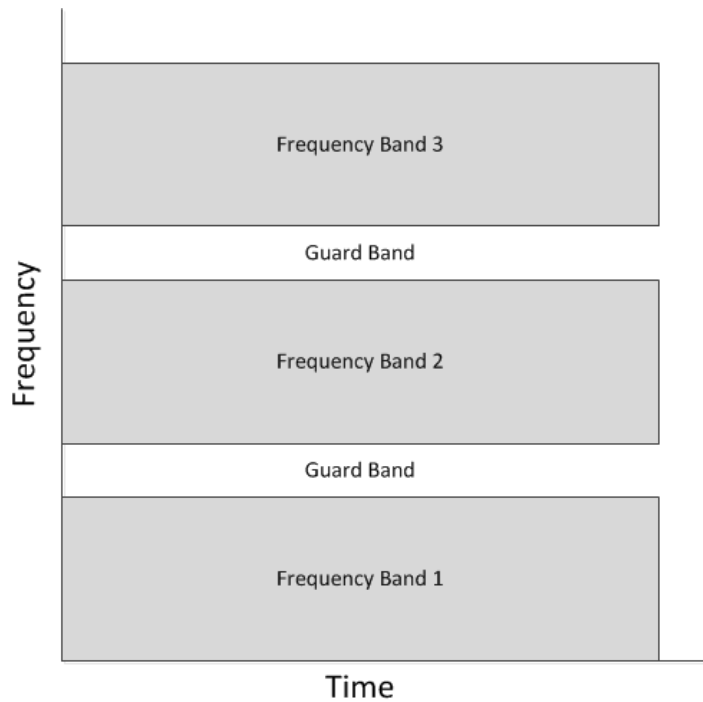
Figure 67 - Diagram of frequency allocation for FDMA with guard bands. A significant amount of the available spectrum is lost due to guard bands

9.4.2. Time Division Multiple Access

Time Division Multiple Access (TDMA) allows each device to use all of the available bandwidth for transmission but allocates time slots for each device to transmit (Figure 68). This allows multiple devices to access the same channel but provides no advantages to compensate for non-uniform channels. The modulation scheme must compensate for the channel but the entire bandwidth of the channel is available for use during the designated time slot. No extra hardware is required to implement TDMA. The Xport protocol implements a TDMA system to allow two-way communication.
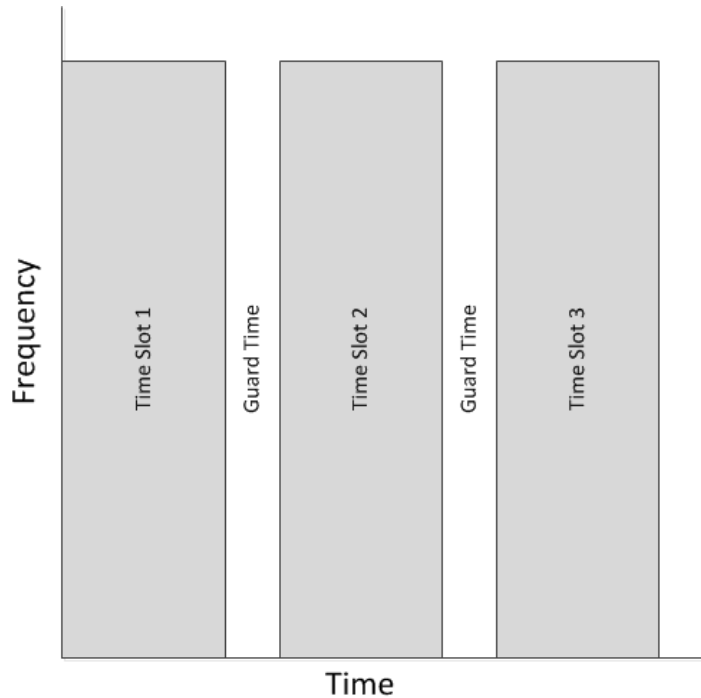
Figure 68 - Diagram of time allocation for TDMA with guard time. A significant amount of time is lost due to guard time slots

9.4.3. Spread Spectrum/Code Division Multiple Access

Spread Spectrum (SS) is a technique for increasing the bandwidth of the signal beyond what is required to modulate the data. This effectively allows the demodulator to spread narrow band noise across a larger number of bits and increase the probability that the message is decoded correctly.

There are two main methods for spreading the signal across a wider bandwidth. The first is called Frequency Hopping Spread Spectrum (FHSS). A sequence of frequency 'hops' are chosen and the sequence is modulated onto the bit stream, repeating the sequence once per bit period. The second method is Direct Sequence Spread Spectrum (DSSS). The bit stream is modulated using a binary code word which is known to both the transmitter and receiver. This has the same effect as spreading with FHSS.

$$G_P(dB) = 10 \log_{10}\left(\frac{W}{B}\right) = 10 \log_{10}\left(\frac{T_c}{T_s}\right)$$

Equation 7 - Processing Gain of a DSSS System [27]

Where G_P = Processing Gain, W = Bandwidth of spread signal, B = Bandwidth of data signal, T_C = chip rate, T_s = symbol rate. An important concept to note is that spread spectrum does not improve a system's BER if the system is only exposed to Additive White Gaussian Noise (AWGN). Its primary advantage is combatting the other forms of noise in the system (i.e. interference and distortion). Equation 7 is the processing gain which the system can gain over sources other than AWGN.

Code Division Multiple Access (CDMA) is an alternative technique for allowing multiple devices to access the channel simultaneously. Each device utilizes the full bandwidth of the channel and is able to transmit at all times by applying a mathematical code to its data stream. The modulated signal produced has a very wide bandwidth and appears as noise to any device which is not demodulating with the same code. The effect of this technique is to raise the noise floor of the channel which limits the number of devices which can transmit simultaneously.

This is functionally identical to DSSS techniques but the focus of SS is to improve the noise performance of the channel rather than enable multiple-access and uses a different group of code words which tend to be longer. The code words for CDMA must also be orthogonal to avoid interference with other code words, such as those produced by a Walsh Matrix [27].

9.4.4. Orthogonal Frequency Division Multiplexing

Orthogonal Frequency Division Multiplexing (OFDM) splits a channel into multiple carriers which is similar in principle to FDMA. However it has a number of significant advantages over FDMA, especially for unpredictable channels such as those found on a fence [28].

OFDM does not require guard bands to separate the sub-carriers which increases the spectral efficiency of the scheme. Each sub-carrier is orthogonal to the adjacent carriers, allowing them to overlap without interference.

As each sub-carrier in an OFDM system uses a much longer symbol duration than a single carrier system (i.e. has a lower bitrate), OFDM is much more resistant to multipath interference. For systems with particularly bad multipath interference, the

number of sub-carriers can be increased and a short guard time added to eliminate the remaining interference.

Due to the narrow bandwidth of each OFDM sub-carrier, it is possible for the modulation scheme to characterize the channel spectrum. This allows the system to compensate for channels with significant notches in the spectrum. Either the transmit power of the sub-carrier can be increased, or the sub-carrier can be dropped entirely for a small performance penalty. No hardware adjustment is required in the modulator as all of this adjustment is made in the DSP software.

Care must be taken when designing the amplification stage of an OFDM system. Because each sub-carrier is completely independent of all other sub-carriers, if certain patterns of symbols combine then the output power of the OFDM system can be significantly higher than it is on average. If the signal exceeds the capabilities of the amplifier, the signal can clip and/or add distortion which degrades the system. This places extra strain on the power amplifier and also requires it to be highly linear across a wide range.

To reduce the requirements of the power amplifier, codes can be used to control the peak power levels. PAR Reduction Codes can be used so that the small subset of symbol combinations which generate the very high peak power signals are removed from the constellation and the overall data rate is reduced to compensate. Other techniques have also been developed and can be found in the relevant literature [28].

Timing and synchronization has a large impact on the required guard time and therefore the overall data rate and BER. The more precise the synchronization can be made, the smaller the guard time slots can be made. This further improves the overall data rate and spectral efficiency.

9.5. Error Correction Techniques

Inevitably errors occur in communication systems, even systems with strong signal to noise ratios. It is possible for the receiver to request that the transmitter resend the required data, but only if the receiver has recognized that there is an error in the transmitter. If in fact there is an error in the received data, it is often more efficient for

the receiver to attempt to correct the error itself. This requires extra redundant information to be sent along with the original data.

9.5.1. Block Codes

Block codes are a family of codes which add extra redundant information to a packet of bits [21]. This is commonly added at the end and is calculated using a predetermined binary algorithm. Cyclic Redundancy Check (CRC) codes are a subset of block codes which are very well suited to simply detecting errors in a packet. The current Gallagher Xport protocol uses a 16 bit CRC code to check for errors in the previous 2056 bits (Chapter 8.1). This gives a block code with the properties in Table 18.

<div align="center">

Table 18 - Properties of Xport Protocol CRC Code

</div>

n (Total Packet Size)	2072
k (Message Length)	2056
r (Redundant Data)	16
R (Efficiency of Code)	99.2 %
d_{min} (Guaranteed Errors Detected)	3
Errors Corrected	0

Assuming that the standard CRC-16 algorithm is in use, this guarantees that the code can detect up to 3 errors and very likely more depending on the nature of the errors [29].

This is a useful approach but can cause problems if it takes a long period of time for the receiver and transmitter to coordinate resending of the original data. Other block codes such as Hamming, Bose-Chaudhuri-Hocquenghem (BCH) and Reed-Solomon Codes also allow the receiver to calculate which bits are incorrect and change them to correct the message. This eliminates the need to resend the data.

The Hamming(31,26) is an example of an simple but efficient block code as shown in Table 19.

Table 19 – Properties of the Hamming(31,26) Linear Block Code

n (total packet size)	31
k (message length)	26
r (redundant data)	5
R (efficiency of code)	83.9%
d_{min} (guaranteed errors detected)	2
Errors corrected	1

The efficiency of this code is lower than that of the CRC code utilized in the Xport protocol but it can detect and correct errors in the received packet. If the data portion of the Xport transmission (1960 bits) was encoded using this code, up to 150 errors could be detected and 75 errors corrected (assuming an even distribution of errors across the message).

This example illustrates a major disadvantage of using block codes. Certain patterns of noise can overpower the block code. Burst noise can eliminate a number of bits in a data sequence. So even if the individual block codes across the entire message are capable of correcting the required number of bits, the single packet which has been severely corrupted cannot be recovered. The extra computation required to decode the block code also adds further demands to the system. Each individual code also has other advantages and disadvantages associated with it due to the manner in which it calculates the redundant data.

9.5.2. Convolutional Codes

Convolutional codes generate a code word based on the current data bit and a predetermined number of previous bits [21].

The encoder is particularly easy to implement in hardware, requiring only flip-flops and XOR gates for the computation and data switches for the input and output. No buffers are required to process the bit stream as the code words are generated sequentially. Powerful decoders are also possible using maximum-likelihood

decoding which determines the code word with the least differences to the received message.

As the convolutional code becomes larger and more complex, the decoder computation and storage requirements become exponentially larger. This is due to the decoder needing to calculate a large number of paths through the possible trellis network to determine the closest match to the message. Convolutional codes are often less efficient than block codes if there are few errors in the channel due to the extra redundant information.

9.5.3. Interleaving

Interleaving is commonly used with block codes to make them resistant to burst errors which degrade a number of sequential bits [21]. As previously mentioned (Chapter 9.5.1), burst noise can overpower a single block code in a message even if over the entire message, the block codes are capable of correcting the errors. If the channel is known to experience burst noise in advance, then a suitable interleaver can be used to spread the burst errors over a number of block codes, allowing the receiver to correctly decode the message.

9.5.4. Trellis Code Modulation

Trellis Code Modulation (TCM) is functionally very similar to convolutional codes, except that it works at the lowest level by selecting the next modulation symbol rather than generating redundant data [22]. By restricting the number of states which the modulator can change to, the distance between symbols can be maximized. This improves the error performance of the system (Table 20).

Table 20 - Processing Gain of 8-PSK with TCM over QPSK [22]

Number of Trellis States	4	8	16	32	64	128	256
Power Saving (dB)	3.0	3.6	4.1	4.6	5.0	5.2	5.8

TCM provides a further processing gain which can be implemented in addition to a combination of convolutional codes, block codes and interleaving to achieve the required processing gain. A reasonable processing gain of 3dB can be achieved with

only 4 states. TCM also does not increase the bandwidth required (i.e. going from QPSK to 8-PSK with TCM) [27].

TCM adds further complexity to the overall system by requiring that the modulator have memory available to store past bits as well as the ability to calculate the next symbol. It also requires increasing the complexity of the demodulator to decode the best path through the trellis using the Viterbi Algorithm. The number of symbols must also be increased to accommodate the extra redundant information.

10. Communication System Design

10.1. Available Spectrum

Possibly the most important consideration when designing a communications system is the available bandwidth for the system to occupy. For wireless systems, this is defined and allocated by the governing body. For this particular system, it is defined predominantly by the geometry of the system.
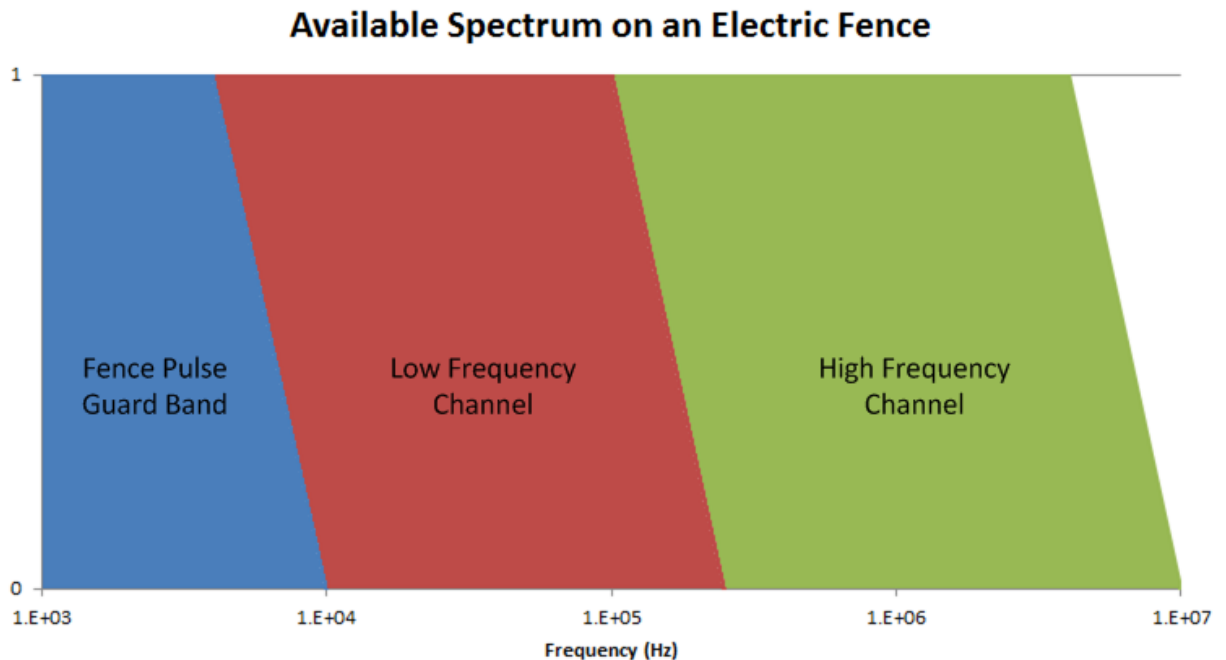
Figure 69 - Available Fence Spectrum including proposed channels. There is no fixed point at which the Low Frequency Channel transitions to the High Frequency Channel and vice-versa. This is indicated on the graph with the non-vertical transitions

The fence pulse transmits at the low end of the spectrum, predominantly between 1 kHz and 3 kHz but components can extend either side so the guard band is set between DC and 10 kHz (Figure 69). It should be noted that due to the extreme voltage levels produced by the fence pulse, interference is seen across all bands and should be taken into account.

The Low Frequency Channel then extends from the limit of the Fence Pulse Guard Band up to approximately 250 kHz. In this region, effects due to the fence radiating

will not be substantial except in very rare cases of fence geometry. The frequency response will gently roll off beyond 100 kHz depending on fence geometry.

The High Frequency Channel extends from the limit of the Low Frequency Channel up to between 5 MHz and 10 MHz. In this region, transmission line effects and radiation are significant and must be taken into account. The high frequency limit is tentatively set but further development could increase this limit further.

The impedance of the human operator decreases as the frequency increases (Chapter 6.6). An asymptote is reached between 5 MHz and 10 MHz after which point there are no further gains to be made. Based on this data, increasing the frequency as high as possible is recommended to reduce the impact of using the operator as part of the receive circuit. This component will have a smaller effect than the response of the fence and should be considered a lower priority.

Bad joints will also be present in the system (Chapter 7). To reduce the impact of these connections, it is also recommended to increase the frequency as high as possible. This component will have a smaller effect than the response of the fence and should be considered a lower priority.

10.2. Modulation Solutions

Given the bandwidth available and the frequency selective fading due to radiation effects and multipath interference, a number of modulation strategies are presented here, each with a focus on a particular performance aspect.

10.2.1. Solution 1

The first solution is to convert the current system to use 2-PSK from 2-FSK (Figure 70 and Table 21). A single bit would be transmitted per symbol in the Low Frequency Channel, preferably between 150 kHz and 250 kHz. No further modifications would be made to the overall system.
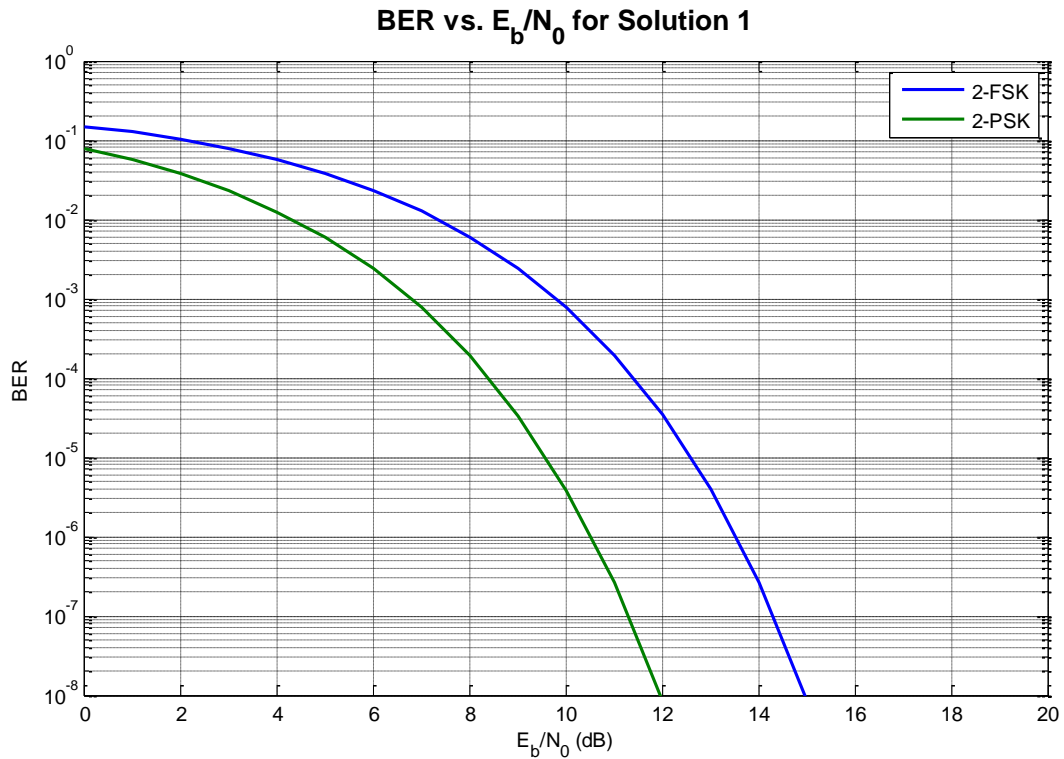
Figure 70 - Plot of BER vs. E_b/N_0 for 2-FSK Modulation and 2-PSK Modulation

Table 21 – Performance Summary at BER = 10^{-5}

Modulation Strategy	Bandwidth	E_b/N_0	Transmit Power Savings
2-FSK	$BW_{0.95} = \dfrac{4}{T_b}$	12.6 dB	0 dB
2-PSK	$BW_{0.95} = \dfrac{3}{T_b}$	9.61 dB	2.99 dB

PSK is spectrally more efficient than FSK which allows more data to be transmitted given a limited bandwidth. This advantage is less important for a system which is not as strictly limited by bandwidth; however it does have advantages for other aspects of the system. For example, both amplifiers and filters need not be as linear as most of the information is contained in a narrower bandwidth. This allows the amplifiers to achieve a higher gain, lower power consumption or a combination of both.

Without increasing the modulation systems resistance to frequency selective fading, this modulation strategy is confined to operate in the Low Frequency Channel. 2-PSK has the same error rate as 4-PSK but only achieves half of the bit rate. With only a single non-configurable modulator/demodulator, this system does not support multiple channels operating concurrently. It is also highly unlikely that CDMA would be possible given the available bitrate. This forces the system to use TDMA to establish multiple accesses. This modulation strategy does not add any extra redundant information and relies on the signal being strong enough for the demodulator to decode. Further signal gain can be achieved in software using FEC.

10.2.2. Solution 2

The second solution is convert the current system to use PPM from 2-FSK. No further modifications are made to the system.

PPM has identical noise performance to FSK so no BER improvements can be made as a direct result of the modulation strategy itself. However since the pulse shape is quite flexible, the modulator and demodulator design can be simplified. The wide bandwidth makes this modulation scheme highly resistant to frequency selective fading and so is suitable for transmission in the High Frequency Channel as well as in the Low Frequency Channel. Due to the low duty cycle of the modulation, it may offer advantages for increasing signal power in certain bands if only the maximum average power is specified. To assess this, the particular standard in question would need to be reviewed.

This modulation strategy is likely to have a very wide bandwidth which makes it unsuitable for multiple access systems other than TDMA. PPM is susceptible to time delays caused by multipath interference. Further research would be required to determine if agricultural fences are sufficiently conductive to return a significant reflection. UWB in its simplest form is highly susceptible to narrow band interference. This can be improved but requires significant improvements to the modulator and demodulator, such as matched filters.

10.2.3. Solution 3

The third solution is to convert the current system to use 8-PSK from 2-FSK (Figure 71 and Table 22). The modulation is further developed by adding TCM and DSSS to the system (Table 23 and Table 24). The carrier frequency could be as high as 5 MHz with sufficiently large spreading codes; although this is a conservative estimate.

Figure 71 - Plot of BER vs. E_b/N_0 for 2-FSK Modulation, 4-PSK Modulation and an estimated curve for 8-PSK with TCM

<div align="center">**Table 22 - Performance Summary at BER = 10^{-5}**</div>

Modulation Strategy	Bandwidth	E_b/N_0	Transmit Power Savings
2-FSK	$BW_{0.95} = \dfrac{4}{T_b}$	12.6 dB	0 dB
4-PSK	$BW_{0.95} = \dfrac{3}{2T_b}$	9.61 dB	2.99 dB
8-PSK with 4-state TCM	$BW_{0.95} = \dfrac{3}{2T_b}$	6.61 dB (Est.)	5.99 dB (Est)

<div align="center">**Table 23 - Performance Summary for possible DSSS Spreading Codes**</div>

Length of Spreading Code	Reduction in bit rate	Processing Gain
Barker Code (Length 7)	$\dfrac{1}{7}$	8.45 dB
Barker Code (Length 13)	$\dfrac{1}{13}$	11.1 dB

<div align="center">**Table 24 - Barker code words for length 7 and 13**</div>

Bit No.	1	2	3	4	5	6	7	8	9	10	11	12	13
Barker-7 Value	+1	+1	+1	-1	-1	+1	-1						
Barker-13 Value	+1	+1	+1	+1	+1	-1	-1	+1	+1	-1	+1	-1	+1

It should be noted that for the estimated plot of 8-PSK with TCM, the approximation of a 3 dB processing gain at BER = 10^{-6} degrades as the BER increases. It is highly likely that the BER of 8-PSK with TCM approaches that of 4-PSK as E_b/N_0 approaches 0dB.

This system is significantly more complex than the previous two solutions. By increasing the number of bits per symbol from one to three, the data rate is increased by a factor of three. This gives a similar BER with that of 2-FSK. TCM is then added

and the distance between symbols is maximised. This results in the data rate being reduced to two bits per symbol but improves the BER beyond that of 2- and 4-PSK. A 4-state encoder is used to generate the TCM but should further increases in performance be desired, the states can be increased up to 256 states which results in approximately 6 dB improvement over 2- and 4-PSK.

A DSSS system is added to the 8-PSK and TCM. A 13 bit Barker code is a possible option but there are a number of other codes available should an increase in processing gain be desired. This code reduces the data rate by a factor of 13 to 1/6.5. This increases the processing gain of the system by 11.1 dB.

This solution adds significant redundancy to the strategy, making the system resistant to all forms of noise, especially narrow band signals. It is also resistant to frequency selective fading along with other multipath effects, allowing it to utilise the High Frequency Channel and Low Frequency Channels as required. The spreading code widens the bandwidth occupied and reduces the average power spectral density (PSD) of the system, possibly allowing it to increase signal power in controlled bands in a similar fashion to Solution 2.

The codes suggested for this modulation scheme are not suitable for CDMA because they do not exist as an orthogonal set which is required by CDMA. The wider bandwidth also makes this system less suitable for FDMA although it is still possible. It is expected that this strategy would be used in conjunction with a TDMA system. The processing demands on the modulator and demodulator are also increased significantly. Two sets of codes are used to provide redundancy and each requires signal processing to operate, particularly at the receiver. The 8-PSK constellation is much closer together than a 2-PSK system and requires that the filters and amplifiers introduce as little phase distortion as possible which makes these modules more complex.

10.2.4. Solution 4

The fourth solution is to convert the current system to use 8-PSK from 2-FSK (Figure 72 and Table 25). The modulation is further developed by adding TCM and CDMA

to the system (Table 26 and Table 27). The carrier frequency could be as high as 5 MHz with sufficiently large spreading codes. This is an estimate only as the use of CDMA can cause complications. This solution is functionally identical to Solution 3 but uses orthogonal spreading codes to allow simultaneous access by multiple devices.
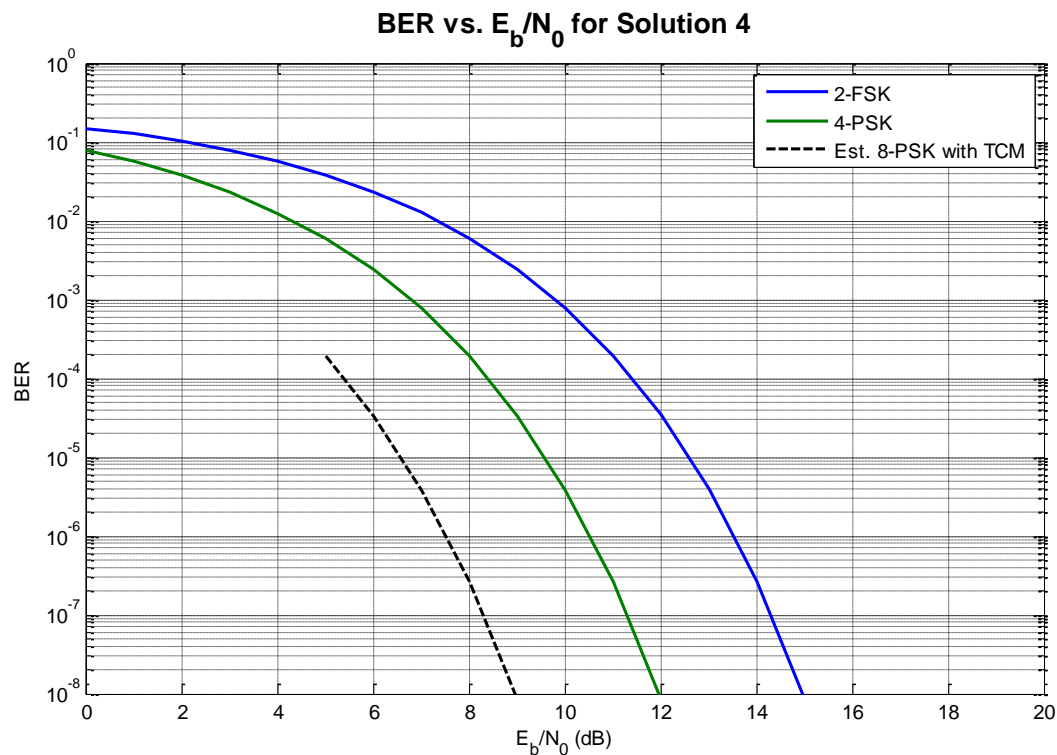
Figure 72 - Plot of BER vs. E_b/N_0 for 2-FSK Modulation, 4-PSK Modulation and an estimated curve for 8-PSK with TCM

Table 25 - Performance Summary at BER = 10^{-5}

Modulation Strategy	Bandwidth	E_b/N_0	Transmit Power Savings
2-FSK	$BW_{0.95} = \dfrac{4}{T_b}$	12.6 dB	0 dB
4-PSK	$BW_{0.95} = \dfrac{3}{2T_b}$	9.61 dB	2.99 dB
8-PSK with 4-state TCM	$BW_{0.95} = \dfrac{3}{2T_b}$	6.61 dB (Est.)	5.99 dB (Est)

Table 26 - Performance Summary for possible CDMA Spreading Codes

Length of Spreading Code	Reduction in bit rate	Maximum Processing Gain
Walsh Code (Length 4)	$\dfrac{1}{4}$	6.02 dB
Walsh Code (Length 16)	$\dfrac{1}{16}$	12.0 dB

Table 27 - Example Walsh code words for CDMA. The complete set of length-16 code words is available in the Appendix

Bit No.	1	2	3	4	5	6	7	8	9	10	11	12	13	14	15	16
Code 1 Value	+1	+1	+1	+1	+1	+1	+1	+1	+1	+1	+1	+1	+1	+1	+1	+1
Code 2 Value	+1	-1	+1	-1	+1	-1	+1	-1	+1	-1	+1	-1	+1	-1	+1	-1
Code 3 Value	+1	+1	-1	-1	+1	+1	-1	-1	+1	+1	-1	-1	+1	+1	-1	-1

It should be noted that for the estimated plot of 8-PSK with TCM, the approximation of a 3 dB processing gain at BER = 10^{-6} degrades as the BER increases. It is highly likely that the BER of 8-PSK with TCM approaches that of 4-PSK as E_b/N_0 approaches 0dB.

The modulation strategy is exactly the same as for Solution 3. This configuration is resistant to frequency selective fading and multi-path effects. It is also highly resistant to narrow band interference. An important modification is made to the spreading code system which affects the performance of the system. The DSSS system is replaced with a CDMA system by changing the code words used. It is important that the code words assigned to each device be orthogonal. This prevents the code words from interfering when transmitted in the same communications channel. Orthogonality of two code words can be verified by calculating the dot-product. The result should be zero.

As the number of devices transmitting in the CDMA system increases, the 'apparent' noise floor also increases. This is a result of the channel being limited according to the Shannon Limit. Increasing the size of the code word increases the number of

devices which can be transmitting simultaneously but reduces the bit rate of each as well.

As well as the advantages outlined in Solution 3, this system has another key advantage. The CDMA system is very flexible and can adapt to a number of situations. If significant amounts of narrow band interference are present, a CDMA system can function as a DSSS system by reducing the number of transmitting devices to one. Using CDMA simplifies the protocol for the system significantly by allowing a device to transmit at any time to another device as long as it has a unique code word. This would be of particular benefit in a mesh network where each device can function as a repeater.

The main disadvantage of CDMA is an increase in complexity of the modulator and demodulator. In order to isolate a particular device's transmission, the signal must be matched to the corresponding code word. This allows a demodulator to demodulate any and all signals in a system but requires that either the demodulator has sufficient processing power to demodulate all code words simultaneously or memory to store the incoming transmission. This adds to the power consumption and cost of the system.

10.2.5. Solution 5

The fifth solution is to convert the current system to use 8-PSK from 2-FSK (Figure 73). The modulation is further developed by adding TCM and OFDM to the system (Table 28 and Table 29). This solution is designed to maximise the bandwidth available on any fence system.

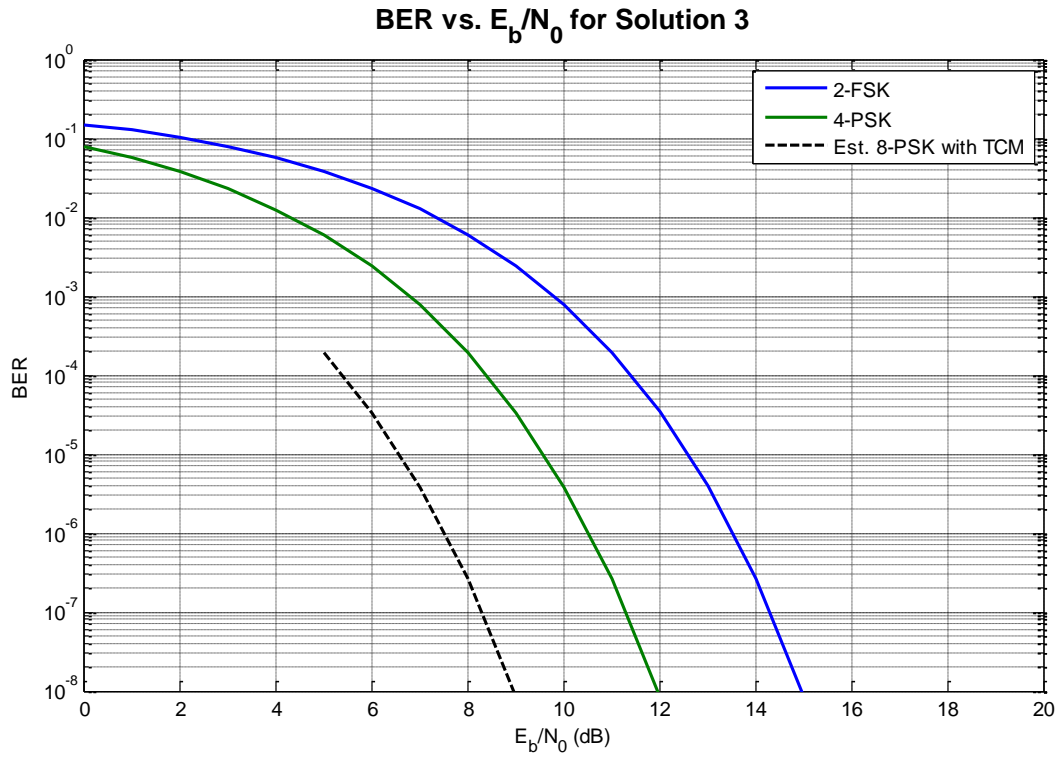**BER vs. E_b/N_0 for Solution 5**
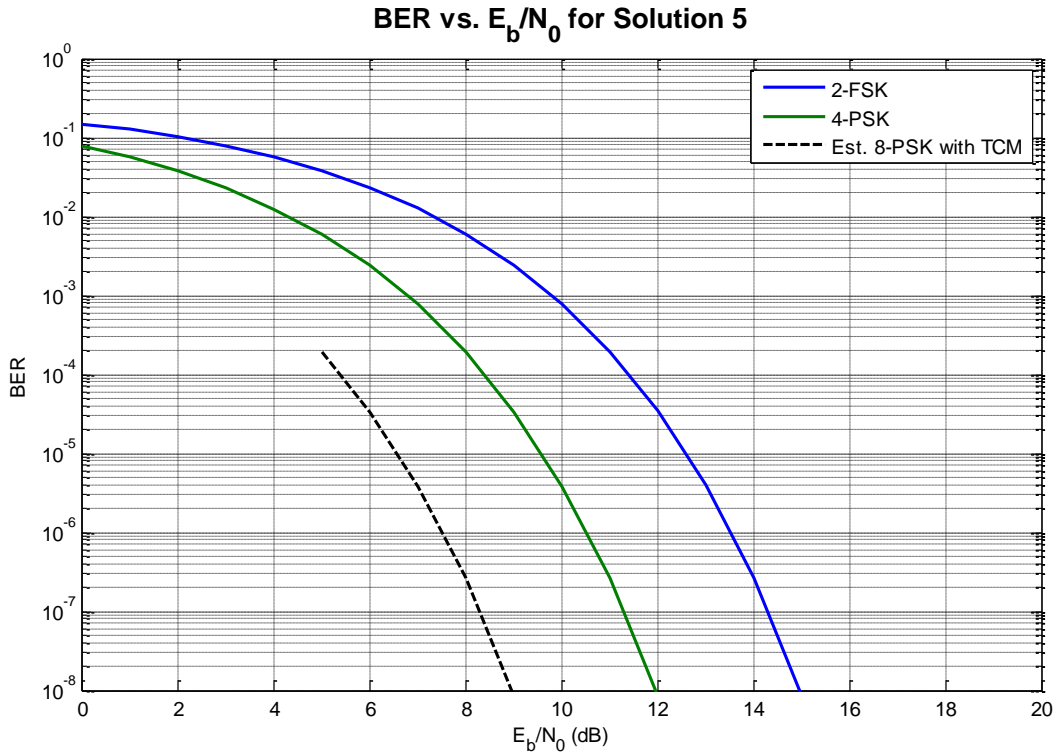
Figure 73 - Plot of BER vs. E_b/N_0 for 2-FSK Modulation, 4-PSK Modulation and an estimated curve for 8-PSK with TCM

Table 28 - Performance Summary at BER = 10^{-5}

Modulation Strategy	Bandwidth	E_b/N_0	Transmit Power Savings
2-FSK	$BW_{0.95} = \dfrac{4}{T_b}$	12.6 dB	0 dB
4-PSK	$BW_{0.95} = \dfrac{3}{2T_b}$	9.61 dB	2.99 dB
8-PSK with 4-state TCM	$BW_{0.95} = \dfrac{3}{2T_b}$	6.61 dB (Est.)	5.99 dB (Est)

Table 29 – Comparison of OFDM configurations with different sub-carrier bandwidths assuming channel from 1 MHz to 6 MHz (5 MHz total)

Number of Sub-carriers	Bandwidth Per Sub-carrier
64	78.1 kHz
128	39.1 kHz
256	19.5 kHz

It should be noted that for the estimated plot of 8-PSK with TCM, the approximation of a 3 dB processing gain at BER = 10^{-6} degrades as the BER increases. It is highly likely that the BER of 8-PSK with TCM approaches that of 4-PSK as E_b/N_0 approaches 0dB.

As with a number of the previous modulation strategies, 8-PSK with TCM is used to minimise the transmit power required. None of the previous strategies were able to maximise the data rate in the bandwidth available because the data rate was limited by the carrier frequency (at least a couple of carrier cycles are required per bit). Each also attempted to prevent the channel from selectively filtering the transmitted signal either by transmitting at a frequency which would minimise the effect or by spreading the bandwidth. This may work but it does not deal with the problem directly and certain fence configurations may overwhelm the systems capabilities.

OFDM measures and characterises the channel as part of its configuration [28]. By splitting the available bandwidth into sufficiently small sub-carriers, each sub-carrier can be approximated to have a flat frequency response. This allows the modulator and demodulator to configure the system based on which sub-carriers have the best signal quality and in turn maximise the available data throughput. Adding a guard-time slot at the end of each OFDM symbol makes the system extremely immune to multipath effects. It is also immune to frequency selective fading.

The number of sub-carriers chosen has a significant effect on how the system reacts if the channel response changes [30]. If the channel response is reasonably static with respect to time, then a large number of sub-carriers can be used to improve the overall

efficiency. If the channel response changes with time quickly, then a smaller number of sub-carriers should be used and the symbol time reduced as much as possible.

Because the sub-carriers are encoded and decoded using FFT methods, OFDM is extremely processor intensive. Digital Signal Processors (DSPs) are rapidly becoming more efficient and are the most common processor for running the required algorithms. It also requires very linear amplifiers and filters to prevent the carriers from interfering and causing inter-symbol interference (ISI). Synchronisation must also be strictly controlled. If the system can drift out of synchronisation quickly, then larger guard-time slots must be used to prevent interference with the following symbols, lowering the overall efficiency of the system. In its standard configuration, OFDM by itself does not allow simultaneous multiple-access such as CDMA does. It must be further modified to support this with further techniques such as CDMA.

10.3. Forward Error Correction Solutions

With any communications system, errors inevitably occur in transmission. For well-behaved systems with very low BER, automatically resending a packet if an error occurs is a viable and efficient scheme. As the signal deteriorates, stronger error correction is needed to ensure correct transmission.

The format of the data being transmitted also has an impact on the configuration of the error correction. Data streams such as uncompressed video are comprised of packets which are not interrelated. So if a packet is lost, only a small fraction of the video frame will be corrupted. Compressed video such as produced by the H.264 codec [31] uses frames which can be dependent on up to 48 other frames to achieve compression. Losing a packet in a H.264 stream would cause much more severe corruption than for an uncompressed stream.

Other sorts of information are transmitted through the fence system such as control commands from a Gallagher Remote and measurements from fence monitors. These are a comprised of short packets and an optimal FEC scheme for continuous data such as video is unlikely to be effective in this situation. The implications of having

short packets as well as continuous streams are beyond the scope of this research and further investigation is required to determine an effective solution for both.

10.3.1. Solution 1

The first solution is to convert the CRC code in the current system to a block code. CRC codes do not allow detected errors in the data to be corrected, only detected. Block codes allow a small number of the detected errors to be corrected, adding a small amount of redundancy to the overall message. The message length is also reduced. The current protocol allows 3 errors to be detected in the packet of 2072 bits. This is extremely efficient but is not suitable for the system which is susceptible to interference.

The Hamming(31,26) code mentioned previously (Chapter 9.5.1) is an efficient code which is capable of detecting 2 errors per message and correcting 1. Over the full message of 1960 bits, up to 75 errors could be corrected. This scheme is capable of correcting a large number of random errors and can efficiently resend for a small packet as required rather than the whole message. Block codes would minimise the number of single bit errors such as occur with small amounts of ISI or when operating at a higher BER. This solution does not require that the data be part of a long transmission and will work effectively with shorter messages as well as longer messages, making it suitable for control packets as well as continuous streams such as video.

This configuration is particularly susceptible to burst errors in the transmission. A number of errors in a packet would overwhelm the block code and require the packet to be resent. The energizer pulse is an example of a burst-error source which would eliminate a number of packets.

10.3.2. Solution 2

The second solution is to convert the CRC code in the current system to a block code as with Solution 1. In addition to the block code, an interleaver is added to the system as well.

The main disadvantage of Solution 1 is its susceptibility to burst errors. In an electric fence system this is most commonly the energizer pulse and it is a regular and predictable source of interference. Because the source is predictable, a systematic interleaver is recommended. The size of the block code is then chosen based on the bitrate and the number of bits which would be lost during the energizer pulse. The system is then able to continue transmitting and receiving data, even if the energizer pulse occurs during the transmission.

This solution is not suitable for short messages because a large number of packets are required for the interleaver to overcome the burst errors present. If only a single packet is sent, then the overall performance is equal to that of the block code alone. If shorter messages were scheduled to send between pulses by the protocol, this disadvantage could be minimised.

Consider the following parameters:

Table 30 - Scenario Parameters

Specified Parameter	Value
Overall bitrate of system	100 kbit/s
Length of Energizer Pulse	200 μs
Chosen Block Code	Hamming (31,26)

The system includes an interleaver so the number of packets which need to be interleaved to allow the receiver to correctly decode the message can be calculated (Table 31). Using this code a single error can be corrected per packet. Using an interleaver, a 200 μs burst error can be compensated for every 6.2 ms at 100 kbit/s given a sufficiently long message.

Table 31 - Calculated Error performance with block code and interleaver

Calculate Parameter	Value
Bit time	10 μs
Number of corrupted bits	20
Number of Packets to correct errors	20
Length of message (time)	6.2 ms

10.3.3. Solution 3

The third solution is to convert the CRC code to a block code as mentioned in Solution 1 and 2. An interleaver and a convolutional code are also added.

Block codes become more efficient as they get longer and require fewer parity check bits. However this reduces the power of the code. A convolutional code on the other hand works very effectively for shorter lengths of data and becomes exponentially more compute intensive as the length of the encoded message increases. It is possible to combine all three of these techniques to exploit their advantages.

Reed-Solomon Codes [32] are a powerful family of block codes but are designed for much longer length blocks. For example the RS(204,188) code operates on 8-bit symbols or bytes. So 204 bytes is a single block, of which 188 bytes are information. Up to 8 incorrect bytes can be corrected from anywhere in the block [33].

This is then encoded again using a convolutional code. Convolutional codes perform best to compensate for data which has single errors in the transmission rather than burst errors. The encoding can be made more or less robust depending on the ratio of parity bits to data bits. After running through the convolutional encoder, the data is interleaved to spread any burst errors. An extra interleaver can be used between the block encoding and the convolutional encoding but is not necessary.

The combination of these three methods makes the transmission resistant to all forms of error patterns and can be adjusted as required to have more redundancy or less redundancy depending on the encoding.

11. Conclusion

The object of this thesis was to evaluate the spectrum available in the electric fence system. The fence comprises of a number of key components, the fence geometry itself, the operator and remote, and any insulating joints which may be present.

In Chapter 5, the frequency response of the fence is evaluated in isolation. The response was flat and well behaved below 250 kHz, but was highly variable beyond this frequency. Significant frequency selective fading is present which can attenuate the signal by up to 15 dB. To operate in the high frequency region, an advanced system will be required to utilise the available bandwidth.

In Chapter 6, the impedance of the human operator was evaluated with regard to a number of important scenarios such as footwear. The impedance of this component is predominantly capacitive with a direct connection to the skin having the lowest impedance and the highest impedance measured when wearing footwear. Due to the biological nature of this component, a fractional-capacitor-resistor model was found to fit the data best which is an interesting effect but has little influence on the performance of the system. With regard to the performance of the overall system, an improvement in signal strength can be achieved by transmitting at a higher frequency up to a limit of 10 MHz.

In Chapter 7, the impedance of an insulating fence joint was evaluated. There is a clear difference in impedance between a joint which is conductive and a joint which is insulative. An insulative joint was best fit by a capacitor-resistor model with a small capacitance. This results in a very high impedance at low frequencies so transmitting at higher frequencies is the preferred method to reduce the effect of the joint. An insulating joint was found to have semi-conductive effect under optimum conditions. It is unlikely that this effect will have a significant impact on the system and can be safely ignored.

In Chapter 9, a number of modulation techniques were evaluated. Due to its simplicity and ease of implementation, Phase Shift Keying (PSK) was recommended

for most of the proposed systems. This was complemented with either Trellis Code Modulation (TCM) or Orthogonal Frequency Division Multiplexing (OFDM) depending on the performance requirements of the system. In addition to evaluating modulation techniques, a number of forward error correction techniques were evaluated. The choice of code is heavily dependent on the overall system and the importance of the information being sent. A simple block code was recommended for non-essential data while a combination of a block code, interleaver and turbo code was chosen for critical data.

In Chapter 10, the available spectrum is split into three main bands based on the technology required to transmit data. From DC to 10 kHz, it is recommended that a Guard Band be designated to isolate the interference caused by the energizer. The impedance of the human operator and of any insulating joints is especially high in this region as well making it unsuitable for data transmission. From 10 kHz to 250 kHz, it is recommended that a Low Frequency Channel be designated. No frequency selective attenuation is generated by the fence in this band which makes it suitable for less robust systems. The impedance of the human operator and insulating joints prioritises transmitting at the higher end of the band to achieve optimal signal strength. From 250 kHz to 10 MHz, it is recommended that a High Frequency Channel be designated. Significant frequency selective attenuation is present although the impedance of the human operator and insulating joints is at its lowest level. A very robust system is required to transmit in this channel.

A number of solutions for improving the efficiency of the modulation and error correction strategies are also presented. It is recommended that Solution 3 which utilises Phase Shift Keying with eight symbols and Trellis Code Modulation be implemented. This is a robust system for transmitting in the entire Low Frequency Channel and the lower part of the High Frequency Channel. A forward error correction strategy as outlined in Solution 1 is also recommended. This utilises a simple block code to eliminate the most common sources of transmission errors. This proposed system provides the best balance between difficulty of implementation and overall system performance.

12. Future Work

A number of other aspects of the electric fence communications system need to be examined in further detail before design decisions can be made on the possible solutions presented. These are predominantly related to how the communications protocol is implemented.

The current protocol assumes that any device connected to the system is capable of transmitting and receiving to and from any other device on the network. This hampers the performance of the system. A number of methods are commonly used in other communications systems to achieve this, such as mesh networks [34] or star networks [35].

A logical first step to designing the hardware for a new system would be to implement Solution 3 as a development board. The 8-PSK modulator/demodulator is the key hardware required by the system. Implementing TCM and DSSS is primarily software based and can be added afterwards as needed. If the carrier can be adjusted through a large range, i.e. from 100 kHz to 10 MHz, then the system could be adapted to simulate the performance of Solutions 1 and 4 as well as Solution 3. Solution 2 is fundamentally different to Solution 3. Solution 5 is significantly more advanced but could be adapted to simulate any of the other solutions.

DSPs are the best choice for running calculations and software filtering on incoming signals for communications. However these have historically required significant amounts of power, which is not commonly available on battery powered products.

13. References

[1]   A. T. Hancock, *"Modelling the Characteristics and Behaviour of Electric Fence Systems", MSc(Tech). Thesis, University of Waikato. New Zealand,* 1991.

[2]   S. B. Saad, *"Detecting Fence Tampering for Security Electric Fencing", MSc(Tech). Thesis, University of Waikato: New Zealand,* 2002.

[3]   P. A. Rizzi, Microwave Engineering, Prentice Hall, 1988.

[4]   Omegatron, *Transmission line element.svg,* http://en.wikipedia.org/wiki/File:Transmission_line_element.svg, 2007.

[5]   B. Hyland, "An Improved and Simple Cable Simulation Model," 22 October 2012. [Online]. Available: http://pdfserv.maximintegrated.com/en/an/AN5141.pdf. [Accessed 2 March 2014].

[6]   ANSYS Inc., "ANSYS HFSS," 2014. [Online]. Available: http://www.ansys.com/Products/Simulation+Technology/Electronics/Signal+Integrity/ANSYS+HFSS. [Accessed 2 March 2014].

[7]   V. De Santis, P. A. Beeckman, D. A. Lampasi and M. Feliziani, "Assessment of Human Body Impedance for Safety Requirements Against Contact Currents for Frequencies up to 110 MHz," *IEEE Trans. Biomed. Eng.,* vol. 58, no. 2, pp. 390-396, 2011.

[8]   C. Gabriel, S. Gabriel and E. Corthout, "The dielectric properties of biological tissues: I. Literature Survey," *Physics in Medicine and Biology,* vol. 41, pp. 2231-2249, 1996.

[9]   S. Gabriel, R. W. Lau and C. Gabriel, "The dielectric properties of biological tissues: II. Measurements in the frequency range 10 Hz to 20 GHz," *Physics in Medicine and Biology,* vol. 41, pp. 2251-2269, 1996.

[10]   K. R. Foster and H. C. Lukaski, "Whole-body impedance--what does it measure?," *The American Journal of Clinical Nutrition,* vol. 64, no. 3, pp. 388S-396S, 1996.

[11]   J. Scott and A. Parker, "Distortion Analysis Using SPICE," *J. Audio Eng. Soc.,* vol. 43, no. 12, December 1995.

[12]   Agilent Technologies, "Agilent E4980A Precision LCR Meter User's Guide," December 2012. [Online]. Available: http://cp.literature.agilent.com/litweb/pdf/E4980-90080.pdf. [Accessed 13 November 2013].

[13]   Rocky Mountain Gear Guide, [Online]. Available: http://www.rockymountaingearguide.com/images/stance-comparison-900.jpg. [Accessed 3 March 2014].

[14]   A. S. Elwakil, "Fractional-Order Circuits and Systems: An Emerging Interdisciplinary Research Area," *IEEE Circuits Syst. Mag.,* pp. 40-50, Fourth Quarter 2010.

[15]   K. S. Cole and R. H. Cole, "Dispersion and absorption in dielectrics: Alternating currect characteristics," *J. Chem. Phys.,* vol. 9, pp. 341-51, 1941.

[16]   J. L. Walley, "A Method of Electronic Control". International Patent WO9413120, 9 June 1994.

[17]   N. May, "Method and apparatus pertaining to communication along a fence line". United States of America Patent US5651025, 22 July 1997.

[18]   P. R. Adamson, R. R. Nilson and J. R. Spray, "Method and apparatus for communication in an electric fence wiring system". United States of America Patent US6081198, 27 June 2000.

[19]   P. C. Lunenburg and R. C. B. Woodhead, "Data Transmission". United States of America Patent US6847298, 27 June 2002.

[20] E. J. Deuss, D. C. Greager and P. Teal, "System and Method for Electronically Signalling Along a Fence Line". United States of America Patent US6911900, 28 June 2005.

[21] S. Haykin, Communication Systems, 4th ed., Hamilton, Ontario: John Wiley & Sons, 2001.

[22] H. H. Nguyen and E. Shwedyk, A First Course in Digital Communications, Cambridge: Cambridge University Press, 2009.

[23] Mobile Reference, Electronics Quick Study Guide for Smartphones and Mobile Devices, Boston: Mobile Reference, 2007.

[24] H. Nikookar and R. Prasad, Introduction to Ultra Wideband for Wireless Communications, New York: Springer Science+Business Media, 2008.

[25] F. Nekoogar, Ultra-Wideband Communications: Fundamentals and Applications, London: Prentice Hall Professional Technical Reference, 2006.

[26] B. M. Donlan, *"Ultra-wideband Narrowband Interference Cancellation and Channel Modeling for Communications", MSc. Thesis, Virginia Polytechnic Institute. United States of America,* 2005.

[27] D. Torrieri, Principles of Spread-Spectrum Communication Systems, 2nd ed., New York: Springer Science+Business Media, 2011.

[28] V. C. Ramasami, "Orthogonal Frequency Division Multiplexing," CReSIS, Kansas, 2002.

[29] P. Koopman and T. Chakravarty, "Cyclic Redundany Code (CRC) Polynomial Selection for Embedded Networks," in *The Internation Conference on Dependable Systems and Networks*, Florence, 2004.

[30] F. Rayal, "The Number of Sub-Carriers in OFDM impacts NLOS Backhaul Performance (More than You Think)," Blinq Networks, 18 June 2012. [Online]. Available:

http://www.blinqnetworks.com/blog/article/the_number_of_sub_carriers_in_of
dm_impacts_nlos_backhaul_performance_more_t. [Accessed 21 February
2014].

[31]   International Telecommunications Union, "H.264 : Advanced video coding for
generic audiovisual services," February 2014. [Online]. Available:
http://www.itu.int/rec/T-REC-H.264. [Accessed 24 February 2014].

[32]   M. Riley and I. Richardson, "Reed-Solomon Codes: An introduction to Reed-
Solomon codes," Carnegie Mellon University, 1998. [Online]. Available:
http://www.cs.cmu.edu/~guyb/realworld/reedsolomon/reed_solomon_codes.ht
ml. [Accessed 24 February 2014].

[33]   European Telecommunications Standards Institute, "DVB; Framing structure,
channel coding and modulation for digital terrestrial television," January 2009.
[Online]. Available:
http://www.etsi.org/deliver/etsi_en/300700_300799/300744/01.06.01_60/en_3
00744v010601p.pdf. [Accessed 24 February 2014].

[34]   ZigBee Alliance, "FAQ," ZigBee Alliance, [Online]. Available:
https://www.zigbee.org/About/FAQ.aspx. [Accessed 19 February 2014].

[35]   L. G. Roberts and B. D. Wessler, "Computer network development to achieve
resource sharing," Advanced Research Projects Agency, Washington D.C.,
1970.

[36]   W. H. Hayt and J. A. Buck, Engineering Electromagnetics, New York:
McGraw-Hill Science Engineering, 2005.

14. Appendices

14.1. Appendix 1 – Tables of Length-4 and Length-16 Walsh Codes for CDMA

Table 32 - Complete set of length-4 Walsh Codes

Bit No.	1	2	3	4
Code 1 Value	+1	+1	+1	+1
Code 2 Value	+1	-1	+1	-1
Code 3 Value	+1	+1	-1	-1
Code 4 Value	+1	-1	-1	1

Table 33 - Complete set of length-16 Walsh Codes

Bit No.	1	2	3	4	5	6	7	8	9	10	11	12	13	14	15	16
Code 1 Value	+1	+1	+1	+1	+1	+1	+1	+1	+1	+1	+1	+1	+1	+1	+1	+1
Code 2 Value	+1	-1	+1	-1	+1	-1	+1	-1	+1	-1	+1	-1	+1	-1	+1	-1
Code 3 Value	+1	+1	-1	-1	+1	+1	-1	-1	+1	+1	-1	-1	+1	+1	-1	-1
Code 4 Value	+1	-1	-1	+1	+1	-1	-1	+1	+1	-1	-1	+1	+1	-1	-1	+1
Code 5 Value	+1	+1	+1	+1	-1	-1	-1	-1	+1	+1	+1	+1	-1	-1	-1	-1
Code 6 Value	+1	-1	+1	-1	-1	+1	-1	+1	+1	-1	+1	-1	-1	+1	-1	+1
Code 7 Value	+1	+1	-1	-1	-1	-1	+1	+1	+1	+1	-1	-1	-1	-1	+1	+1
Code 8 Value	+1	-1	-1	+1	-1	+1	+1	-1	+1	-1	-1	+1	-1	+1	+1	-1
Code 9 Value	+1	+1	+1	+1	+1	+1	+1	+1	-1	-1	-1	-1	-1	-1	-1	-1
Code 10 Value	+1	-1	+1	-1	+1	-1	+1	-1	-1	+1	-1	+1	-1	+1	-1	+1
Code 11 Value	+1	+1	-1	-1	+1	+1	-1	-1	-1	-1	+1	+1	-1	-1	+1	+1
Code 12 Value	+1	-1	-1	+1	+1	-1	-1	+1	-1	+1	+1	-1	-1	+1	+1	-1
Code 13 Value	+1	+1	+1	+1	-1	-1	-1	-1	-1	-1	-1	-1	+1	+1	+1	+1
Code 14 Value	+1	-1	+1	-1	-1	+1	-1	+1	-1	+1	-1	+1	+1	-1	+1	-1
Code 15 Value	+1	+1	-1	-1	-1	-1	+1	+1	-1	-1	+1	+1	+1	+1	-1	-1
Code 16 Value	+1	-1	-1	+1	-1	+1	+1	-1	-1	+1	+1	-1	+1	-1	-1	+1

14.2. Appendix 2 – Photos of Remotes used for Fence Communications

Figure 74 - Gallagher iSeries Remote (Front)

Figure 75 - Gallagher iSeries Remote (Back)

Figure 76 - Gallagher SmartPac (Front)

Figure 77 - Gallagher SmartPac (Back)

Figure 78 - Gallagher XR1 Remote (Front)

Figure 79 - TruTest Fence Compass (Front)

Figure 80 - TruTest Fence Compass (Back)

14.3. Appendix 3 – ENZCON Paper

Title: Impact of Repair Joints in Fencing Wire on Data Communications: How to Receive Radio and Block Data using No. 8 Wire

Authors: Jonathon McMullan and Jonathan Scott

Abstract: Modern electric fences have remote controls and remote monitors that communicate with the energizer through the active fence wire. This manuscript looks at the impact of repair joints on the data communications between energizer and remotes. We report measurements of nonlinear rust-induced characteristics in joints and we draw conclusions about their effects in the context of an electric fence carrying data communications signals. We furthermore demonstrate how their nonlinear characteristics can cause mixing and detection effects that could account for radio reception.

Intended Venue: Electronics New Zealand Conference 2014

Impact of Repair Joints in Fencing Wire on Data Communications: How to Receive Radio and Block Data using No. 8 Wire

Jonathon McMullan
School of Engineering
University of Waikato
Hamilton, New Zealand
Email: jgm14@waikato.ac.nz

Jonathan Scott
School of Engineering
University of Waikato
Hamilton, New Zealand
Email: scottj@waikato.ac.nz

Abstract—**Modern electric fences have remote controls and remote monitors that communicate with the energizer through the active fence wire. This manuscript looks at the impact of repair joints on the data communications between energizer and remotes. We report measurements of nonlinear rust-induced characteristics in joints and we draw conclusions about their effects in the context of an electric fence carrying data communications signals. We furthermore demonstrate how their nonlinear characteristics can cause mixing and detection effects that could account for radio reception.**

I. Introduction

Modern electric fence energizers offer the possibility of remote control and remote measurement of pulse voltage level. These energizers use the fence wire as the transmission medium for the data. The idea was first patented in 1993 [1], and a number of other patents appeared in the following decade [2]–[5]. The communication can be bi-directional, and is typically a low bit-rate FSK modulation operating at a few tens of kilohertz.

It is common for fence wire to be joined during repair or modification of the fence layout. After being exposed to the elements, a joint may develop an insulating layer. This is obviously known to have little effect upon the high tension pulses, but could the increased impedance of the joint be detrimental to the signal strength of the transmitted data sent between the pulses? This manuscript examines the characteristics of corroding joints and the impact of such joins on low-level signals travelling along the fence network.

No research could be found in the engineering literature on faults which occur in agricultural fencing. The non-linear effects of dry joints have been exploited to detect faults in buried cables [6]. The wireless base station industry has problems with intermodulation occurring in passive components, especially cables and antennas, with corrosion being supposed to possibly contribute, but investigations are usually limited to measuring and eliminating faulty components, and the signal levels are typically quite low even given high RF power [7]. Passive intermodulation distortion (PIMD) is known to arise from a multitude of other reasons, though in RF transmitters it

is chiefly attributed to thermal effects [8]. There are predictions of distortion arising from corrosion, but they are mathematical and not directly supported by measurements [9].

We report here some experiments on the properties of deteriorating fence joints. We disclose a novel theory that can explain demodulation of radio signals within an electric fence structure.

II. Characterising a Corroded Joint

Standard agricultural fencing wire is galvanised steel, 2.65mm in diameter, usually described as "number 8", short for number 8 gauge. A reef knot is the common configuration used to join two lengths of wire. When the joint is exposed to the elements, water ingress occurs and the joint corrodes. The zinc layer deteriorates first due to sacrificial galvanic corrosion before the steel rusts, at which point an iron oxide layer forms in the joint. [10] Ultimately this layer will stop the joint from conducting. At specific thicknesses, the joint can exhibit non-linear impedance characteristics.

In order to investigate the impedance characteristics of rusty steel contact an arrangement resembling a "cat's whisker" was constructed with a rusty bar and a needle. The schematic diagram appears in figure 1, and a photograph of the setup appears in figure 2. A signal generator was used to produce sine and triangle waves at a frequency of 10 kHz with varying amplitudes. A Tektronix TBS1062 Oscilloscope was used to sample the voltage and current waveforms. By dragging the needle across the rust layer and applying more or less pressure, the quality of the connection could be varied. Mostly the joint would appear either as an open or a short circuit. Nevertheless, the oscilloscope would sometimes display a distorted waveform when a certain rust layer thickness was achieved. This method is delicate and it could take a significant period of time to achieve a joint that was neither completely isolated nor fully conducting, but the outcome was repeatable.

Some measurements are presented in figure 3. Initially the nonlinear characteristic appeared with a source voltage of 3.3 V peak. The signal amplitude was then increased from 3.3 to 3.8 V. This increased the current through the junction and
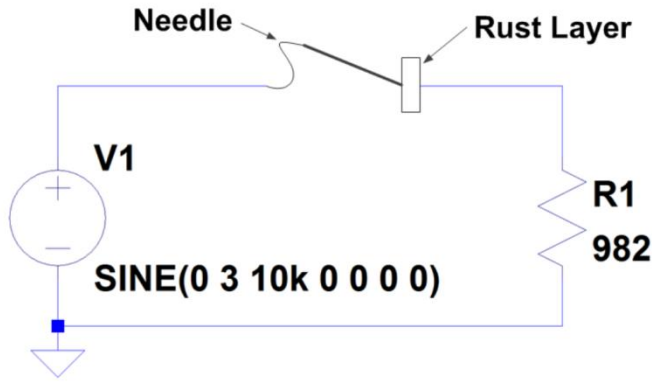
Fig. 1.   Schematic of test circuit

Fig. 2.   Photo showing experimental setup of Rust Joint

Fig. 3.   Measured I-V characteristic of a rust layer demonstrating non-linear conductivity.

reduced the voltage drop as shown in the figure. Increasing the signal amplitude eventually resulted in the junction failing to a short circuit.

III.   IMPLICATIONS FOR DATA TRANSMISSION

These findings have implications for data transmission using the active wire of an electrified fence. Fence line impedance is highly variable. The fence itself acts as a transmission line with a characteristic impedance of typically several hundred Ohms. [11] A fence can terminate in an open circuit, or may suffer significant "vegetation loading" through grass growing up or branches leaning down. The operator of a remote control unit appears as a load, and this load varies greatly with frequency. [12] Operator series impedance and fence characteristic impedance have been measured to change with circumstances such as weather, through its effect upon ground conductivity and operator clothing [13]. It is very difficult, even by design, to get a matched termination on a fence with low return loss [13].

A rusty joint can appear as a capacitor of about 30 pico-farads. At frequencies typical of fence remote controls, this is effectively an open circuit. If the insulating layer is thin, it will be destroyed by the high-tension (HT) pulse, and the wires effectively welded together. Unfortunately, if a joint fails while the fence is off, there will be no pulses to clear the fault, and a remote control might be unable to restart the fence.
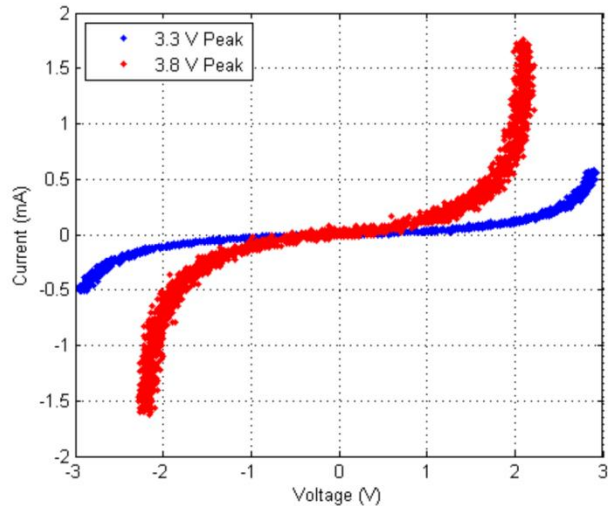
The implication is that a remote should be able to develop a substantial voltage on typical fence loads. One remote studied[1] is capable of producing signal amplitudes in excess of 100 V at light loads. This is intended to be sufficient to cause a rusty junction to fail back to a conducting status.

It should be noted that a communications protocol based at a much higher frequency, where 30pF is a lower magnitude of reactance, would withstand even (dc) open-circuit joints. Similarly, a complex-modulation signal, even at high frequency, would suffer intermodulation interference in the presence of such a joint.

IV.   POTENTIAL FOR NONLINEAR ACTION OF A FENCE JOINT

Observation of the highly nonlinear, albeit symmetrical characteristic observed in figure 3 lead us to recall stories of radio reception in agricultural fencing and dental fillings. Could this be a source of the nonlinearity required for signal detection?

We propose a novel application of a corroded fence joint as an AM radio transmission demodulator. The component arrangement is depicted in figure 4. The fence joint is biased using two fencing staples, one galvanised, and the other rusted steel. These produce two electrochemical cells when they react with the fence wire. Each cell is supposed for our purposes to produce a different potential, giving a total biasing of 0.8V, which is considered quite typical. [10] This allows the fence joint to operate in the non-linear region to one side of the centre of the characteristic, where it has an exponential type of I-V characteristic. The RF picked up by a long stretch of fence acting as an antenna is passed through the joint and thence a low-pass filter, before supposedly being connected to an audio reproduction system, say a crystal ear piece.
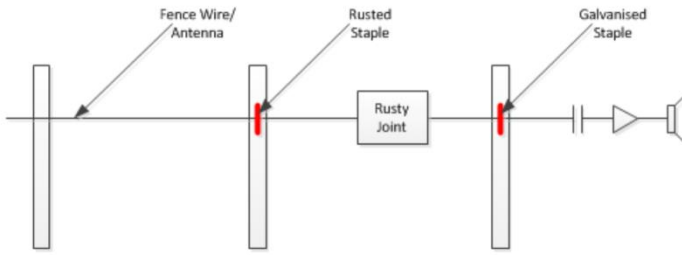
[1]A Gallagher iSeries Remote control.

Fig. 4. The arrangement that is proposed for causing a corroded fence joint to demodulate AM radio transmissions. The rusty and galvanised staples produce a small dc potential to bias the rusty joint in order to achieve asymmetry in its characteristic.
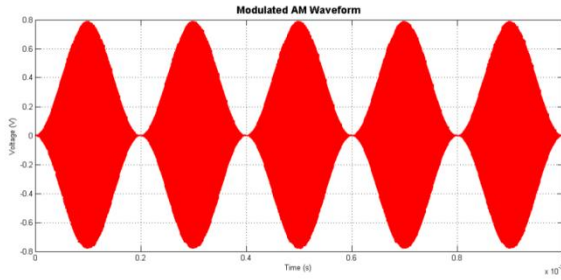

Fig. 6. The Amplitude Modulated (AM) waveform collected by the fence acting as an antenna.

In order to demonstrate the viability of this arrangement we simulate a model of it using SPICE. We model the fence joint as two silicon diodes, see figure 5. A 20 kHz sinusoidal waveform is impressed upon a 1 MHz carrier using Amplitude Modulation (AM). The resulting demodulated waveform is reproduced in figure 7. It is noticeably distorted but does clearly demonstrate demodulation of the original waveform from the carrier wave.

V. CONCLUSION

A thin layer of rust has been measured to have non-linear conductivity. The circumstances required to achieve such a characteristic are quite specific and mechanically fragile, and so are unlikely to occur often in practice. We attribute the nonlinearity to a tunnelling effect associated with a thin layer of material (iron oxide?) separating the steel of the wires. A modest voltage, such as occurs in the case of an operating electric fence, can destroy the thin isolating layer. A well-
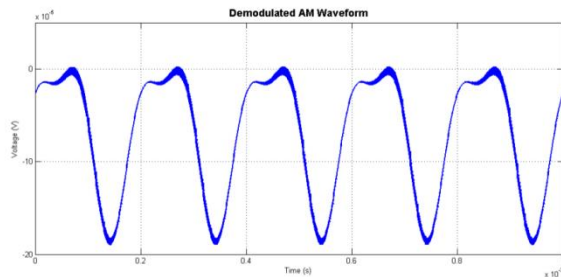
designed remote will also deliver a sufficient voltage to break through such non-linear joints.

Furthermore, the nonlinear effect can produce mixing and detection effects. We show how a fence might demodulate AM radio transmissions.

REFERENCES

[1] J. L. Walley, "Method of Electronic Control", International Patent WO9413120, 9 June 1994.
[2] N. May, "Method and apparatus pertaining to communication along a fence line", United States of America Patent US5651025, 22 July 1997.
[3] P. R. damson, R. R. Nilson and J. R. Spray, "Method and apparatus for communication in an electric fence wiring system", United States of America Patent US6081198, 27 June 2000.
[4] P. C. Lunenburg and R. C. B. Woodhead, "Data Transmission", United States of America Patent US6847298, 27 June 2002.
[5] E. J. Deuss, D. C. Greager and P. Teal, "System and Method for Electronically Signalling Along a Fence Line", United States of America Patent US6911900, 28 June 2005.
[6] J. Rhodes, "A Method of Locating Dry Joints in Telecommunications Cable", *Proc. IEE - Part B. Elec. and Comm. Eng.*, vol. 106, no. 29, pp. 470-472, Sep. 1959.
[7] Jargon, Jeffrey A., DeGroot, D.C., and Reed, Kristopher L., "NIST Passive Intermodulation Measurement Comparison for Wireless Base Station Equipment," 52nd Fall ARFTG Conference Digest, vol.34, pp.128–139, Dec 1998.
[8] Wilkerson, J.R.; Lam, P.G.; Gard, K.G.; and Steer, M.B., "Distributed Passive Intermodulation Distortion on Transmission Lines," IEEE Transactions on Microwave Theory and Techniques, vol. 59, no. 5, pp.1190–1205, May 2011.
[9] Abuelma'atti, M.T., "Prediction of passive intermodulation arising from corrosion," IEE Proceedings on Science, Measurement and Technology, vol. 150, no. 1, pp30–34, 6 Jan 2003.
[10] P. Roberge, *Handbook of Corrosion Engineering*, 2nd ed. New York City, New Yord: McGraw-Hill Professional, 2012.
[11] A. T. Hancock, "Modelling the Characteristics and Behaviour of Electric Fence Systems", MSc(Tech). Thesis, University of Waikato. New Zealand, 1991.
[12] V. De Santis, P. Beeckman, D. Lampasi, and M. Feliziani, "Assessment of Human Body Impedance for Safety Requirements Against Contact Currents for Frequencies up to 110 MHz," IEEE Transactions on Biomedical Engineering, vol. 58, no. 2, pp390–396, 2011.
[13] Jonathon McMullan, "FREQUENCY RESPONSE OF AN AGRICULTURAL FENCE AND THE IMPLICATIONS FOR DATA TRANSMISSION", MPhil thesis, University of Waikato, 2014.

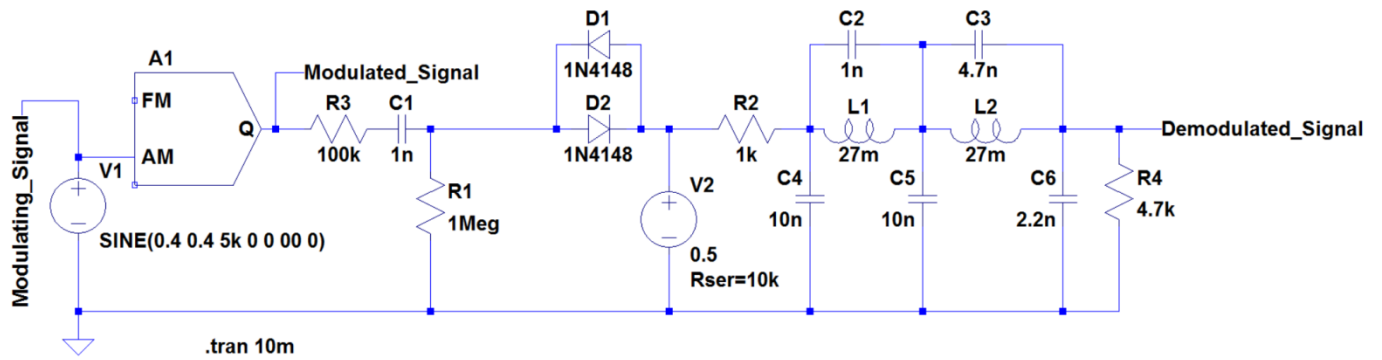Fig. 7. Demodulated AM Waveform that results from the circuit of figure 5.

Fig. 5.   Demodulator circuit as simulated in LTspice